



Ramos-Román, M. J. et al. (2018) Millennial-scale cyclical environment and climate variability during the Holocene in the western Mediterranean region deduced from a new multi-proxy analysis from the Padul record (Sierra Nevada, Spain). *Global and Planetary Change*, 168, pp. 35-53.(doi:[10.1016/j.gloplacha.2018.06.003](https://doi.org/10.1016/j.gloplacha.2018.06.003))

This is the author's final accepted version.

There may be differences between this version and the published version. You are advised to consult the publisher's version if you wish to cite from it.

<http://eprints.gla.ac.uk/163105/>

Deposited on: 29 May 2018

Enlighten – Research publications by members of the University of Glasgow
<http://eprints.gla.ac.uk>

Manuscript Details

Manuscript number	GLOPLACHA_2018_155_R2
Title	Millennial-scale cyclical environment and climate variability during the Holocene in the western Mediterranean region deduced from a new multi-proxy analysis from the Padul record (Sierra Nevada, Spain)
Short title	Millennial-scale cyclical environment and climate variability during the Holocene in the western Mediterranean region
Article type	Research paper

Abstract

A high-resolution multi-proxy approach, integrating pollen, inorganic and organic geochemical and sedimentological analyses, has been carried out on the Holocene section of the Padul sedimentary record in the southern Iberian Peninsula reconstructing vegetation, environment and climate throughout the last ~ 11.6 cal kyr BP in the western Mediterranean. The study of the entire Holocene allows us to determine the significant climate shift that occurred during the middle-to-late Holocene transition. The highest occurrence of deciduous forest in the Padul area from ~ 9.5 to 7.6 cal kyr BP represents the Holocene humidity optimum probably due to enhanced winter precipitation during a phase of highest seasonal anomaly and maximum summer insolation. Locally, insolation maxima induced high evaporation, counterbalancing the effect of relatively high precipitation, and triggered very low water table in Padul and the deposition of peat sediments. A transitional environmental change towards more regional aridity occurred from ~ 7.6 to 4.7 cal kyr BP and then aridification enhanced in the late Holocene most likely related to decreasing summer insolation. This translated into higher water levels and a sedimentary change at ~ 4.7 cal kyr BP in the Padul wetland, probably related to reduced evaporation during summer in response to decreased seasonality. Millennial-scale variability is superimposed on the Holocene long-term trends. The Mediterranean forest regional climate proxy studied here shows significant cold-arid events around ~ 9.6, 8.5, 7.5, 6.5 and 5.4 cal kyr BP with cyclical periodicities (~1100 and 2100 yr) during the early and middle Holocene. A change is observed in the periodicity of these cold-arid events towards ~1430 yr in the late Holocene, with forest declines around ~ 4.7-4, 2.7 and 1.3 cal kyr BP. The comparison between the Padul-15-05 data with published North Atlantic and Mediterranean paleoclimate records suggests common triggers for the observed climate variability, with the early and middle Holocene forest declines at least partially controlled by external forcing (i.e. solar activity) and the late Holocene variability associated with internal mechanisms (oceanic-atmospheric).

Keywords	Holocene; Padul; wetland; Sierra Nevada; western Mediterranean; atmospheric-oceanic dynamics; wavelet analysis; arid events
Corresponding Author	María J. Ramos-Román
Corresponding Author's Institution	University of Granada
Order of Authors	María J. Ramos-Román, Gonzalo Jimenez-Moreno, Jon Camuera Bidaurreta, Antonio Garcia-Alix, R. Scott Anderson, Francisco J. Jimenez-Espejo, Dirk Sachse, Jaime Toney, José Carrión, Cole Webster, Y. Yanes

Submission Files Included in this PDF

File Name [File Type]

Letter to the editor.pdf [Cover Letter]

Authors response-marked version.pdf [Response to Reviewers]

Highlights.docx [Highlights]

MS MJRR.docx [Manuscript File]

Fig 1.tif [Figure]

Fig 2.tif [Figure]

Fig 3.tif [Figure]

Fig 4.tif [Figure]

Fig 5.tif [Figure]

Fig 6.tif [Figure]

Fig 7.tif [Figure]

Fig 8.tif [Figure]

Table 1.docx [Figure]

Table 2.docx [Figure]

Table 3.docx [Figure]

Table 4.docx [Figure]

Supplementary Information.pdf [Figure]

To view all the submission files, including those not included in the PDF, click on the manuscript title on your EVISE Homepage, then click 'Download zip file'.



ugr | **Universidad
de Granada**

Facultad de Ciencias
Departamento de Estratigrafía y Paleontología

Avda. Fuente Nueva S/N
18002, Granada, Spain
+34 – 958 241000

29 May 2018

Dr. Fabienne Marret-Davies, Editor Global and Planetary Change (Ref. GLOPLACHA_2018_155)

Dear Fabienne,

Thank so much for accepting our new manuscript version “*Millennial-scale cyclical environment and climate variability during the Holocene in the western Mediterranean region deduced from a new multi-proxy analysis from the Padul record (Sierra Nevada, Spain)*”, in response to the reviewers comments.

Here we are submitting a new reviewed version of our manuscript in response to your suggestions. We have gone in detail over the correction and suggestions that you made, which improved it significantly.

Sincerely,
María J. Ramos-Román

Author's response to the editor

The editor comments are displayed in black, and our answer in blue. We indicate the lines in which we made the modifications according to the marked-up manuscript version (see below; in red text that was deleted, in blue text that was modified).

General comments

Can you please modify the age format in the text (I have corrected a few but you need to check all the text):

Absolute ages are given in units of “ka”, which are read as “billions of years ago”, “thousands of years ago”. Durations of time, including for rates and fluxes, are given in units of “kyr”, which are read and “thousands of years”. For Quaternary studies, note that “ka B.P.” is redundant because “ka” is equivalent to “thousands of years ago”. However, “kyr B.P.” is fine. “cal B.P.” alone is not acceptable; “cal yr B.P.” or “cal kyr B.P.” are fine. By analogy, “a” stands for “years ago”, so “a B.P.” is also redundant.

Thank you so much for your valuable suggestion and corrections about the age format. We corrected this throughout the text.

Comments and corrections over the manuscript

Line 108. Could it be possible to add mean winter and summer T and P?

Yes. We added mean summer and winter T and P. See added text between lines 108-110.

Line 217. Could you please give the dilution in %?

Yes. We have added the dilution.

Lines 756-757. I would also like to suggest to the reviewers.

Thank you for reminding us. We would like to thank the reviewers and the editor (lines 756-757).

Lines 1051-1053. Whose photos are these? You need to give a source to comply with copyright.

Ok. We added the author (line 1053).

Lines 1058. Same comment here about the photo's ownership.

Ok. We added this in lines 1058-1059. This information was also previously added in the methodology (please see in lines 166-167).

1 **Millennial-scale cyclical environment and climate variability during the Holocene in the western**
2 **Mediterranean region deduced from a new multi-proxy analysis from the Padul record (Sierra**
3 **Nevada, Spain)**

4

5 María J. Ramos-Román¹, Gonzalo Jiménez-Moreno¹, Jon Camuera¹, Antonio García-Alix^{1,2}, R. Scott
6 Anderson³, Francisco J. Jiménez-Espejo⁴, Dirk Sachse⁵, Jaime L. Toney⁶, José S. Carrión⁷, Cole Webster³,
7 Yurena Yanes⁸

8 ¹ Departamento de Estratigrafía y Paleontología, Universidad de Granada, Spain

9 ² Instituto Andaluz de Ciencias de la Tierra (IACT), CSIC-UGR, Armilla, Spain

10 ³ School of Earth Sciences and Environmental Sustainability, Northern Arizona University, USA.

11 ⁴ Department of Biogeochemistry, Japan Agency for Marine-Earth Science and Technology (JAMSTEC),
12 Japan.

13 ⁵ Helmholtz Centre Potsdam, German Research Centre for Geosciences GFZ, Section 5.1
14 Geomorphology, Organic Surface Geochemistry Lab., Germany

15 ⁶ School of Geographical and Earth Sciences, University of Glasgow, UK

16 ⁷ Departamento de Biología Vegetal, Facultad de Biología, Universidad de Murcia, Murcia, Spain

17 ⁸ Department of Geology, University of Cincinnati, USA

18

19 *Correspondence to:* María J. Ramos-Román (mjrr@ugr.es)

20 **Abstract**

21 A high-resolution multi-proxy approach, integrating pollen, inorganic and organic geochemical and
22 sedimentological analyses, has been carried out on the Holocene section of the Padul sedimentary record
23 in the southern Iberian Peninsula reconstructing vegetation, environment and climate throughout the last ~
24 11.6 cal ka-kyr BP in the western Mediterranean. The study of the entire Holocene allows us to determine

25 the significant climate shift ~~that has~~ occurred during the middle-to-late Holocene transition. The highest
26 occurrence of deciduous forest in the Padul area from ~ 9.5 to 7.6 cal ~~ka~~-kyr BP represents the Holocene
27 humidity optimum probably due to enhanced winter precipitation during a phase of highest seasonal
28 anomaly and maximum summer insolation. Locally, insolation maxima induced high evaporation,
29 counterbalancing the effect of relatively high precipitation, and triggered very low water table in Padul and
30 the deposition of peat sediments. A transitional environmental change towards more regional aridity
31 occurred from ~ 7.6 to 4.7 cal ~~ka~~-kyr BP and then aridification enhanced in the late Holocene most likely
32 related to decreasing summer insolation. This translated into higher water levels and a sedimentary change
33 at ~ 4.7 cal ~~ka~~-kyr BP in the Padul wetland, probably related to reduced evaporation during summer in
34 response to decreased in seasonality. Millennial-scale variability is superimposed on the Holocene long-
35 term trends. The Mediterranean forest regional climate proxy studied here shows significant cold-arid
36 events around ~ 9.6, 8.5, 7.5, 6.5 and 5.4 cal ~~ka~~-kyr BP with cyclical periodicities (~1100 and 2100 yr)
37 during the early and middle Holocene. A change is observed in the periodicity of these cold-arid events
38 towards ~1430 yr in the late Holocene, with forest declines around ~ 4.7-4, 2.7 and 1.3 cal ~~ka~~-kyr BP. The
39 comparison between the Padul-15-05 data with published North Atlantic and Mediterranean paleoclimate
40 records suggests common triggers for the observed climate variability, ~~being-with~~ the early and middle
41 Holocene forest declines at least partially controlled by external forcing (i.e. solar activity) and the late
42 Holocene variability associated with internal mechanisms (oceanic-atmospheric).

43 **Keywords:** Holocene, Padul, wetland, Sierra Nevada, western Mediterranean, atmospheric-oceanic
44 dynamics, wavelet analysis, arid events

45 1. Introduction

46 The western Mediterranean region, located ~~between-in the~~ subtropical ~~and-tropical~~ latitudes (Alpert et
47 al., 2006), is a sensitive area to detect past climate variability and has been the focus of several previous
48 Holocene studies (e.g., Fletcher et al., 2013; Zielhofer et al., 2017). Present-day climate in this area is

49 characterized by a strong seasonality, principally dominated by dry (hot) summers and wetter (mild) winters
50 (Lionello et al., 2006) and one of the main mechanisms driving climate variations is the North Atlantic
51 Oscillation (NAO) (Hurrell, 1995; Moreno et al., 2005).

52 During the Holocene, orbital-scale (i.e. insolation) variations triggered climate changes that in turn
53 produced significant environmental changes worldwide. Paleoclimate records show a Holocene climatic
54 optimum between 9.5-7.5 ka-kyr BP (Dormoy et al., 2009), characterized in the western Mediterranean area
55 by high temperatures and precipitation, which has been related with high summer insolation (Lamb and van
56 der Kaars, 1995; Fletcher and Sánchez-Goñi, 2008; Anderson et al., 2011). Regional climate models
57 described that the most important climatic transition towards cooler and drier conditions during the
58 Holocene occurred around ~ 6 ka BP (Huntley and Prentice, 1988; Cheddadi et al., 1997). This shift has
59 also been documented in the western Mediterranean, suggesting the establishment of the current NAO-like
60 system at ~ 6 cal ka-kyr BP (Fletcher et al., 2013). However, other studies differ in the timing of this climate
61 shift indicating a transition phase between 7 and 5.5 cal ka-kyr BP (Jalut et al., 2009). These differences
62 could be related with changes in altitudinal vegetation gradient, geomorphological changes in the study
63 area and/or human perturbation of the landscape (Anderson et al., 2011). According to Roberts et al. (2011),
64 combining different proxies indicative of vegetation and geomorphological changes is a useful tool to
65 discern the timing and the main forcing triggering this mid-Holocene environmental changes.

66 During the last few decades, a multitude of continental, marine and ice records worldwide have shown
67 millennial-scales climate variability during the Holocene (e.g. Johnsen et al., 1992; Bar-Matthews et al.,
68 2003; Mayewski et al., 2004). Numerous studies have detected this climate variability in the North Atlantic
69 area (i.e., Bond et al., 2001; Debret et al., 2007, 2009), with a prominent ~ 1500 yr cyclicality throughout the
70 Holocene (Bond et al., 2001). However, others studies have demonstrated that Holocene climate variability
71 was not stationary and exhibited variable periodicity at different times-intervals (Debret et al., 2007; 2009).
72 In this respect, high-resolution Mediterranean records have also shown rapid environmental variability
73 related to millennial-scale climate variability (Cacho et al., 2001; Fletcher and Sánchez-Goñi, 2008; Peyron
74 et al., 2013). Previous palynological analyses from the western Mediterranean, showed vegetation

75 responses at millennial-scales that seem to co-vary with climate variability from North Atlantic records,
76 demonstrating hemispheric-scale teleconnections during the Holocene (Combourieu-Nebout et al., 2009;
77 Fletcher et al., 2013; Rodrigo-Gámiz et al., 2014a). Other marine and terrestrial studies found centennial
78 and millennial-scale Holocene frequency climatic patterns (Rodrigo-Gámiz et al., 2014a; Ramos-Román et
79 al., 2016; García-Alix et al., 2017). However, there is a lack of non-stationary time-series analysis at
80 millennial-scales from terrestrial records in the western Mediterranean area, which is necessary to
81 understand terrestrial-ocean-atmospheric dynamics and the connections with high-latitude North Atlantic
82 climate records. This is key for learning about past environmental change and climate variability in the
83 western Mediterranean region.

84 Multi-proxy studies ~~in~~on continental records in southern Iberia and the western Mediterranean that
85 could help understanding this environmental variability during the Holocene are rare. In order to improve
86 our knowledge about this subject, we present a high-resolution multidisciplinary analysis integrating
87 sedimentation, geochemistry, vegetation, and climate change and variability during the Holocene (from
88 ~11.6 cal ~~ka~~kyr BP to Present) from the Padul-15-05 wetland record. Previous sedimentary records and
89 paleoecological studies have been carried out on the Padul archive, detecting climate variability from the
90 Pleistocene to the middle Holocene (Florschütz et al., 1971; Pons and Reille, 1988; Ortiz et al., 2004).
91 Nevertheless, a high-resolution multi-proxy analysis on the same sediment samples has never been
92 performed ~~in~~at this site for the entire Holocene epoch. Recently, a multi-proxy analysis [studying pollen,
93 spores, magnetic susceptibility (MS), total organic carbon (TOC) and X-ray fluorescence (XRF)] has been
94 done focusing on the late Holocene part of the Padul-15-05 record. That study ~~shows~~ an aridification trend
95 ~~during the last~~since ~~~ca.~~ 4.7 cal ~~ka~~kyr BP and enhanced human influence on the environments in the area
96 since the last 1.5 cal ~~ka~~kyr BP (Ramos-Román et al., 2018), renewing the interest to carry out a more
97 complete study for the entire Holocene. The present study uses high-resolution radiocarbon dating,
98 inorganic and organic geochemistry (biomarkers and bulk sediment), pollen, lithology and macrofossil
99 ~~analys~~is to reconstruct the Padul area paleoenvironmental evolution and millennial-scale vegetation and
100 climate fluctuations in the western Mediterranean region over the last ~~11.6 cal ka~~11,600 yearsBP. This

101 research seeks two main goals: 1) understanding regional vegetation changes and local environmental
102 evolution and making climate interpretations during the early, middle and late Holocene, specifically
103 focusing on the transitions, and 2) comparing millennial-scale vegetation and water-level oscillations
104 (regional and local signal) with global climatic events.

105 *1.1. Location and environmental setting*

106 The Padul basin is an endorheic area at around 725 m of elevation at the foothill of the southwestern
107 Sierra Nevada in Andalusia, southern Spain (Fig. 1). Today's climate in the [Padul region](#) ~~area~~ is
108 characterized by a mean annual temperature of 14.4 °C and a mean annual precipitation of 445 mm, and by
109 [hot and dry summers \(mean temperature of 22.8 °C and precipitation of 25 mm\) and mild and wetter winters](#)
110 [\(mean temperature of 8 °C and precipitation of 140 mm\) \(<http://agroclimap.aemet.es/>\)](#). [FM1]The Sierra
111 Nevada mountain range shows strong thermal and precipitation differences due to the altitudinal gradient
112 (from ~700 to more than 3400 m), which controls plant taxa distribution in different bioclimatic vegetation
113 belts due to the variability in temperature and precipitation (Valle Tendero, 2004). According to this
114 climatophilous series classification (Table 1), the Padul basin is situated in the Mesomediterranean
115 vegetation belt (from ~ 600 to 1400 m of elevation), which is largely defined by the dominance of *Quercus*
116 *rotundifolia* (evergreen *Quercus* pollen morphotype) and, to a lesser extent, *Q. faginea* (deciduous *Quercus*
117 pollen morphotype), which is normally accompanied by *Pistacia terebinthus*. *Q. coccifera* (evergreen
118 *Quercus* pollen morphotype) also occur in crests and very sunny rocky outcrops.

119 Sedimentation in the Padul basin results from (1) allochthonous detritic material coming for the
120 surrounding mountains, principally from Sierra Nevada, which is characterized at higher elevations by
121 Paleozoic siliceous metamorphic rocks (mostly mica-schists and quartzites) from the Nevado-Filabride
122 complex and, at lower elevations and acting as bedrock, by Triassic dolomites, limestones and phyllites
123 from the Alpujarride Complex (Sanz de Galdeano et al., 1998), (2) autochthonous organic material coming
124 from plants growing in the wetland area of the basin itself and (3) biogenic carbonates from charophytes,
125 ostracods and gastropod shells, prominent organisms that lived in the lake. The water contribution to the

126 Padul wetland primarily comes from groundwater input and, to a lesser degree, from rainfall. Groundwater
127 comes from different aquifers: the Triassic carbonate aquifers to the north and south edge of the basin, the
128 out-flow of the Granada Basin to the west and the conglomerate aquifer to the east (Castillo Martín et al.,
129 1984; Ortiz et al., 2004). The main water output is through evaporation and evapotranspiration and more
130 recently also by water wells and by canals (locally called “madres”) (Castillo Martín et al., 1984). The
131 canals were built around the end of the XVIII century with the goal of draining the basin water to the Dúrcal
132 river to the southeast for cultivation purposes (Villegas Molina, 1967). In the early 2000s the Padul wetland
133 was placed under environmental protection and the peat mine stopped pumping water out of the basin and
134 the Padul lake increased its size considerably.

135 The Padul-15-05 drilling site is located around 50 m south of the present-day Padul lake-shore area.
136 The edge of the lake area is at present principally dominated by the grass *Phragmites australis*. The lake
137 environment is also characterized by emerged and submerged macrophytes communities dominated by
138 *Chara vulgaris*, *Myriophyllum spicatum*, *Potamogeton pectinatus*, *Potamogeton coloratus*, *Typha*
139 *dominguensis*, *Apium nodiflorum*, *Juncus subnodulosus*, *Carex hispida*, *Juncus bufonius* and *Ranunculus*
140 *muricatus* among others (Pérez Raya and López Nieto, 1991). *Populus alba*, *Populus nigra*, *Ulmus minor*
141 and several species of *Salix* and *Tamarix* grow on the northern lake shore (Ramos-Román et al., 2018).

142 **2. Methodology**

143 *2.1. Padul site core drilling*

144 The Padul-15-05 sediment core (37°00'39.77''N; 3°36'14.06''W) with a length of 42.64 m, was
145 collected in 2015 from the Padul lake shore (Fig. 1). The core was taken with a Rolatec RL-48-L drilling
146 machine equipped with a hydraulic piston corer from the Scientific Instrumentation Center of the University
147 of Granada (CIC-UGR). The sediment core was wrapped in film, put in core boxes, transported and stored
148 in a dark cool room at +4 °C at the University of Granada. In this study, we focus on the uppermost ~ 3.67
149 m from the 42.6-m-long Padul-15-05 core.

150 *2.2. Chronology and sedimentation rates*

151 The age model for the uppermost ~ 3.27 m is based on fourteen AMS radiocarbon dates previously
152 shown in Ramos-Román et al. (2018). Six more radiocarbon samples have been analyzed in the lower part
153 of the study record in order to improve the chronology of older sediments. Three of these samples were
154 rejected, because one plant sample was too young and two gastropod shell samples provided old dates due
155 to the reservoir effect. As a result, the sedimentary record chronology from ~ 4.24 m to 0.21 m depth was
156 constrained using a total of seventeen AMS radiocarbon dates (Table 2). The age model was built using the
157 R-code package ‘Clam 2.2’ employing the calibration curve IntCal 13 (Reimer et al., 2013), a 95%
158 confident range, a smooth spline (type 4) with a 0.20 smoothing value and 1000 iterations (Fig. 2). The
159 chronology of the uppermost 21 cm of the record was built using a linear interpolation between the last
160 radiocarbon date and the top of the record, which was assigned the age when coring (2015 CE).

161 In this paper we followed the three principal subdivisions for the Holocene defined by Walker et al.,
162 2012. They proposed an Early-Middle Holocene boundary at 8.2 cal kyr~~a~~ BP and Middle-Late Holocene at
163 4.2 cal kyr~~a~~ BP.

164 *2.3. Lithology and magnetic susceptibility (MS)*

165 The Padul-15-05 core was split longitudinally and was described in the laboratory with respect to
166 lithology and color (Fig. 3). High-resolution continue scanning images were taken with an Avaatech core
167 scanner at the University of Barcelona (UB). MS was measured with a Bartington MS3 operating with a
168 MS2E sensor. MS measurements (in SI units) were obtained directly from the core surface every 0.5 cm
169 (Fig. 3). Lithological description and MS data of the same record of the uppermost 1.15 m of the record
170 were previously described in Ramos-Román et al. (2018).

171 *2.4. Inorganic geochemistry*

172 High-resolution XRF was applied continuously throughout the core surface, taking measurements of
173 elemental geochemical composition. An Avaatech X-Ray fluorescence (XRF) core scanner® located at the
174 UB was used. Chemical elements were measured in the XRF core scanner at 10 mm of spatial resolution,
175 using 10 s count time, 10 kV X-ray voltage and an X-ray current of 650 μ A for lighter elements and 35 s
176 count time, 30 kV X-ray voltage, X-ray current of 1700 μ A for heavier elements. Thirty-three chemical
177 elements were measured but only the most representative with a significant number of counts were
178 considered (Si, K, Ca, Ti, Fe, Zr, Br, S and Sr). Results for each element are expressed as intensities in
179 counts per second (cps) and normalized for the total sum in cps in every measure (Fig. 4), being the upper
180 part of the record (from 1.15 m to the top) previously shown in Ramos-Román et al. (2018).

181 2.5. Organic geochemistry

182 Several organic geochemical proxies have been studied from bulk sediment samples throughout the
183 record: total organic carbon (TOC), atomic Carbon-Nitrogen ratio (C/N) and atomic Hydrogen-Carbon ratio
184 (H/C). In addition, several indices of leaf wax biomarkers (*n*-alkanes) were calculated: the average chain
185 length (ACL), the carbon preference index (CPI) and the portion of aquatic (Paq). In addition, three new
186 indices have been calculated based on the relative abundance of odd carbon number from nC_{17} to nC_{33}
187 alkanes, except for nC_{27} alkanes (See Section 3.2.2 for justification of new indices).

188 Samples for elemental analyses in bulk sediment were analyzed every 2 or 3 cm throughout the Padul-
189 15-05 record, with a total of 206 samples analyzed. Samples were decalcified with 1:1 HCl to eliminate the
190 carbonate fraction. Carbon, nitrogen and hydrogen content of the decalcified samples were measured in an
191 Elemental Analyzer Thermo Scientific Flash 2000 model at the CIC-UGR. Percentage of TOC (note that
192 TOC of the uppermost 1.15 m of the record was previously described; Ramos-Román et al., 2018), total
193 nitrogen (TN) and total hydrogen (TH) per gram of sediment was calculated from the percentage of organic
194 carbon, nitrogen and hydrogen yielded by the elemental analyzer, and recalculated by the weight of the

195 sample prior to decalcification. The atomic C/N and H/C ratio was calculated from the carbon, nitrogen and
196 hydrogen measurements (Fig. 4).

197 Biomarkers from the Padul-15-05 record were extracted every 5 cm from sedimentary record, with a
198 total of 68 samples analyzed. Furthermore, thirty-one modern plant leaves/algae and bryophyte samples
199 were taken from the surroundings of the Padul basin and analyzed for biomarkers. The total lipid extraction
200 (TLE) from the freeze-dried samples was obtained using an accelerated solvent extractor (ASE) Thermo
201 DIONEX 350, with a dichloromethane:methanol (9:1). Plant biomarkers were extracted manually using
202 dichloromethane:methanol (9:1) by means of sonication and low temperature (38°C). The TLE from plants
203 and sediments was separated into three different fractions using a silica gel column. Before the separation
204 three internal standards were added to the TLE (5 α -androstane, 5 β -androstane-17-one and 5 α -androstane-
205 3 β -ol) in order to assess the biomarker extraction as well as to quantify them. Compounds of the aliphatic
206 fraction (*n*-alkanes) were recovered in the first fraction eluted with Hexane. The *n*-alkanes were identified
207 and quantified using a Gas Chromatography flame detection and mass spectrometry (GC-FID and GC-MS)
208 by means of an Agilent 5975C MSD by comparison to an external *n*-alkane standard mixture from *n*C₁₀ to
209 *n*C₄₀.

210 2.6. Pollen

211 Samples for pollen analysis (1-3 cm³) were taken with a resolution between 1-5 cm throughout the
212 core. A total of 73 samples between 1.15 and 3.67 m have been analysed in this study and were summed to
213 the previous 103 pollen samples analysed between 0-1.15 m (Ramos-Román et al., 2018), ~~the~~ with a mean
214 pollen resolution ~~is~~ around 65 yr (~ 95 yr between 11.6 and 4.7 cal ~~ka~~ kyr BP and ~ 50 yr for the last ~~4.7~~
215 ~~ka~~ 4,700 years). Pollen extraction methods followed a modified Faegri and Iversen, (1989) methodology.
216 Processing included the addition of *Lycopodium* spores for calculation of pollen concentration. Sediment
217 was treated with 10 % NaOH, 10% HCl, 10% HF [FM2] and the residue was sieved at 250 μ m before an
218 acetolysis solution. Counting was performed using a transmitted light microscope at 400 magnifications to

219 an average pollen count of around ~250 terrestrial pollen grains. Fossil pollen was identified using
220 published keys (Beug, 2004) and modern reference collections at the UGR. Pollen counts were transformed
221 to pollen percentages based on the terrestrial pollen sum, excluding aquatics. Non-pollen palynomorphs
222 (NPP) include algal spores. The NPP percentages were also calculated and represented with respect to the
223 terrestrial pollen sum. Several pollen and NPP taxa were grouped according to present-day ecological data
224 in Mediterranean forest, xerophytes and algae (Fig. 5). The Mediterranean forest taxa include *Quercus* total,
225 *Olea*, *Phillyrea*, *Pistacia* and Cistaceae. The Xerophyte group includes *Artemisia*, *Ephedra*, and
226 Amaranthaceae. The Algae group is composed of *Botryococcus*, *Zygnema* type, *Mougeotia* and *Pediastrum*.
227 ~~The palynological analysis was executed~~ Zonation was obtained with ~~by~~ a cluster analysis using four
228 representative pollen taxa Mediterranean forest, *Pinus* total, Ericaceae and *Artemisia* (Grimm, 1987; Fig.
229 5).

230 2.7. Statistical analysis

231 Statistical treatment was performed using the *PAST 3.12* software ([Hammer et al., 2001](#)). Principal
232 component analysis (PCA) was conducted on different geochemical elements (XRF data) to clarify the
233 lithological elemental composition of the core (Supplementary; Figure S1). Prior to the PCA analysis, we
234 pretreated the data normalizing the element counts by subtracting the mean and dividing by the standard
235 deviation (Davis and Sampson, 1986). As data spacing was different in all the study proxies, the data were
236 also resampled to the average value of 80-yr (linear interpolation) to obtained equally spaced time series.
237 Posteriorly, a Pearson correlation was made to different organic/inorganic geochemistry and pollen proxies
238 to find affinities between the different proxies.

239 In this study, spectral analysis was accomplished on the Mediterranean forest pollen taxa time series,
240 to identify regional millennial-scale periodicities in the Padul-15-05 record. We used REDFIT software
241 (Schulz and Mudelsee, 2002) on the unevenly spaced pollen time series in order to identify cyclical changes. In
242 addition, we carried out a Wavelet transform analysis by the ~~Past~~ [PAST](#) software (Torrence and Compo,
243 1998) with the goal of identifying non-stationary cyclical variability in the regional vegetation evolution,

244 the pollen was previously detrended and resampled at 80-yr age increments. In this study, a Morlet wavelet
245 was chosen, the significant level (plotted as contour) corresponded to a p-value = 0.05, and a white-noise
246 model was implemented.

247 *2.8. Correlations for the environment reconstruction*

248 Linear r (Pearson) correlation analyses between the obtained local proxy dataset (MS, Ca, S, Br, Sr,
249 K/Si ratio, C/N ratio, H/C ratio, TOC, short-chain, mid-chain and long-chain abundances, Poaceae, Algae
250 and Hygrophytes) ~~is~~ are shown in table 4. These analyses were performed to identify the associations
251 between proxies and to understand environmental change in the Padul area. This analysis assisted us in
252 identifying (a) different proxies characteristic of organic-rich sediments, primarily that peatland
253 environment under very shallow lake conditions (higher TOC, C/N ratio, S, Br, Sr and mid-chain
254 abundance) and (b) a second group of proxies characteristic of deeper shallow water environments depicted
255 by the increase in endogenic carbonates and more influenced by terrestrial-clays input (higher Ca, K/Si,
256 MS, Algae).

257 **3. Results and proxy interpretation**

258 *3.1. Chronology and sedimentary rates*

259 The age-model of the studied Padul-15-05 core (Fig. 2) is constrained by ~~seventeen-17~~ AMS ¹⁴C
260 radiocarbon dates from the top 4.24 m of the record (Table 2). In this work, we studied the uppermost ~
261 3.67 m that continuously cover the last ~ 11.6 cal ~~kyr~~ BP. This interval is chronologically constrained by
262 ~~sixteen-16~~ AMS radiocarbon dates. Fifteen distinct sediment accumulation rates (SAR) intervals are
263 differentiated between 3.67 m and the top of the record (Fig. 2).

264 *3.2. Lithology, inorganic and organic geochemistry*

265 *3.2.1. Lithology and inorganic geochemistry*

266 Inorganic geochemistry informs us about variations in the lithology and the local depositional
267 environment. Variations in these proxies could also be useful for estimating water level fluctuations in the
268 wetland environment. Sediments bearing aquatic fossil remains (i.e. gastropods and charophytes) ~~and as~~
269 ~~well as being~~ rich in carbonates have previously been related to shallow water lakes (Riera et al., 2004).
270 Lower water levels, more subjected to be occupied by wetland vegetation, and ephemeral lakes are
271 characterized by the increase in organics and clastic input and more influenced by terrestrial-fluvial
272 deposition (Martín-Puertas et al., 2008). Magnetic susceptibility (MS) measures the propensity of the
273 sediments to bring a magnetic charge (Snowball and Sandgren, 2001).

274 Framboidal pyrite (FeS_2) and barite (BaSO_4) with Sr have been found covering exceptionally preserved
275 mammals remains from 40 to 30 ka ~~ago~~ at the Padul Peat bog (García-Alix et al., 2012) pointing towards a
276 peat-bog environment with enhanced anoxic conditions. The presence of pyrite and organic-sulfur
277 compounds is common in peat bogs (Wieder and Lang, 1988; Feijtel et al., 1989; Chapman, 2001) and
278 other organic rich sediments under anoxic conditions (López-Buendía et al., 2007). Increasing values of
279 organic carbon, and bromine have been related with higher organic matter deposition generated in high
280 productivity environments (Kalugin et al., 2007). In marine records, Br XRF scanning counts can be used
281 to estimate sedimentary total organic carbon (Ziegler et al., 2008).

282 A visual lithological inspection was made for the upper ~ 3.67 m of the Padul-15-05 sediment core and
283 was compared with the elemental geochemical composition (XRF) and the MS data (Fig. 3). For the
284 geochemical elements, we conducted a PCA ~~analysis~~ to summarize and better understand the correlation
285 between the visual lithological features and the geochemical signal of the sediments (Supplementary Fig.
286 S1 and Table S1). The PCA ~~analysis~~ in the ~~studied~~ sedimentary sequence identifies three main groups of
287 sediments consisting of clays with variable content in (1) carbonates of endogenic formation with high
288 values of Ca, related with the occurrence of shells and charophyte remains, (2) siliciclastics (Si, K, Ti, Fe,
289 Zr) and (3) vegetal organics (related with S and Br) probably associated with reducing environment under
290 anoxic conditions showing high values of S, Sr and Br. The K/Si ratio was calculated to differentiate the

291 clays input into the basin. The K/Si ratio is based on the fact that clay fraction is enriched in phyllosilicates
292 (illite, muscovite), whereas the coarser particles that are mainly quartz, dolomite and schists. This
293 correlation between K and clay content has been observed in other lacustrine systems (e.g. Lake Enol,
294 Iberian Peninsula) and associated with an increase in detrital input (Moreno et al., 2011). Four different
295 lithological units were identified (Fig. 3). Units 1 and 2 are principally made up of peat sediments and Unit
296 3 and 4 by clays with variable carbonates (Fig. 3). Unit 1 (SAR ~ 0.04 cm/yr, from the bottom (3.67 m; ~
297 11.6 cal kyr BP) to around 2.31 m (~ 7.6 cal kyr BP), is characterized by *facies* 1 - dark organic peat –
298 high S, Sr and Br values. Unit 2 (SAR ~ 0.05 cm/yr), from 2.31 to 1.15 m (~ 7.6 to 4.7 cal kyr BP), is
299 also generally characterized by *facies* 1 but with the intercalation of three other different *facies*; *facies* 2
300 from 2.31 to 2.21 m (~ 7.6 to 7.3 cal kyr BP) depicted by grey clays with gastropod remains (featured
301 by the increase in Ca and K/Si ratio), *facies* 3 from 1.95 to 1.85 m (~ 6.6 to 6.4 cal kyr BP) made up of
302 brown clays with the occurrence of gastropods and charophytes (showing a decrease in S, Br and Sr and
303 higher values of Ca) and *facies* 4 around 1.46 to 1.40 m (~ 5.7 to 5.4 cal kyr BP) characterized by grey
304 clays (related with the increase in siliciclastic material and clays input). Units 3 (SAR ~ 0.03 cm/yr) and 4
305 (SAR ~ 0.13 cm/yr) correspond with the uppermost 1.15 m (4.7 cal kyr BP) of the record were previously
306 described in Ramos-Román et al. (2018) as clays with high Ca values and showing an increasing trend in
307 K/Si ratio to the top of the record.

308 3.2.2. Organic geochemistry

309 Variations in TOC, C/N and H/C ratios reflect changes in paleoenvironmental dynamics in bogs and
310 lakes (Meyers and Lallier-Vergés, 1999; Ortiz et al., 2010; García-Alix et al., 2017). TOC concentration is
311 the principal indicator of organic matter content in sediments. Typical organic matter contains 50 % of
312 carbon so the concentration of organic matter in sediments is twice the TOC (Meyers et al., 1999). C/N
313 ratio informs about the proportion of algae and terrestrial vascular plant organic matter in the sediments
314 (Meyers, 1994). Fresh organic matter from algae exhibits molar C/N values that are between 4 and 10,
315 whereas cellulose-rich terrestrial plants show values above 20 and greater (Meyers et al., 1994). H/C values

316 are a good proxy for the source of the organic matter in sediments, as algal/bacterial/amorphous remains
317 are richer in hydrogen than herbaceous and woody plant material, with values over 1.7 indicative of
318 algal/amorphous organisms. In addition, lower values of H/C (<0.8) could also be indicative of organic
319 matter transport or diagenesis after deposition (Talbot, 1988; Talbot and Livingstone, 1989).

320 *n*-alkane biomarker abundance and distribution can provide information about different biological
321 sources of organic matter that accumulated in bog and lake sediments (Meyers and Lallier-Vergés, 1999;
322 Ficken et al., 2000; Sachse et al., 2006). Several of these sources are characterized by distinct predominant
323 *n*-alkane chain-lengths that have been identified according to the biological sources to the sediments : (1)
324 In general, *n*-alkanes with 17 or 19 carbon atoms (nC_{17} or nC_{19}) are found predominantly in algae (Gelpi et
325 al., 1970; Cranwell, 1984) and in photosynthetic bacteria (Cranwell et al., 1987), (2) nC_{21} , nC_{23} and nC_{25}
326 are associated with submerged and floating aquatic plants (Cranwell, 1984; Ficken et al., 2000), while (3)
327 *n*-alkane distribution with predominant $> nC_{27}$, nC_{29} , nC_{31} represents higher terrestrial plant input (Cranwell
328 et al., 1987) as well as emergent macrophytes (e.g. *Juncus* sp., *Typha* sp. or *Phragmites australis*)
329 (Cranwell, 1984; Ogura et al., 1990; Ficken et al., 2000). CPI (illustrating the relative abundance of odd vs.
330 even carbon chain lengths) is a proxy for preservation of organic matter in the sediments, with values lower
331 than 2 indicating diagenetic alteration or algal/bacterial influence and, higher than 2 (see Bush et al., 2013
332 review) indicating terrestrial influence and thermal immaturity of the source rock. Ficken et al. (2000)
333 formulated the Paq (proportion of aquatics) to discern the origin of the organic inputs in the sediments,
334 giving average values for present-day plants of <0.1 for terrestrial plants, 0.1-0.4 for emerged aquatics and
335 0.4-1 for submerged/floating aquatic species.

336 García-Alix et al. (2017), however, showed that the interpretation of these *n*-alkane chain length indices
337 cannot be generalized, and the modern *n*-alkanes distribution of the vegetation in the study site should be
338 well understood prior to paleoenvironmental interpretations from core records. Accordingly, to better
339 constrain the origin of the organic input in the Padul-15-05 record, we analyzed *n*-alkanes from present day
340 terrestrial and aquatic plants as well as algae/bryophyte in the Padul basin area (Supplementary information;
341 Figs. S2 and S3). Our results show that the predominant *n*-alkanes in the samples are nC_{27} , nC_{29} and nC_{31} .

342 There is also a strong odd-over-even carbon number predominance (CPI values higher than 2). This basin
 343 is currently dominated by wetland plants, such as *Phragmites australis* with predominant carbon chain
 344 between C₂₇ and C₂₉ *n*-alkane. The Paq for present-day plants average values of 0.16 ± 0.16 for terrestrial
 345 plants, 0.29 ± 0.34 for aquatic plants and 0.32 ± 0.21 for algae-bryophyte. ACL average values were around
 346 28.23 ± 0.74 for emerged-terrestrial plants, 28.78 ± 1.86 for aquatic plants and 27.97 ± 0.74 for algae-
 347 bryophyte (Table 3; Supplementary Fig. S3). These results led us to the need to create three new *n*-alkane
 348 indices with the goal of characterizing the source of organic matter in our sediment samples from the Padul-
 349 15-05 record, taking in consideration the relative abundances of the odd carbon chains except for *n*C₂₇ (due
 350 to higher values in all the plant/algae samples): (1) Short-chain (%), where higher values are typical from
 351 algae or bacterial, (2) Mid-chain (%), where higher values are typical of aquatic plants, and (3) Long-chain
 352 (%), where higher values are obtained when the source is vascular emerged aquatic or terrestrial plants
 353 (Table 3).

- 354 1. Short-chain: $[C_{17}-C_{19}] = [(C_{17}+C_{19})/(C_{17}+C_{19}+C_{21}+C_{23}+C_{25}+C_{29}+C_{31}+C_{33})] \times 100$
- 355 2. Middle-chain: $[C_{21}-C_{23}-C_{25}] = [(C_{21}+C_{23}+C_{25})/(C_{17}+C_{19}+C_{21}+C_{23}+C_{25}+C_{29}+C_{31}+C_{33})] \times 100$
- 356 3. Long-chain: $[C_{29}-C_{31}-C_{33}] = [(C_{29}+C_{31}+C_{33})/(C_{17}+C_{19}+C_{21}+C_{23}+C_{25}+C_{29}+C_{31}+C_{33})] \times 100$

357 The results for the organic geochemistry (TOC, C/N ratio, H/C ratio and *n*-alkane indices) from the
 358 Padul-15-05 record are illustrated in Figure 4. TOC values range from 0.8 to 61%, with an average value
 359 of 27.5 %. Highest TOC values are registered during the deposition of sedimentary Unit 1 averaging values
 360 of 41 %, associated with the peatland environment and higher values of anoxic/reducing proxies (showing
 361 higher correlation with S, Br; Table 4). Higher TOC variability occurred during Unit 2. The transition
 362 between Unit 1 and 2 is marked by a TOC decrease with values around 14 % at ~ 7.6 cal ka-kyr BP. Other
 363 decreases occurred between 2-1.89 m (~ 6.9 to 6.4 cal ka-kyr BP) and between 1.48-1.39 m (~ 5.7 to 5.4
 364 cal ka-kyr BP), reaching values around 20 and 30 %, respectively. The transition between Unit 2 and 3 (~
 365 4.7 cal ka-kyr BP/~ 1.13 m) is marked by a significant decline to values below 15 %. The lowest TOC
 366 values are recorded during Units 3 and 4 with average values around 4.6 %. Atomic C/N ratios were higher

367 during the lithological Units 1 and 2 and ranged between 53 and 11, with an average value of 26. A decrease
368 in C/N occurred during the transition from Units 2 to 3 down to average values of 17. The lowest values
369 occurred during Unit 1, recording C/N values in a range between 14 and 10. Atomic H/C ratios ranged
370 between 1.13 and 6.66 with an average value of 1.65. The lowest values were recorded between the bottom
371 of the record and approximately 0.77 m (~ 3.9 cal ~~ka~~-kyr BP) with ranging values between 1.13 and 2.26
372 with an average of 1.39. Highest values are depicted from 0.77 m to the top of the record averaging values
373 of 2.62.

374 The *n*-alkane data obtained from the Padul-15-05 sediments show that shorter carbon chains were
375 abundant during Unit 1. CPI values were higher than 2, averaging values of around 7 and representing an
376 odd over even carbon chain and a good preservation of the organic matter in the sediments, the lowest
377 values, with an average of 2.6, occurred during the Unit 1 around 3.07-2.31 m depth (~ 9.7 to 7.6 cal ~~ka~~-kyr
378 BP), and the highest values averaging 11.8 occurred between 2.31 and 2.15 m depth (from ~~ca.~~7.5 to 7.2
379 cal kyr BP). Short-chain abundance shows peaks of higher values at 3.10 m (~9.6 cal ~~ka~~-kyr BP), 2.55 m
380 (~ 8.5 cal ~~ka~~-kyr BP), 2.30 m (~ 7.5 cal ~~ka~~-kyr BP), 1.40 m (~ 5.4 cal ~~ka~~-kyr BP), from 1.10 to 0.8 m (~ 4.6-
381 4 cal ~~ka~~-kyr BP), 0.52 m (~ 2.7 cal ~~ka~~-kyr BP) and from 0.4-0.33 m (~ 1.3-0.8 cal ~~ka~~-kyr BP). Mid-chain
382 abundance shows the highest values between the bottom and 2.26 m (between ~11.6 and 7.6 cal ~~ka~~-kyr BP)
383 with an average of approximately 24 %, depicting a maximum between 2.90 and 2.31 m (~9.5 to 7.6 cal ~~ka~~
384 kyr BP) with average values of around 40 %. The lowest values are recorded during the last 1.15 m (~4.7
385 cal ~~ka~~-kyr BP). Long-chain abundance shows high values averaging ~ 81 % between 2.26 and 1.40 m (~
386 7.5 to 5.4 cal ~~ka~~-kyr BP) and reached maximum values around 0.60 m (~3.2 cal ~~ka~~-kyr BP) and between
387 0.45 m (~ 1.9 cal ~~ka~~-kyr BP), and the last 0.22 cm (~ 0.1 cal ~~ka~~-kyr BP).

388 3.3. Pollen and Spores

389 Pollen grains from terrestrial, aquatic species and spores were identified and the taxa higher than around
390 1 % were plotted in the pollen diagrams (Supplementary Figures S4, S5 and S6). The most representative
391 taxa are plotted in a summary pollen diagram (Fig. 5). In this study, we used the variations between
392 Mediterranean forest taxa, xerophytes, hygrophytes and algae for paleoenvironmental and paleoclimatic
393 variability in the study area. The fluctuations in arboreal pollen (AP, including Mediterranean tree species)
394 have previously been used in other nearby Sierra Nevada records as a proxy for regional humidity changes
395 (Jiménez-Moreno and Anderson, 2012; Ramos-Román et al., 2016). The abundance of the Mediterranean
396 woods (i.e., evergreen and deciduous *Quercus*, *Olea*, *Pistacia*) has been used as a proxy for climate change
397 in many other studies in the western Mediterranean region, with higher forest development generally
398 meaning higher humidity (Fletcher and Sánchez-Goñi, 2008; Fletcher et al., 2013). On the other hand,
399 increases in xerophyte pollen taxa (i.e., *Artemisia*, *Ephedra*, *Amaranthaceae*), representative of steppe
400 vegetation, have been used as an indication of aridity in this area (Carrión et al., 2007; Anderson et al.,
401 2011). Variability in wetland angiosperms and algae could be indicative of local change in the surrounding
402 vegetation and lake level fluctuations. Singh et al. (1990) suggested that Cyperaceae and *Typha* could be
403 considered swamp- indicative when co-occurring with freshwater algae (*Cosmarium*, *Zygnemataceae*).
404 Currently, the dominant plant species in the Padul wetland is the common reed, *Phragmites australis*, in
405 fact very common in semi-arid wetlands with shallow water levels (Moro et al., 2004). This species has
406 thrives whenever a wetlands becomes drier (Hudon, 2004). Van Geel et al. (1983) described the occurrences
407 of *Zygnema* and *Mougeotia* as characteristic of shallow lake water environments. The chlorophyceae
408 *Botryococcus* is an indicator of freshwater environments in relatively productive fens, temporary pools,
409 ponds or lakes (Guy-Ohlson, 1992). Clausen (1999) point out that *Botryococcus* abundance is higher in
410 sediment of shallow water lakes and/or littoral environment in deeper lakes. Three pollen zones were
411 visually identified with the help of a cluster analysis using the program CONISS (Grimm, 1987).

412 The pollen results are described subsequently, distinguishing three major phases during the Holocene:

413 3.3.1. From ~ 11.6 to 7.6 cal ~~ka~~-kyr BP (from ~ 3.67 to 2.31 m)

414 The early and early middle Holocene, from ~ 11.6 to 7.6 cal ~~ka~~-kyr BP, is characterized by high
415 abundance of Mediterranean forest, averaging relative percentage values of approximately 58%. The most
416 representative arboreal tree taxon between ~ 11.6 to 9.7 cal ~~ka~~-kyr BP is evergreen *Quercus*, reaching
417 maximum values of ~~around~~ ca. 50 %. A decrease in the Mediterranean forest and an increase in hygrophytes
418 and Poaceae occurred between 10.1 and 9.6 cal ~~ka~~-kyr BP (from 3.28 to 3.01 m). Deciduous *Quercus* show
419 increasing trends between 9.5 and 7.6 cal ~~ka~~-kyr BP (~ 2.91 to 2.31 m), recording average maxima with
420 values of around 22% at that time. Hygrophytes reach maxima average values of approximately 17%, from
421 ~ 9.8 to 8.8 cal ~~ka~~-kyr BP (from 3.16 to 2.63 m). Algae display a decreasing trend from around 9 % (from
422 ~ 11.6 to 9.9 cal ~~ka~~-kyr BP/3.67 to 3.20 m) to 2 % (from ~ 9.9 to 7.6 cal ~~ka~~-kyr BP/3.20 to 2.34 m). ~~The~~ is
423 ~~algae~~ decline between ~ 11.6 and 9.9 cal ~~ka~~-kyr BP is due to the lowering of *Zygnema* spores. An increase
424 in the soil mycorrhizal fungus *Glomus* type occurs from ~9.6 to 9.3 cal ~~ka~~-kyr BP (from 3.01 to 2.80 m).
425 This transition between the early and middle Holocene is featured by a slight decrease in deciduous *Quercus*
426 and in wetland plants such as Cyperaceae and *Typha* type.

427 3.3.2. From ~ 7.6 to 4.7 cal ~~ka~~-kyr BP (from ~ 2.34 to 1.15 m)

428 The middle Holocene from ~ 7.6 to 4.7 cal ~~ka~~-kyr BP ~~was~~ is still characterized by high values of
429 Mediterranean forest (averaging values of ~~ca.~~ ca. 58 %) interrupted by several events of forest decrease. One
430 of the most significant Mediterranean forest declines (up to 26 %) parallel hygrophyte and Poaceae rise
431 between ~ 7.5 and 7.3 cal ~~ka~~-kyr BP (2.28 to 2.21 m). A slight increase in algae also occurred around ~ 7.6
432 to 7.1 cal ~~ka~~-kyr BP (2.31 to 2.11 m). A second decrease in the Mediterranean forest occurred at ~ 6 cal ~~ka~~
433 ~~kyr~~ BP (from around 1.65 m), also characterized by the increase in hygrophytes to maximum values around
434 40 %, and the increase in *Pinus* of around 5 to 12 %. A third remarkable decrease in Mediterranean forest
435 occurred between ~ 5.5 to 5.4 cal ~~ka~~-kyr BP (around 1.43 to 1.39 m), also characterized by the increase of

436 the aquatic component. These three previous events of decrease in forest decline are accompanied by slight
437 *Glomus* type increases.

438 3.3.3. From ~ 4.7 [cal kyr BP](#) to Present (from ~ 1.15 m to top)

439 The middle to late Holocene transition (~ 4.7 cal ~~ka~~-[kyr](#) BP/~ 1.15 m) is characterized by the decrease
440 in Mediterranean forest, in particular in the deciduous tree taxa, and the increase in *Pinus*, shrubs (i.e.,
441 Ericaceae) and xerophytes and Asteraceae (mainly Cichorioideae) (Ramos-Román et al., 2018).

442 3.4. Spectral analysis

443 Spectral analysis was performed [on the pollen percentage record](#) in order to find cyclical periodicities
444 in the Mediterranean forest from the Padul-15-05 record using REDFIT analysis (Schulz and Mudelsee,
445 2002) detecting a periodicities of around ~ 2070, 1430 and 1100 yr. Wavelet analyses show significant
446 cycles ($p = 0.05$) in the Mediterranean forest taxa time series with periodicities around ~ 2070 and 1100 yr
447 during the early and middle Holocene period and ~ 1430 yr periodicity ~~during the last~~[since](#) ~ 4.7 cal [kyr](#)
448 [BP to Present](#) (Supplementary Figure S7).

449 4. Discussion

450 4.1. Holocene climate change in Padul and the western Mediterranean region

451 4.1.1. The earliest Holocene

452 During the earliest Holocene (~ 11 to 10 cal ~~ka~~-[kyr](#) BP) a transition period from glacial to interglacial
453 conditions occurred in the Padul area and the pollen assemblages were dominated by evergreen *Quercus*
454 and to a lesser extent, mesic forest species such as deciduous *Quercus*. Local environment proxies show a
455 development of a peatland environment in the Padul basin (organic facies featured by higher values of TOC
456 and C/N and lower values of mid-chain, short-chain and S; Fig. 6), which indicate low water levels at that
457 time. The increase in Mediterranean forest taxa may be interpreted as a regional vegetation response to a

458 climate change to warmer and more humid conditions than earlier on during the cold and dry Younger
459 Dryas, agreeing with the increasing trend in SSTs reconstructions from the Alboran Sea (Cacho et al., 1999;
460 Martrat et al., 2004; Rodrigo-Gámiz et al., 2014b; Fig. 7; Supplementary Fig. S8). The observed peak of
461 evergreen *Quercus* is consistent with previously described glacial-interglacial vegetation transition from
462 Southern Europe indicating that a cold-dry steppe was followed by pre-temperate open woodland [including
463 *Juniperus*, *Pinus*, *Betula*, *Quercus*; van der Hammen et al. (1971)]. These results agree with the previous
464 pollen records from Padul, which also show a widespread evergreen *Quercus* forest after the postglacial
465 epoch (Pons and Reille, 1988) and other high-resolution pollen studies in the western Mediterranean
466 region that show a similar forest change with high abundance of Mediterranean taxa (Fletcher and Sanchez-
467 Goñi et al., 2008; Fig. 7). These results are also consistent with vegetation variability in the Middle Atlas
468 Mountains of Morocco depicting high values of evergreen *Quercus rotundifolia* at that time (Lamb and van
469 der Kaars, 1995). A forest expansion is also observed in the nearby, but higher elevation site, Laguna de
470 Rio Seco in Sierra Nevada (Supplementary Fig. S8), but in this case, it is mostly due to *Pinus* expansion
471 after a pollen assemblage dominated by steppe vegetation (Anderson et al., 2011; Fig. 7). This dissimilarity
472 is probably explained by the altitudinal difference between the two sites (Padul=750 m vs. Laguna de Rio
473 Seco=3000 m), being influenced by different vegetation belts (mesomediterranean vs. oromediterranean
474 belt; see Table 1). The continental pollen record of the cave site Carihuela, inland Granada at the
475 supramediterranean altitude, also shows a clear oak dominance during this period (Carrión et al., 1999;
476 Fernández et al., 2007).

477 A punctual increase in algae (principally dominated by *Zygnema* type) also occurred within this peat-
478 dominated and shallow water period at around ~ 10.5 cal ka-kyr BP. We suggest that this increase in algae
479 could probably be linked with an increase in productivity in the wetland resulting from increased
480 temperatures during a warm pulse recorded in the North Atlantic ice record (Bond et al., 2001; Fig. 8).

481 4.1.2. Early and middle Holocene and Humidity optimum

482 The early to middle Holocene (from ~ 10 to 4.7 cal ka-kyr BP) in the Padul-15-05 record is featured by

483 the highest values of Mediterranean forest showing the expansion in mesic components (e.g. deciduous
484 *Quercus*), agreeing with the temperate phase of vegetation transition during interglacial periods (described
485 by van der Hammen et al., 1971 and reviewed by Tzedakis et al., 2007; Supplementary Fig. S9). The local
486 Padul wetland environment within this period (~ 10 to 4.7 cal ka-kyr BP) was characterized by generally
487 low water levels, triggering high occurrence of wetland plants, which accumulated in great amounts,
488 generating peat sedimentation related with higher organic content and/or anoxic/reducing conditions and
489 associated geochemical signals (i.e. higher values of TOC, C/N, S and an increase in mid-chain; Figs. 4 and
490 6). There is an apparent contradiction between the regional vegetation signal, which indicates high
491 humidity, and local sedimentary proxies, which pointing to low water levels in the area. This contradiction
492 could be explained due to very strong evapotranspiration rates during Holocene summer insolation maxima
493 (Laskar et al., 2004) even if annual (mostly winter) precipitation was the highest (Fig. 6). Low lake levels
494 during the regionally humid early Holocene have also been observed in other records from the southern
495 Mediterranean area, pointing to the same high-evaporative summer insolation phenomenon (Lamb and van
496 der Kaars, 1995; Reed et al., 2001; Magny et al., 2007).

497 Despite the overall humid conditions interpreted for the early and middle Holocene, millennial-scale
498 climate variability occurred (see section 4.1.4 below) and wettest conditions are observed between ~ 9.5 to
499 7.6 cal ka-kyr BP in the Padul-15-05 record. This humidity optimum is indicated regionally by the maximum
500 expansion of mesic forest species (deciduous *Quercus*). Our new results from Padul agree with the
501 previously described Holocene climate evolution in the western Mediterranean region, which also show a
502 wetter early and middle Holocene and a transition to drier conditions during the late Holocene (Fletcher et
503 al., 2013; Anderson et al., 2011; Carrión et al., 2010 among others). The maximum in humidity occurred
504 during summer insolation maxima and thus during the warmest Holocene conditions shown by paleoclimate
505 records such as the Greenland ice core record temperature reconstruction (Alley, 2000), the decrease in the
506 Drift Ice Index in the north Atlantic records and in total solar irradiance (TSI) and regionally the SST
507 reconstructions in the Alboran Sea (Bond et al., 2001; Cacho et al., 1999; Rodrigo-Gámiz et al., 2014b;
508 Steinhilber et al., 2009; Figs. 7 and 8). Support for the timing of the Holocene humidity optimum recorded

509 in Padul-15-05 comes from a number of paleoclimatic studies from nearby places. For example, previous
510 pollen results from the Padul sedimentary sequence show a similar increase in deciduous *Quercus* and
511 maximum humidity at the same time (Pons and Reille, 1988; Fig. 7). The nearby alpine site of Laguna de
512 Rio Seco in Sierra Nevada indicates that the early and middle Holocene is characterized by more abundant
513 mesic vegetation and the maximum in algae and aquatic plants, indicating that humid maximum occurred
514 prior to ~ 7.8 cal ka-kyr BP (Anderson et al., 2011). Jimenez-Espejo et al., (2008) in a study in the Algero-
515 Balearic basin described that the end of the Holocene, humid conditions occurred between ~ 7.7 and 7.2 cal
516 kyr BP and a synthesis about circum-Mediterranean vegetation change analysis determined that two
517 principal climatic phases occurred during the early and middle Holocene, with a more humid phase from
518 11 to 7.5 cal kyr BP and a transition phase from 7 to 5.5 cal ka-kyr BP, the later one mostly related to
519 decreasing insolation and the installation of the present climate dynamics (Jalut et al., 2009). Dormoy et al.
520 (2009) also described the maximum in humidity in the Mediterranean region during the early and middle
521 Holocene between 9.5 and 7.5 cal ka-kyr BP, resulting from maximum seasonal anomaly characterized by
522 greatest winter precipitation and minima in precipitation during summer. However, some discrepancies
523 exist about the timing of the mesic maximum within this generally humid period in the Mediterranean
524 region and continental and marine records from southern Iberia and north Africa pointed out that the mesic
525 maximum occurred later on during the middle Holocene (Lamb and van der Kaars, 1995; Carrión, 2002;
526 Fletcher and Sánchez-Goñi, 2008). Supporting our hypothesis, Anderson et al. (2011) suggested that this
527 difference in timing between montane and subalpine forest development and water lake levels could be
528 associated to the different effect that summer insolation maxima and higher seasonality provoked in
529 effective precipitation and water levels during the early Holocene. In lower elevation with higher
530 evaporations rates during summer, compared to higher elevation areas and alpine lakes with lower summer
531 temperatures and higher snowpack during winter and subsequently high lake level.

532 The early Holocene thermal maximum could be explained by maximum orbital-scale summer
533 insolation (Laskar et al., 2004; Figs. 6 and 8). The early Holocene humidity maximum was likely due to
534 enhanced fall/winter precipitation, consistent with global climate models predicting that summer insolation

535 maxima favor the land/sea temperature contrast in the Mediterranean thus enhancing the winter rainfall
536 (Meijer and Tuenter, 2007).

537 This occurred at the same time that the Intertropical Convergence Zone was displaced northward (prior
538 to ~ 6 ka-~~BP~~) into the Sahara and Arabian deserts (Gasse and Roberts, 2004). However, Arz et al. (2003)
539 and Tzedakis (2007) concluded that summer monsoon did not reach further than the African subtropical
540 desert during the early and middle Holocene and would not have had a direct influence over the northern
541 Mediterranean coast.

542 Sedimentation at that time in the Padul basin is homogeneous peat but the local proxies show some
543 oscillations (see in section 4.1.4).

544 4.1.3. *End of the humid period and significant environmental change around 4.7 cal ~~ka~~-kyr BP*

545 The Padul-15-05 record shows the most significant climatic change affecting both regional and local
546 environment at ~ 4.7 cal kyr BP, right at the middle to late Holocene transition. This paleoenvironmental
547 change is regionally depicted by the beginning of a strong decrease in Mediterranean (especially in the
548 deciduous) forest, indicating progressive climate drying conditions, a slight increase in *Pinus*, and an
549 increase in Ericaceae (Ramos-Román et al., 2018). The significant development of heathlands (Ericaceae)
550 during the middle to late Holocene transition could be indicative of reduced insolation under still a relatively
551 humid climate. This agrees with other studies that show that heathlands increased under increasing
552 precession (decreasing summer insolation), suggesting a thriving response to reduced thermal seasonality
553 (Fletcher and Sánchez-Goñi et al., 2008). Similar vegetation changes, with the decline in mesic forest
554 species and the increase in shrubs such as Ericaceae, have previously been recorded in other terrestrial and
555 marine pollen archives from the western Mediterranean region during the transition to the late Holocene
556 (e.g., Carrión 2002; Carrión et al., 2003; 2007; 2010b; Fletcher and Sánchez-Goñi, 2008;) pointing to a
557 regional response to climate aridification and reduction in seasonality (i.e. cooler summers and warmer
558 winters). The timing of this change agrees with Magny et al. (2002) who described the period at 4.5 cal ~~ka~~

559 kyr BP, as a crucial transition from wetter to drier climate in the Mediterranean region. In addition, Jalut et
560 al. (2009), described the aridification process in the Mediterranean region since 5.5 cal ka-kyr BP.

561 This climatic change also locally affected the Padul wetland environment, and sedimentation changed
562 drastically from mostly peat (unit 2) to carbonate-rich clays (unit 3) rich in aquatic organisms (charophytes
563 and gastropods; between ~ 4.7 to 1.5 cal ka-kyr BP; Ramos-Román et al., 2018) pointing to an increase in
564 the lake level. This sedimentary change is principally featured in the geochemistry by a decrease in organic
565 content, a decrease in the aquatic plants in the lake [lower values of TOC (Ramos-Román et al., 2018), C/N
566 and generally decrease in mid-chain abundance], an increase in Ca and in the palynomorph record by a
567 continuously increase in algae (principally dominated by *Botryococcus*; Ramos-Román et al., 2018). In
568 addition, a higher terrestrial and detrital input occurred during the aridification trend, observed in the Padul-
569 15-05 sequence by a slight increasing trend in soil erosion (*Glomus*) and clastic input (higher K/Si), most
570 likely due to the decrease in Mediterranean forest in the area.

571 As discussed above, there seems to be a contradiction between regional proxies, showing increased
572 aridity, and local proxies showing increasing lake levels. This could be explained due to varied effect of
573 the orbital-scale decrease in summer insolation in both environments. A decrease in summer insolation
574 would trigger a decrease in the sea surface temperature reducing the wind system and precipitation from
575 sea to shore during winter (Marchal et al., 2002) and would also shorten the length of the growing season
576 thus provoking forest depletion. However, decreasing summer insolation would also reduce the seasonality
577 and would lower evapotranspiration during summer, affecting the evaporation/precipitation balance. This
578 along with the continuous groundwater supply in the Padul basin would explain the increasing lake levels
579 in the Padul wetland during the late Holocene (Fig. 6). Some authors also related this aridification trend to
580 the establishment of the current atmospheric dynamics with a northward shift of the westerlies -and as
581 consequence a long-term NAO-like positive mode- affecting the western Mediterranean region (Magny et
582 al., 2012). In addition, this climatic shift coincided with the end of the African Humid Period (5.5 ka-BP;
583 deMenocal et al., 2000). Shanahan et al. (2015) suggested that the decrease in rainfall at this time shown in

584 the African paleoclimate records (tropical and subtropical Africa) is related to declining summer insolation
585 and the gradual southward migration of the tropical monsoon.

586 A general decreasing trend in SST is recorded in the Alboran Sea since around 4-3 cal ka-kyr BP (Figs.
587 7 and 8; Cacho et al., 1999; Martrat et al., 2004; Rodrigo-Gámiz et al., 2014b), which supports our
588 hypothesis of a lower sea/land temperature contrast. However, the higher resolution study of Rodrigo-
589 Gámiz et al. (2014b) shows increasing SST superimposed between the generally decreasing trend,
590 coinciding with wetter periods such as for example the end of the Iberian-Roman Humid Period.

591 Within the context of regional progressive aridification, the late Holocene (*sensu lato*) from Padul could
592 mainly be divided into two phases, a first phase from ~ 4.7 to 3 cal ka-kyr BP characterized by the slight
593 increasing trend in *Botryococcus* and the declining trend in mid-chain abundance, and a second phase from
594 ~ 3 to 1.5 cal ka-kyr BP featured by maximum values in *Botryococcus* and a minimum in mid-chain
595 abundance (Fig. 6). Relative maxima in Mediterranean forest between ~ 2.6 and 1.6 cal ka-kyr BP,
596 indicating regional humidity, co-occurred with the maximum in *Botryococcus* algae also indicating either
597 high relative lake level and/or more productivity in the lake (Ramos-Román et al., 2018). High relative
598 humidity in this region is supported by the fact that this mild climatic event occurred during the well-known
599 Iberian Roman Humid Period (IRHP) between 2.6 to 1.6 cal ka-kyr BP (Martín-Puertas et al., 2009).

600 The aridification trend enhanced around ~ 1.5 cal ka-kyr BP and culminated with a further
601 environmental change to an ephemeral lake (even emerged during the last centuries). This is deduced by
602 the remarkable increase in detritic sedimentation (K/Si; Fig. 6), probably due to higher soil erosion (increase
603 in *Glomus* type) partially enhanced by human activities in the surroundings of the lake since this time
604 (Ramos-Román et al., 2018), and by a continuous increase in mid-chain, short-chain abundance and wetland
605 plants while *Botryococcus* and other aquatic organisms (especially charophytes) declined. Aquatic plants
606 probably expanded in the Padul wetland area when the water levels dropped. This increasing trend in mid-
607 chain and short-chain abundances started to decline during the last centuries when the wetland became
608 emerged and higher human impact occurred (for more information about human activities see Ramos-
609 Román et al., 2018).

610 The ~ 4.7 to Present natural aridification process was interrupted by millennial-scale climate variability
611 with several especially arid events occurring around ~ 4.7-4, 2.7 and 1.3 cal ~~ka~~-kyr BP (see next section;
612 4.1.4)

613 4.1.4. *Millennial-scale Holocene climate variability*

614 In addition to the long-term trends observed in the Padul paleoenvironments, likely driven by
615 insolation-related climate changes during the Holocene, the high-resolution multi-proxy record from Padul-
616 15-05 record shows millennial-scale vegetation, lake level and sedimentary oscillations that can be related
617 with global climate variability and cooling events detected in North Atlantic archives. In this respect, the
618 Padul-15-05 sequence shows arid-cooling climatic events around ~ 9.6, 8.5, 7.5, 6.5, 5.4, 4.7-4, 2.7 and 1.3
619 cal ~~ka~~-kyr BP, generally identified in both regional (decreases in the Mediterranean forest suggesting
620 regional cooling and aridity) and local proxies (increases in clays input, short-chain, mid-chain and
621 hygrophyte) and with periodicities of about 2100 and 1100 years. These short-scale climatic changes
622 affected sedimentation and local lake level in the Padul environment, generally with increases in carbonate
623 (charophytes and gastropods) and clastic sedimentation, hygrophytes, short-chain and mid-chain
624 abundances pointing to higher lake levels probably triggered by cooling and less evaporation in the wetland,
625 enhanced erosion due to deforestation and increase in plants adapted to more aquatic wetland environments
626 (Fig. 6). Some of these events are manifested in the Padul-15-05 record clearly in both regional and local
627 proxies (~ 9.6, 7.5, 5.4, 4.7-4, 2.7, 1.3 cal ~~ka~~-kyr BP) but some others are more evident in the local signal
628 (for example events at 8.5 and 6.5 cal ~~ka~~-kyr BP). The two latter ones probably indicating that those events
629 were less severe and/or problems recording them sufficiently well in the pollen. During the last ~ 4.7 cal
630 ~~ka~~-kyr BP, during the establishment of the modern climatic dynamics and the decrease in summer insolation,
631 a shallow lake formed and these cold events are also associated with declines in the lake productivity (for
632 example, reductions in algae before and after the IRHP; Fig. 6).

633 Most of these climatic events have been described in other Mediterranean paleoclimate records, considering
634 the radiocarbon age uncertainties between the different studies. For example, Jalut et al. (2000) also

635 described aridification phases for the western Mediterranean region around ~10.9-9.7, 8.4-7.6 and 5.3- 4.2,
636 4.3-3.4, 2.8-1.7 and 1.3-0.75 cal [ka-kyr BP](#), showing that [this-these](#) events were correlated with glacial
637 advances, ¹⁴C anomalies, North Atlantic records and paleohydrological changes in European mid-latitudes
638 suggesting that they were a regional response to global climate change. Some arid events around ~ 9.6-9.5,
639 8.4-8 and 6-5.5 [cal kyr BP](#), have been also identified as arid and cool events in a study from the eastern and
640 western Mediterranean region (Dormoy et al., 2009). Fletcher and Zielhofer (2013) detected this rapid
641 climate changes relating these arid periods with high-latitude cooling events around 6-5 and 3.5-2.5 cal [kyr](#)
642 [BPa-BP](#). Recently, Zielhofer et al. (2017) show a decrease in western Mediterranean winter rain at 11.4,
643 10.3, 9.2, 8.2, 7.2, 6.6, 6.0, 5.4, 5.0, 4.4, 3.5, 2.9, 2.2, 1.9, 1.7, 1.5, 1.0, 0.7, and 0.2 cal [kyra BP](#). They
644 associated these events during the early Holocene with Atlantic coolings probably related with meltwater
645 discharges and weakening of the Atlantic overturning circulation. In contrast, after ~ 5 cal [kyra BP](#), they
646 related these Atlantic cooling episodes to humid winters and negative NAO conditions evidencing a change
647 in the ocean-atmospheric system in response to the external forcing. In the nearby Sierra Nevada, arid
648 events are detected around 3.8-3.1 and 1.8-0.7 cal [kyra BP](#) (Laguna de la Mula; Jiménez-Moreno et al.,
649 2013). Cold and arid events detected in the Padul-15-05 record at ~ 9.6, 8.5, 7.5, 6.5, 5.4, 4.7-4, 2.7 and 1.3
650 cal [kyra BP](#) have been also identified in North Atlantic records (Bond events 6, 5, 4, 3, 2, 1; Bond et al.,
651 2001; Fig. 8), which indicate that these events were recorded at hemispheric scales. The good
652 correspondence with the timing of these cold events with decreases in solar activity recorded by the TSI
653 anomaly during the Holocene could show a link between them (Steinhilber et al., 2009; Fig. 8). The
654 correlation between the Mediterranean forest from Padul and TSI anomaly ($r = 0.43$; $p < 0.001$ between ~
655 9.4 to 4.7 cal [ka-kyr BP](#) and $r = 0.37$; $p < 0.001$ between 4.7 cal [ka-kyr BP](#) to present) seems to show that a
656 link exists between solar and environmental variability in the Mediterranean area. This would agree with
657 previous studies showing a sun-climate-environment relationship (Zielhofer et al., 2017). However, we are
658 still far to understanding how solar activity affects climate and deeper studies are necessary in order to
659 provide with information about the behavior between solar, climate and environmental relationships and
660 the link between the Mediterranean and North Atlantic regions.

661 4.1.5. *Forcing mechanisms of Holocene millennial-scale climate variability in the western Mediterranean*
662 *region*

663 The time series analysis done on the Mediterranean forest (regional proxy) from the Padul-15-05 record
664 using wavelet analysis ~~evidence~~ shows millennial-scale cyclical periodicities during the early, middle and
665 late Holocene. This analysis helps to understand the relationship between the regional paleoenvironmental
666 periodicity in the proxy data from the Padul record and external (i.e. solar activity) and internal (oceanic-
667 atmospheric dynamics) forcings during the Holocene in the western Mediterranean. Cyclicities of around
668 ~ 2100 yr and ~ 1100 yr are detected in the Mediterranean forest taxa time series with a statistically strong
669 cyclical pattern during the early and middle Holocene (the ~ 1100 yr cycle is absent in the late Holocene),
670 and a predominant ~ 1430 yr cycle between the transition of the middle-late Holocene and during the late
671 Holocene (Supplementary Fig. S7). This later cycle ~~should be carefully taken linked to carefully as~~ human
672 impact, ~~who-which~~ could have altered the natural climatic signal, ~~and is evident-recorded~~ in this area since
673 the last ~ 1500 yr (Ramos-Román et al., 2018).

674 Our results are consistent with similar cyclical patterns detected throughout the North Atlantic records
675 and related with solar activity also describing ~ 2500 and 1000 yr periodicities during the early Holocene
676 (Debret et al., 2007; 2009). A similar periodicity of about 2300 yr is recognized in the $\Delta^{14}\text{C}$ residual series
677 from the Greenland Ice Sheet record (Mayewski et al., 1997). This periodicity has also been evidenced in
678 sea surface temperatures (SST) reconstructions in the Aegean Sea in the NE Mediterranean related with
679 glacier advance and suggesting a solar modulation (Rohling et al., 2002). The ~ 1000 yr periodicity is also
680 established as a signal of solar activity in many other records in the Mediterranean and the North Atlantic
681 region (e.g. Debret; 2007; 2009 and references therein). Previous cyclostratigraphic analysis performed in
682 the nearby Sierra Nevada alpine area also described cyclical climatic fluctuations with periodicities around
683 2200 yr (Jiménez-Espejo et al., 2014). In contrast, other spectral analyses carried out in other records in the
684 North Atlantic and western Mediterranean region detected a periodicity of around ~ 1500 yr (e.g. Bond et
685 al., 2001; Rodrigo-Gámiz et al., 2014a). This ~ 1500 yr cycle is also common in other Sierra Nevada records

686 (Jiménez-Espejo et al., 2014; García-Alix et al., 2017) and was interpreted as a solar and atmospheric-
687 oceanic forcing mechanism. In addition, a cycle of ~ 800-760 yr has also been detected in the detailed
688 studied of the late Holocene part of the Padul-15-05 record (Ramos-Román et al., 2018) and in other records
689 in the Sierra Nevada (Ramos-Román et al., 2016). This cycle could be related to the second harmonic of
690 the ~ 1600-1500 yr cycle. These results show very mixed interpretations with both solar and/or oceanic
691 forcing mechanisms being described to explain cyclicities in the different proxies. Debret et al. (2009) in a
692 non-stationary time series analysis ~~tried~~s to differentiate the different forcing mechanisms for the different
693 cyclicities and also described an intensification of the ~ 1600 yr period detected in the North Atlantic area
694 (terrestrial and marine records and interpreted of both solar and oceanic origin) in the last ~~5 cal ka BP~~[5000](#)
695 [years](#). Those authors then interpret this cyclical periodicity change as a shift in dynamics from mostly
696 external (solar) forcing to mostly internal (oceanic) forcing.

697 According to this, the ~~Holocene~~ results from the Padul-15-05 Holocene record suggest that the regional
698 climate variability during the early and middle Holocene was partially due to external forcing (i.e. solar
699 irradiance) and variability during the late Holocene (since ~ 4.7 cal ~~ka~~[kyr](#) BP) was dominated by the effect
700 of internal forcing (atmospheric-oceanic dynamic) -established since the NAO system influencing the
701 western Mediterranean region- enhanced since ~ 5 cal ~~ka~~[kyr](#) BP (Debret et al., 2007; 2009). Fletcher et al.
702 (2013) described a shift in the millennial-scale periodicity since around ~ 6 cal ~~ka~~[kyr](#) BP related with the
703 establishment of the actual climate system in the western Mediterranean region. The similarities between
704 the millennial-scale oscillations observed in the Padul-15-05 record with the total solar irradiance anomaly
705 (TSI) and cooling events in the North Atlantic region (e.g. Bond et al., 2001; Steinhilber et al., 2009; Fig.
706 8) support the solar-atmospheric-oceanic link in the Atlantic-western Mediterranean region previously
707 suggested (Debret et al., 2009).

708 5. Conclusions

709 Variations in regional and local paleoenvironmental and paleoclimate proxies from the Padul-15-05
710 ~~core~~[Holocene record](#) helped ~~us~~ to interpret climate and paleoenvironmental change during the last 11, ~~600~~[600](#)

711 ~~years-cal ka BP~~ in southern Iberia and the western Mediterranean region. The comparison of our record
712 with other regional and global oceanic-atmospheric-terrestrial studies aided to comprehend the origin of
713 these paleoenvironmental changes.

714 The early and middle Holocene was characterized by overall humid and warm conditions and a
715 humidity optimum between ~ 9.5 and 7.6 cal kyr BP, humid winters and very hot and dry summers and a
716 higher seasonality, occurred in this area due to summer insolation maxima. These interpretations come from
717 the highest occurrence of deciduous tree species and humid conditions in the local environment (higher
718 mid-chain abundance) in the Padul-15-05 core. Summer insolation maxima translated into very high
719 evaporation rates and lowest lake level conditions triggering the abundance of wetland plants and the
720 deposition of peat related with the higher TOC. A transition phase towards drier conditions is recorded in
721 the middle Holocene between ~ 7.6 and 4.7 cal ka-kyr BP through a decrease in deciduous forest and a
722 higher water level variability mainly associated with variations in Ca, S, K/Si ratio and TOC content. This
723 environmental change was probably due to a reduction in seasonality and decreasing summer insolation,
724 which also locally triggered less evaporation and the alternation of water level increase within a peatland
725 environment. This climate transition culminated in the Padul area with a significant environmental change
726 at ~ 4.7 cal ka-kyr BP, featured by a regional aridification trend that produced a decreasing trend in the
727 Mediterranean forest. Precipitation decreased in the late Holocene but the decrease in summer insolation
728 locally triggered less evaporation and the development of a shallow water lake environment and a
729 significant sedimentary change characterized by higher values of Ca an increasing trend in clay minerals
730 (K/Si ratio), and the decrease in TOC. The Padul shallow lake environment became ephemeral since ~ 1.5
731 cal kyr BP and even emerged during the last centuries probably induced by human impact.

732 The Padul-15-05 record also shows millennial-scale climate variability with declines in Mediterranean
733 forest showing cool-arid events and variability in the lake level around 9.6, 8.5, 7.5, 6.5, 5.4, 4.7-4, 3, 2.7
734 and 1.3 cal ka-kyr BP, associated with cold events in the North Atlantic records. According to the regional
735 (Mediterranean forest taxa) paleoclimate results from the non-stationary time-series analyses, climate
736 during the early and middle Holocene could have been influenced by external solar forcing with typical

737 periodicities around 1100 and 2100 yrs, and the last ~ ~~4.7 cal ka BP~~ 4700 years could have been associated
738 ~~by~~ with an internal oceanic/atmospheric control (also in part related with solar forcing) as periodicities
739 changed towards ~ 1430 yr in the regional paleoclimate proxy. However, this later periodicity has to be
740 taken carefully as human impact is evident in the area during the last 1500 yr, probably altering somehow
741 the climatic record.

742 We would like to ~~remark~~ emphasise on the importance of carrying out multi-proxy analyses containing
743 both regional and local signals and a non-stationary time-series analysis in order to clarify the links between
744 terrestrial-oceanic-atmospheric connections in Holocene paleoclimatic studies.

745 **Acknowledgments**^[FM3]

746 This work was supported by the project P11-RNM-7332 funded by Consejería de Economía,
747 Innovación, Ciencia y Empleo de la Junta de Andalucía, the project CGL2013-47038-R funded by
748 Ministerio de Economía y Competitividad of Spain and fondo Europeo de desarrollo regional FEDER and
749 the research group RNM0190 (Junta de Andalucía). M. J. R.-R. acknowledges the predoctoral and
750 postdoctoral funding provided by Consejería de Economía, Innovación, Ciencia y Empleo de la Junta de
751 Andalucía (P11-RNM-7332). J.C. acknowledges the PhD funding provided by Ministerio de Economía y
752 Competitividad (CGL2013-47038-R). J.S.C. acknowledges the support of projects CGL-BOS-2012-34717,
753 CGL-BOS 2015-68604, and Fundación Séneca 19434/PI/14. A.G.-A. was also supported by a Ramón y
754 Cajal Fellowship RYC-2015-18966 of the Spanish Government (Ministerio de Economía y Competitividad).
755 Javier Jaimez (CIC-UGR) is thanked for graciously helping with the coring, the drilling equipment and
756 logistics. We would also like to thank to two anonymous reviewers and the editor (Fabienne Marret-Davies)
757 for their valuable suggestions.

- 759 Alpert, P., Baldi, M., Ilani, R., Krichak, S., Price, C., Rodó, X., Saaroni, H., Ziv, B., Kishcha, P., Barkan, J., Mariotti,
760 A., Xoplaki, E., 2006. Chapter 2 Relations between climate variability in the Mediterranean region and the
761 tropics: ENSO, South Asian and African monsoons, hurricanes and Saharan dust. *Developments in Earth and*
762 *Environmental Sciences* 4, 149–177. doi:10.1016/S1571-9197(06)80005-4
- 763 Anderson, R.S., Jiménez-Moreno, G., Carrión, J.S., Pérez-Martínez, C., 2011. Postglacial history of alpine vegetation,
764 fire, and climate from Laguna de Río Seco, Sierra Nevada, southern Spain. *Quaternary Science Reviews* 30,
765 1615–1629. doi:https://doi.org/10.1016/j.quascirev.2011.03.005
- 766 Arz, H.W., Lamy, F., Pätzold, J., Müller, P.J., Prins, M., 2003. Mediterranean Moisture Source for an Early-Holocene
767 Humid Period in the Northern Red Sea. *Science* 300, 118. doi:10.1126/science.1080325
- 768 Bar-Matthews, M., Ayalon, A., Gilmour, M., Matthews, A., Hawkesworth, C.J., 2003. Sea–land oxygen isotopic
769 relationships from planktonic foraminifera and speleothems in the Eastern Mediterranean region and their
770 implication for paleorainfall during interglacial intervals. *Geochimica et Cosmochimica Acta* 67, 3181–3199.
771 doi:https://doi.org/10.1016/S0016-7037(02)01031-1
- 772 Beug, H.-J.: Leitfaden der Pollenbestimmung für Mitteleuropa und angrenzende Gebiete, Fisch. Stuttg., Leitfaden der
773 Pollenbestimmung für Mitteleuropa und angrenzende Gebiete, Friedrich Pfeil, München, 61, 2004.
- 774 Bond, G., Kromer, B., Beer, J., Muscheler, R., Evans, M.N., Showers, W., Hoffmann, S., Lotti-Bond, R., Hajdas, I.,
775 Bonani, G., 2001. Persistent Solar Influence on North Atlantic Climate During the Holocene. *Science* 294,
776 2130. doi:10.1126/science.1065680
- 777 Cacho, I., Grimalt, J.O., Pelejero, C., Canals, M., Sierro, F.J., Flores, J.A., Shackleton, N., 1999. Dansgaard-Oeschger
778 and Heinrich event imprints in Alboran Sea paleotemperatures. *Paleoceanography* 14, 698–705.
779 doi:10.1029/1999PA900044
- 780 Cacho, I., Grimalt, J.O., Canals, M., Sbaiffi, L., Shackleton, N.J., Schönfeld, J., Zahn, R., 2001. Variability of the
781 western Mediterranean Sea surface temperature during the last 25,000 years and its connection with the
782 Northern Hemisphere climatic changes. *Paleoceanography* 16, 40–52. doi:10.1029/2000PA000502
- 783 Carrión, J.S., 2002. Patterns and processes of Late Quaternary environmental change in a montane region of
784 southwestern Europe. *Quaternary Science Reviews* 21, 2047–2066. doi:https://doi.org/10.1016/S0277-
785 3791(02)00010-0
- 786 Carrión, J.S., Fernández, S., González-Sampériz, P., Gil-Romera, G., Badal, E., Carrión-Marco, Y., López-Merino,
787 L., López-Sáez, J.A., Fierro, E., Burjachs, F., 2010b. Expected trends and surprises in the Lateglacial and
788 Holocene vegetation history of the Iberian Peninsula and Balearic Islands. *Review of Palaeobotany and*
789 *Palynology* 162, 458–475. doi:http://dx.doi.org/10.1016/j.revpalbo.2009.12.007
- 790 Carrión, J.S., Munuera, M., Navarro, C., Burjachs, F., Dupré, M., Walker, M.J., 1999. The palaeoecological potential
791 of pollen records in caves: the case of Mediterranean Spain. *Quaternary Science Reviews* 18, 1061–1073.
792 doi:10.1016/S0277-3791(98)00002-X
- 793 Carrión, J.S., Sánchez-Gómez, P., Mota, J.F., Yll, R., Chaín, C., 2003. Holocene vegetation dynamics, fire and grazing
794 in the Sierra de Gádor, southern Spain. *The Holocene* 13, 839–849. doi:10.1191/0959683603hl662rp
- 795 Carrión, J.S., Fuentes, N., González-Sampériz, P., Quirante, L.S., Finlayson, J.C., Fernández, S., Andrade, A., 2007.
796 Holocene environmental change in a montane region of southern Europe with a long history of human
797 settlement. *Quaternary Science Reviews* 26, 1455–1475. doi:https://doi.org/10.1016/j.quascirev.2007.03.013
- 798 Castillo Martín, A., Benavente Herrera, J., Fernández Rubio, R., Pulido Bosch, A., 1984. Evolución y ámbito
799 hidrogeológico de la laguna de Padul (Granada). *Las Zonas Húmedas en Andalucía; Monografías de DGMA-*
800 *MOPU*.
- 801 Chapman, S.J., 2001. Sulphur Forms in Open and Afforested Areas of Two Scottish Peatlands. *Water, Air, and Soil*
802 *Pollution* 128, 23–39. doi:10.1023/A:1010365924019
- 803 Cheddadi, R., Yu, G., Guiot, J., Harrison, S.P., Prentice, I.C., 1997. The climate of Europe 6000 years ago. *Climate*
804 *Dynamics* 13, 1–9. doi:10.1007/s003820050148
- 805 Clausen, A., 1999. Palaeoenvironmental significance of the green alga *Botryococcus* in the lacustrine rotliedend
806 (upper carboniferous - lower permian). *Historical Biology* 13, 221–234. doi:10.1080/08912969909386582
- 807 Combourieu-Nebout, N., Peyron, O., Dormoy, I., Desprat, S., Beaudouin, C., Kotthoff, U., Marret, F., 2009. Rapid
808 climatic variability in the west Mediterranean during the last 25 000 years from high resolution pollen data.
809 *Clim. Past* 5, 503–521. doi:10.5194/cp-5-503-2009
- 810 Cranwell, P., Eglinton, G., Robinson, N., 1987. Lipids of aquatic organisms as potential contributors to lacustrine
811 sediments—II. *Organic Geochemistry* 11, 513–527.

- 812 Cranwell, P.A., 1984. Lipid geochemistry of sediments from Upton Broad, a small productive lake. *Organic*
813 *Geochemistry* 7, 25–37. doi:10.1016/0146-6380(84)90134-7
- 814 Davis, J.C., Sampson, R.J., 1986. *Statistics and data analysis in geology*. Wiley New York.
- 815 Debret, M., Bout-Roumazeilles, V., Grousset, F., Desmet, M., McManus, J.F., Massei, N., Sebag, D., Petit, J.-R.,
816 Copard, Y., Trentesaux, A., 2007. The origin of the 1500-year climate cycles in Holocene North-Atlantic
817 records. *Clim. Past* 3, 569–575. doi:10.5194/cp-3-569-2007
- 818 Debret, M., Sebag, D., Crosta, X., Massei, N., Petit, J.-R., Chapron, E., Bout-Roumazeilles, V., 2009. Evidence from
819 wavelet analysis for a mid-Holocene transition in global climate forcing. *Quaternary Science Reviews* 28,
820 2675–2688. doi:https://doi.org/10.1016/j.quascirev.2009.06.005
- 821 deMenocal, P., Ortiz, J., Guilderson, T., Sarnthein, M., 2000. Coherent High- and Low-Latitude Climate Variability
822 During the Holocene Warm Period. *Science* 288, 2198–2202. doi:10.1126/science.288.5474.2198
- 823 Dormoy, I., Peyron, O., Combourieu Nebout, N., Goring, S., Kotthoff, U., Magny, M., Pross, J., 2009. Terrestrial
824 climate variability and seasonality changes in the Mediterranean region between 15 000 and 4000 years BP
825 deduced from marine pollen records. *Clim. Past* 5, 615–632. doi:10.5194/cp-5-615-2009
- 826 El Aallali, A., Nieto, J. M. L., Raya, F. A. P., and Mesa, J. M.: Estudio de la vegetación forestal en la vertiente sur de
827 Sierra Nevada (Alpujarra Alta granadina), *Itinera Geobot.*, 11, 387–402, 1998.
- 828 Faegri, K., Iversen, J., 1989. *Textbook of Pollen Analysis*. Wiley, New York.
- 829 Feijtel, T.C., Salingar, Y., Hordijk, C.A., Sweerts, J.P.R.A., Van Breemen, N., Cappenberg, T.E., 1989. Sulfur cycling
830 in a dutch moorland pool under elevated atmospheric S-deposition. *Water, Air, and Soil Pollution* 44, 215–
831 234. doi:10.1007/BF00279256
- 832 Fernández, S., Fuentes, N., Carrión, J.S., González-Sampériz, P., Montoya, E., Gil, G., Vega-Toscano, G., Riquelme,
833 J.A., 2007. The Holocene and Upper Pleistocene pollen sequence of Carihuela Cave, southern Spain. *Geobios*
834 40, 75–90. doi:10.1016/j.geobios.2006.01.004
- 835 Ficken, K.J., Li, B., Swain, D., Eglinton, G., 2000. An n-alkane proxy for the sedimentary input of submerged/floating
836 freshwater aquatic macrophytes. *Organic geochemistry* 31, 745–749.
- 837 Fletcher, W.J., Sánchez-Goñi, M.F., 2008. Orbital- and sub-orbital-scale climate impacts on vegetation of the western
838 Mediterranean basin over the last 48,000 yr. *Quaternary Research* 70, 451–464.
839 doi:10.1016/j.yqres.2008.07.002
- 840 Fletcher, W.J., Zielhofer, C., 2013. Fragility of Western Mediterranean landscapes during Holocene Rapid Climate
841 Changes. Long-term degradation of fragile landscape systems 103, 16–29. doi:10.1016/j.catena.2011.05.001
- 842 Fletcher, W.J., Debret, M., Goñi, M.F.S., 2013. Mid-Holocene emergence of a low-frequency millennial oscillation
843 in western Mediterranean climate: Implications for past dynamics of the North Atlantic atmospheric
844 westerlies. *The Holocene* 23, 153–166. doi:10.1177/0959683612460783
- 845 Florschütz, F., Amor, J.M., Wijmstra, T.A., 1971. Palynology of a thick quaternary succession in southern Spain.
846 *Palaeogeography, Palaeoclimatology, Palaeoecology* 10, 233–264. doi:http://dx.doi.org/10.1016/0031-
847 0182(71)90049-6
- 848 García-Alix, A., Delgado Huertas, A., Martín Suárez, E., 2012. Unravelling the Late Pleistocene habitat of the
849 southernmost woolly mammoths in Europe. *Quaternary Science Reviews* 32, 75–85.
850 doi:10.1016/j.quascirev.2011.11.007
- 851 García-Alix, A., Jiménez-Espejo, F.J., Toney, J.L., Jiménez-Moreno, G., Ramos-Román, M.J., Anderson, R.S.,
852 Ruano, P., Queralt, I., Delgado Huertas, A., Kuroda, J., 2017. Alpine bogs of southern Spain show human-
853 induced environmental change superimposed on long-term natural variations. *Scientific Reports* 7, 7439.
854 doi:10.1038/s41598-017-07854-w
- 855 Gasse, F., Roberts, C.N., 2004. Late Quaternary Hydrologic Changes in the Arid and Semiarid Belt of Northern Africa.
856 In: Diaz, H.F., Bradley, R.S. (Eds.), *The Hadley Circulation: Present, Past and Future*. Springer Netherlands,
857 Dordrecht, pp. 313–345. doi:10.1007/978-1-4020-2944-8_12
- 858 Geel, B. van, Hallewas, D.P., Pals, J.P., 1983. A late holocene deposit under the Westfriese Zeedijk near Enkhuizen
859 (Prov. of Noord-Holland, The Netherlands): Palaeoecological and archaeological aspects. *Review of*
860 *Palaeobotany and Palynology* 38, 269–335. doi:http://dx.doi.org/10.1016/0034-6667(83)90026-X
- 861 Gelpi, E., Schneider, H., Mann, J., Oró, J., 1970. Hydrocarbons of geochemical significance in microscopic algae.
862 *Phytochemistry* 9, 603–612. doi:10.1016/S0031-9422(00)85700-3
- 863 Grimm, E.C., 1987. CONISS: a Fortran 77 program for stratigraphically constrained cluster analysis by the method
864 of incremental sum of squares. *Comput. Geosci.* 13, 13-35
- 865 Guy-Ohlson, D., 1992. Botryococcus as an aid in the interpretation of palaeoenvironment and depositional processes.
866 *Review of Palaeobotany and Palynology* 71, 1–15. doi:http://dx.doi.org/10.1016/0034-6667(92)90155-A

- 867 Hammer, O., Harper, D.A.T., Ryan, P.D., 2001. PAST: paleontological statistics software package for education and
868 data analysis. *Palaeontologia Electronica* 4 (1), 9.
- 869 Hudon, C., 2004. Shift in wetland plant composition and biomass following low-level episodes in the St. Lawrence
870 River: looking into the future. *Canadian Journal of Fisheries and Aquatic Sciences* 61, 603–617.
871 doi:10.1139/f04-031
- 872 Huntley, B., Prentice, I.C., 1988. July Temperatures in Europe from Pollen Data, 6000 Years Before Present. *Science*
873 241, 687–690. doi:10.1126/science.241.4866.687
- 874 Hurrell, J.W., 1995. Decadal Trends in the North Atlantic Oscillation: Regional Temperatures and Precipitation.
875 *Science* 269, 676. doi:10.1126/science.269.5224.676
- 876 Jalut, G., Esteban Amat, A., Bonnet, L., Gauquelin, T., Fontugne, M., 2000. Holocene climatic changes in the Western
877 Mediterranean, from south-east France to south-east Spain. *Palaeogeography, Palaeoclimatology, Palaeoecology* 160,
878 255–290. doi:10.1016/S0031-0182(00)00075-4
- 879 Jalut, G., Dedoubat, J.J., Fontugne, M., Otto, T., 2009. Holocene circum-Mediterranean vegetation changes: Climate
880 forcing and human impact. *Quaternary International* 200, 4–18.
881 doi:https://doi.org/10.1016/j.quaint.2008.03.012
- 882 Jimenez-Espejo, F.J., Martinez-Ruiz, F., Rogerson, M., González-Donoso, J.M., Romero, O.E., Linares, D.,
883 Sakamoto, T., Gallego-Torres, D., Rueda Ruiz, J.L., Ortega-Huertas, M., Perez Claros, J.A., 2008. Detrital
884 input, productivity fluctuations, and water mass circulation in the westernmost Mediterranean Sea since the
885 Last Glacial Maximum. *Geochemistry, Geophysics, Geosystems* 9, n/a-n/a. doi:10.1029/2008GC002096
- 886 Jiménez-Espejo, F.J., García-Alix, A., Jiménez-Moreno, G., Rodrigo-Gámiz, M., Anderson, R.S., Rodríguez-Tovar,
887 F.J., Martínez-Ruiz, F., Giral, S., Delgado Huertas, A., Pardo-Igúzquiza, E., 2014. Saharan aeolian input and
888 effective humidity variations over western Europe during the Holocene from a high altitude record. *Chemical*
889 *Geology* 374–375, 1–12. doi:10.1016/j.chemgeo.2014.03.001
- 890 Jiménez-Moreno, G., Anderson, R.S., 2012. Holocene vegetation and climate change recorded in alpine bog sediments
891 from the Borreguiles de la Virgen, Sierra Nevada, southern Spain. *Quaternary Research* 77, 44–53.
892 doi:https://doi.org/10.1016/j.yqres.2011.09.006
- 893 Jiménez-Moreno, G., García-Alix, A., Hernández-Corbalán, M.D., Anderson, R.S., Delgado-Huertas, A., 2013.
894 Vegetation, fire, climate and human disturbance history in the southwestern Mediterranean area during the
895 late Holocene. *Quat. Res.* 79, 110–122. https://doi.org/10.1016/j.yqres.2012.11.008
- 896 Johnsen, S.J., Clausen, H.B., Dansgaard, W., Fuhrer, K., Gundestrup, N., Hammer, C.U., Iversen, P., Jouzel, J.,
897 Stauffer, B., Steffensen, J.P., 1992. Irregular glacial interstadials recorded in a new Greenland ice core. *Nature*
898 359, 311–313. doi:10.1038/359311a0
- 899 Kalugin, I., Daryin, A., Smolyaninova, L., Andreev, A., Diekmann, B., Khlystov, O., 2007. 800-yr-long records of
900 annual air temperature and precipitation over southern Siberia inferred from Teletskoye Lake sediments.
901 *Quaternary Research* 67, 400–410. doi:https://doi.org/10.1016/j.yqres.2007.01.007
- 902 Kaushal, S., Binford, M.W., 1999. Relationship between C:N ratios of lake sediments, organic matter sources, and
903 historical deforestation in Lake Pleasant, Massachusetts, USA. *Journal of Paleolimnology* 22, 439–442.
904 doi:10.1023/A:1008027028029
- 905 Lamb, H.F., Kaars, S. van der, 1995. Vegetational response to Holocene climatic change: pollen and
906 palaeolimnological data from the Middle Atlas, Morocco. *The Holocene* 5, 400–408.
907 doi:10.1177/095968369500500402
- 908 Laskar, J., Robutel, P., Joutel, F., Gastineau, M., Correia, A.C.M., Levrard, B., 2004. A long-term numerical solution
909 for the insolation quantities of the Earth, *Astron. Astrophys.*, 428, 261–285. doi:10.1051/0004-
910 6361:20041335
- 911 Lionello, P., Malanotte-Rizzoli, P., Boscolo, R., 2006. *Mediterranean climate variability*. Elsevier.
- 912 Magny, M., Beaulieu, J.-L. de, Drescher-Schneider, R., Vannière, B., Walter-Simonnet, A.-V., Miras, Y., Millet, L.,
913 Bossuet, G., Peyron, O., Brugiapaglia, E., Leroux, A., 2007. Holocene climate changes in the central
914 Mediterranean as recorded by lake-level fluctuations at Lake Accesa (Tuscany, Italy). *Quaternary Science*
915 *Reviews* 26, 1736–1758. doi:http://dx.doi.org/10.1016/j.quascirev.2007.04.014
- 916 Magny, M., Peyron, O., Sadori, L., Ortu, E., Zanchetta, G., Vannière, B., Tinner, W., 2012. Contrasting patterns of
917 precipitation seasonality during the Holocene in the south- and north-central Mediterranean. *Journal of*
918 *Quaternary Science* 27, 290–296. doi:10.1002/jqs.1543
- 919 Marchal, O., Cacho, I., Stocker, T.F., Grimalt, J.O., Calvo, E., Martrat, B., Shackleton, N., Vautravers, M., Cortijo,
920 E., Van Kreveld, S., Andersson, C., Koç, N., Chapman, M., Saffi, L., Duplessy, J.-C., Sarnthein, M., Turon,
921 J.-L., Duprat, J., Jansen, E., 2002. Apparent long-term cooling of the sea surface in the northeast Atlantic and

922 Mediterranean during the Holocene. *Quaternary Science Reviews* 21, 455–483. doi:10.1016/S0277-
923 3791(01)00105-6

924 Martín-Puertas, C., Valero-Garcés, B.L., Mata, M.P., González-Sampériz, P., Bao, R., Moreno, A., Stefanova, V.,
925 2008. Arid and humid phases in southern Spain during the last 4000 years: the Zoñar Lake record, Córdoba.
926 *The Holocene* 18, 907–921. doi:10.1177/0959683608093533

927 Martín-Puertas, C., Valero-Garcés, B.L., Brauer, A., Mata, M.P., Delgado-Huertas, A., Dulski, P., 2009. The Iberian-
928 Roman Humid Period (2600-1600 cal yr BP) in the Zoñar Lake varve record (Andalucía, southern Spain).
929 *Quaternary Research* 71, 108–120. doi:10.1016/j.yqres.2008.10.004

930 Martrat, B., Grimalt, J.O., López-Martínez, C., Cacho, I., Sierro, F.J., Flores, J.A., Zahn, R., Canals, M., Curtis, J. H.,
931 Hodell, D. A., 2004. Abrupt Temperature Changes in the Western Mediterranean over the Past 250000 years.
932 *Science* 306, 1762. <https://doi.org/10.1126%2Fscience.1101706>

933 Mayewski, P.A., Meeker, L.D., Twickler, M.S., Whitlow, S., Yang, Q., Lyons, W.B., Prentice, M., 1997. Major
934 features and forcing of high-latitude northern hemisphere atmospheric circulation using a 110,000-year-long
935 glaciochemical series. *Journal of Geophysical Research: Oceans* 102, 26345–26366. doi:10.1029/96JC03365

936 Mayewski, P.A., Rohling, E.E., Stager, J.C., Karlén, W., Maasch, K.A., Meeker, L.D., Meyerson, E.A., Gasse, F.,
937 Kreveld, S. van, Holmgren, K., Lee-Thorp, J., Rosqvist, G., Rack, F., Staubwasser, M., Schneider, R.R.,
938 Steig, E.J., 2004. Holocene climate variability. *Quaternary Research* 62, 243–255.
939 doi:<https://doi.org/10.1016/j.yqres.2004.07.001>

940 Meijer, P.T., Tuenter, E., 2007. The effect of precession-induced changes in the Mediterranean freshwater budget on
941 circulation at shallow and intermediate depth. *Journal of Marine Systems* 68, 349–365.
942 doi:10.1016/j.jmarsys.2007.01.006

943 Meyers, P.A., 1994. Preservation of elemental and isotopic source identification of sedimentary organic matter.
944 *Chemical Geology* 114, 289–302. doi:10.1016/0009-2541(94)90059-0

945 Meyers, P.A., Lallier-Vergés, E., 1999. Lacustrine Sedimentary Organic Matter Records of Late Quaternary
946 Paleoclimates. *Journal of Paleolimnology* 21, 345–372. doi:10.1023/A:1008073732192

947 Moreno, A., Cacho, I., Canals, M., Grimalt, J.O., Sánchez-Goñi, M.F., Shackleton, N., Sierro, F.J., 2005. Links
948 between marine and atmospheric processes oscillating on a millennial time-scale. A multi-proxy study of the
949 last 50,000 yr from the Alboran Sea (Western Mediterranean Sea). *Quaternary Science Reviews* 24, 1623–
950 1636. doi:<https://doi.org/10.1016/j.quascirev.2004.06.018>

951 Moreno, A., López-Merino, L., Leira, M., Marco-Barba, J., González-Sampériz, P., Valero-Garcés, B.L., López-Sáez,
952 J.A., Santos, L., Mata, P., Ito, E., 2011. Revealing the last 13,500 years of environmental history from the
953 multiproxy record of a mountain lake (Lago Enol, northern Iberian Peninsula). *Journal of Paleolimnology*
954 46, 327–349. doi:10.1007/s10933-009-9387-7

955 Moro, M.J., Domingo, F., López, G., 2004. Seasonal transpiration pattern of *Phragmites australis* in a wetland of semi-
956 arid Spain. *Hydrological Processes* 18, 213–227. doi:10.1002/hyp.1371

957 Ogura, K., Machihara, T., Takada, H., 1990. Diagenesis of biomarkers in Biwa Lake sediments over 1 million years.
958 *Organic Geochemistry* 16, 805–813.

959 Ortiz, J.E., Torres, T., Delgado, A., Julià, R., Lucini, M., Llamas, F.J., Reyes, E., Soler, V., Valle, M., 2004. The
960 palaeoenvironmental and palaeohydrological evolution of Padul Peat Bog (Granada, Spain) over one million
961 years, from elemental, isotopic and molecular organic geochemical proxies. *Organic Geochemistry* 35, 1243–
962 1260. doi:<https://doi.org/10.1016/j.orggeochem.2004.05.013>

963 Ortiz, J.E., Torres, T., Delgado, A., Llamas, J.F., Soler, V., Valle, M., Julià, R., Moreno, L., Díaz-Bautista, A., 2010.
964 Palaeoenvironmental changes in the Padul Basin (Granada, Spain) over the last 1Ma based on the biomarker
965 content. *Palaeogeography, Palaeoclimatology, Palaeoecology* 298, 286–299.
966 doi:10.1016/j.palaeo.2010.10.003

967 Pérez Raya, F., López Nieto, J., 1991. Vegetación acuática y helofítica de la depresión de Padul (Granada). *Acta Bot.*
968 *Malacitana* 16, 373–389.

969 Peyron, O., Magny, M., Goring, S., Joannin, S., Beaulieu, J.-L. de, Brugiapaglia, E., Sadori, L., Garfi, G., Kouli, K.,
970 Ioakim, C., Combourieu-Nebout, N., 2013. Contrasting patterns of climatic changes during the Holocene
971 across the Italian Peninsula reconstructed from pollen data. *Clim. Past* 9, 1233–1252. doi:10.5194/cp-9-1233-
972 2013

973 Pons, A., Reille, M., 1988. The holocene- and upper pleistocene pollen record from Padul (Granada, Spain): A new
974 study. *Palaeogeography, Palaeoclimatology, Palaeoecology* 66, 243–263.
975 doi:[http://dx.doi.org/10.1016/0031-0182\(88\)90202-7](http://dx.doi.org/10.1016/0031-0182(88)90202-7)

976 Ramos-Román, M.J., Jiménez-Moreno, G., Anderson, R.S., García-Alix, A., Toney, J.L., Jiménez-Espejo, F.J.,
977 Carrión, J.S., 2016. Centennial-scale vegetation and North Atlantic Oscillation changes during the Late

978 Holocene in the southern Iberia. *Quaternary Science Reviews* 143, 84–95.
979 doi:<https://doi.org/10.1016/j.quascirev.2016.05.007>

980 Ramos-Román, M.J., Jiménez-Moreno, G., Camuera, J., García-Alix, A., Anderson, R.S., Jiménez-Espejo, F.J.,
981 Carrión, J.S., 2018. Holocene climate aridification trend and human impact interrupted by millennial- and
982 centennial-scale climate fluctuations from a new sedimentary record from Padul (Sierra Nevada, southern
983 Iberian Peninsula). *Clim. Past.*, 14 (1), 117–137. <https://doi.org/10.5194/cp-14-117-2018>

984 Reed, J.M., Stevenson, A.C., Juggins, S., 2001. A multi-proxy record of Holocene climatic change in southwestern
985 Spain: the Laguna de Medina, Cádiz. *The Holocene* 11, 707–719. doi:10.1191/09596830195735

986 Reimer, P.J., Bard, E., Bayliss, A., Beck, J.W., Blackwell, P.G., Ramsey, C.B., Buck, C.E., Cheng, H., Edwards, R.L.,
987 Friedrich, M., Grootes, P.M., Guilderson, T.P., Haflidason, H., Hajdas, I., Hatté, C., Heaton, T.J., Hoffmann,
988 D.L., Hogg, A.G., Hughen, K.A., Kaiser, K.F., Kromer, B., Manning, S.W., Niu, M., Reimer, R.W., Richards,
989 D.A., Scott, E.M., Southon, J.R., Staff, R.A., Turney, C.S.M., Plicht, J. van der, 2013. IntCal13 and Marine13
990 Radiocarbon Age Calibration Curves 0–50,000 Years cal BP. *Radiocarbon* 55, 1869–1887.
991 doi:10.2458/azu_js_rc.55.16947

992 Riera, S., Wansard, G., Julià, R., 2004. 2000-year environmental history of a karstic lake in the Mediterranean Pre-
993 Pyrenees: the Estanya lakes (Spain). *Catena*, 55, 293–324. doi:[https://doi.org/10.1016/S0341-](https://doi.org/10.1016/S0341-8162(03)00107-3)
994 [8162\(03\)00107-3](https://doi.org/10.1016/S0341-8162(03)00107-3)

995 Rodrigo-Gámiz, M., Martínez-Ruiz, F., Rodríguez-Tovar, F.J., Jiménez-Espejo, F.J., Pardo-Igúzquiza, E., 2014a.
996 Millennial- to centennial-scale climate periodicities and forcing mechanisms in the westernmost
997 Mediterranean for the past 20,000 yr. *Quaternary Research* 81, 78–93.
998 doi:<https://doi.org/10.1016/j.yqres.2013.10.009>

999 Rodrigo-Gámiz, M., Martínez-Ruiz, F., Rampen, S.W., Schouten, S., Sinninghe Damsté, J.S., February 1, 2014b. Sea
1000 surface temperature variations in the western Mediterranean Sea over the last 20 kyr: A dual-organic proxy
1001 (UK'37 and LDI) approach. *Paleoceanography* 29, 87–98. doi:10.1002/2013PA002466

1002 Rohling, E., Mayewski, P., Abu-Zied, R., Casford, J., Hayes, A., 2002. Holocene atmosphere-ocean interactions:
1003 records from Greenland and the Aegean Sea. *Climate Dynamics* 18, 587–593. doi:10.1007/s00382-001-
1004 0194-8

1005 Sachse, D., Radke, J., Gleixner, G., 2006. δD values of individual n-alkanes from terrestrial plants along a climatic
1006 gradient – Implications for the sedimentary biomarker record. *Organic Geochemistry* 37, 469–483.
1007 doi:10.1016/j.orggeochem.2005.12.003

1008 Sanz de Galdeano, C., El Hamdouni, R., Chacón, J., 1998. Neotectónica de la fosa del Padul y del Valle de Lecrín.
1009 Itinerarios Geomorfológicos por Andalucía Oriental, Publicacions de la Universitat de Barcelona, Barcelona
1010 65–81.

1011 Schulz, M., Mudelsee, M., 2002. REDFIT: estimating red-noise spectra directly from unevenly spaced paleoclimatic
1012 time series. *Computers & Geosciences* 28, 421–426. doi:[https://doi.org/10.1016/S0098-3004\(01\)00044-9](https://doi.org/10.1016/S0098-3004(01)00044-9)

1013 Shanahan, T.M., McKay, N.P., Hughen, K.A., Overpeck, J.T., Otto-Bliesner, B., Heil, C.W., King, J., Scholz, C.A.,
1014 Peck, J., 2015. The time-transgressive termination of the African Humid Period. *Nature Geoscience* 8, 140.

1015 Singh, G., Wasson, R.J., Agrawal, D.P., 1990. Vegetational and seasonal climatic changes since the last full glacial in
1016 the Thar Desert, northwestern India. *The Proceedings of the 7th International Palynological Congress (Part*
1017 *I)* 64, 351–358. doi:10.1016/0034-6667(90)90151-8

1018 Snowball, I., Sandgren, P., 2001. Application of mineral magnetic techniques to paleolimnology. *Developments in*
1019 *Paleoenvironmental Research. Tracking Environmental Change Using Lake Sediments: Physical and*
1020 *Geochemical Methods* 2, 217–237.

1021 Steinhilber, F., Beer, J., Fröhlich, C., 2009. Total solar irradiance during the Holocene. *Geophysical Research Letters*
1022 36, 19. doi:10.1029/2009GL040142

1023 Talbot, M., 1988. The origins of lacustrine oil source rocks: evidence from the lakes of tropical Africa. *Geological*
1024 *Society, London, Special Publications* 40, 29–43.

1025 Talbot, M.R., Livingstone, D.A., 1989. Hydrogen index and carbon isotopes of lacustrine organic matter as lake level
1026 indicators. *The Phanerozoic Record of Lacustrine Basins and Their Environmental* 70, 121–137.
1027 doi:10.1016/0031-0182(89)90084-9

1028 Torrence, C., Compo, G.P., 1998. A Practical Guide to Wavelet Analysis. *Bulletin of the American Meteorological*
1029 *Society* 79, 61–78. doi:10.1175/1520-0477(1998)079<0061:APGTWA>2.0.CO;2

1030 Tzedakis, P., 2007. Seven ambiguities in the Mediterranean palaeoenvironmental narrative. *Quaternary Science*
1031 *Reviews* 26, 2042–2066.

1032 Valle, F.: Mapa de series de vegetación de Andalucía 1: 400 000, Editorial Rueda, Madrid, 2003.

- 1033 Valle Tendero, F., 2004. Modelos de Restauración Forestal: Datos botánicos aplicados a la gestión del Medio Natural
1034 Andaluz II: Series de vegetación. Consejería de Medio Ambiente de la Junta de Andalucía, Sevilla.
- 1035 Villegas Molina, F., 1967. Laguna de Padul: Evolución geológico-histórica. *Estudios Geográficos* 28, 561.
- 1036 Wieder, R.K., Lang, G.E., 1988. Cycling of inorganic and organic sulfur in peat from Big Run Bog, West Virginia.
1037 *Biogeochemistry* 5, 221–242. doi:10.1007/BF02180229
- 1038 Walker, M. J., Berkelhammer, M., Björck, S., Cwynar, L. C., Fisher, D. A., Long, A. J., Lowe, J. J., Newnham, R.
1039 M., Rasmussen, S. O. and Weiss, H., 2012. Formal subdivision of the Holocene Series/Epoch: a Discussion
1040 Paper by a Working Group of INTIMATE (Integration of ice-core, marine and terrestrial records) and the
1041 Subcommission on Quaternary Stratigraphy (International Commission on Stratigraphy). *J. Quaternary Sci.*,
1042 27: 649-659. doi:10.1002/jqs.2565
- 1043 Ziegler, M., Jilbert, T., Lange, G.J. de, Lourens, L.J., Reichert, G., 2008. Bromine counts from XRF scanning as an
1044 estimate of the marine organic carbon content of sediment cores. *Geochemistry, Geophysics, Geosystems* 9.
- 1045 Zielhofer, C., Fletcher, W.J., Mischke, S., De Batist, M., Campbell, J.F.E., Joannin, S., Tjallingii, R., El Hamouti, N.,
1046 Junginger, A., Stele, A., Bussmann, J., Schneider, B., Lauer, T., Spitzer, K., Strupler, M., Brachert, T.,
1047 Mikdad, A., 2017. Atlantic forcing of Western Mediterranean winter rain minima during the last 12,000
1048 years. *Quaternary Science Reviews* 157, 29–51. doi:10.1016/j.quascirev.2016.11.037

1049 **Figure captions**

1050 **Figure 1.** Location and pictures of Padul wetland. (a) Location of Padul wetland in Sierra Nevada, southern
1051 Iberian Peninsula, with an inset showing south western Europe. (b) Padul basin area showing the coring
1052 location. (c) Picture of Padul wetland, peat bog and crops area in the Padul basin, and the alluvial fans and
1053 Sierra Nevada mountains in the background. [Picture from M.J. Ramos-Román.](#) [FM4] Software use: Above,
1054 Sierra Nevada map was performed using the GIS software Global Mapper (<http://www.globalmapper.com>)
1055 and modified with Adobe Illustrator. The inset map (the western Mediterranean region) was created with
1056 Adobe Illustrator (<https://www.adobe.com/>). Below, left, is the Google earth image
1057 (<http://www.google.com/earth/index.html>) of the Padul basin showing the coring locations.

1058 **Figure 2.** Picture of the Padul-15-05 sediment core ([images were taken with an Avaatech core scanner at](#)
1059 [the University of Barcelona](#)) [FM5] with the age-depth model showing the part of the record that was studied
1060 here (red rectangle) corresponding with the last ~~~11.6 cal ka BP~~ [11.600 years](#), based on a previous age-depth
1061 model (Ramos-Román et al., 2018). The sediment accumulation rates (SAR; unit= cm/yr) between
1062 radiocarbon dates are marked. See the body of the text for the explanation of the age reconstructions.

1063 **Figure 3.** Inorganic geochemistry results for the ~3.67 m of the upperpart from Padul 15-05 record. Picture
1064 of the Padul-15-05 record, facies interpretations with paleontology, magnetic susceptibility (MS) and X-
1065 ray fluorescence (XRF). XRF elements (Ca, Sr, Br, S, Si, K, Ti, Fe, Zr) are represents as counts per second
1066 normalized to the total counts (norm.). (a) MS in SI, (b) Calcium normalized (Ca norm.) (c) Strontium
1067 normalized (Sr norm.) (d) Bromine normalized (Br norm.) (e) Sulfur normalized (S norm.) (f) Silica
1068 normalized (Si norm.), (g) Potassium normalized (K norm.), (h) Titanium normalized (Ti norm.), (i) Iron
1069 normalized (Fe norm.), (j) Zirconium normalized (Zr norm.), (k) K/Si ratio. Note that uppermost ~ 1.15 m
1070 inorganic geochemistry results of the record were previously shown in Ramos-Román et al. (2018).

1071 **Figure 4.** Organic geochemistry results for the ~3.67 m of the upperpart (Holocene part) from Padul-15-05
1072 record and comparison with inorganic index calculated from the PCA analysis performed to XRF elements

1073 in the same record. (a) K/Si ratio, (b) Ca (norm.), (c) Total organic carbon percentage (TOC %), (d) Carbon-
1074 Nitrogen ratio (C/N), (e) Hydrogen-Carbon ratio (H/C), (f) Average chain length (ACL), (g) Carbon
1075 preference index (CPI), (h) Short-chain (%), (i) Mid-chain (%), (j) Long-chain (%). Note that the uppermost
1076 ~ 1.15 m TOC values were previously shown (Ramos-Román et al., 2018).

1077 **Figure 5.** Percentages of selected pollen taxa and non-pollen palynomorphs (NPPs) from the Holocene part
1078 of Padul-15-05 record, represented with respect to terrestrial pollen sum. Silhouettes show 7-time
1079 exaggerations of pollen percentages. Tree and shrubs are showing in green, herbs and grasses in yellow,
1080 aquatics in dark blue, algae in blue and fungi in brown. The Mediterranean forest taxa is composed of
1081 *Quercus* total, *Olea*, *Phillyrea* and *Pistacia*. The xerophyte group includes *Artemisia*, *Ephedra*, and
1082 Amaranthaceae. The hygrophytes group is composed by Cyperaceae and *Typha* type. Algae group is formed
1083 by *Zygea* type, *Botryococcus*, *Mougeotia* and *Pediastrum*. U: Unit. Note that uppermost ~ 1.15 m pollen
1084 and NPPs results of the record were previously depicted (Ramos-Román et al., 2018).

1085 **Figure 6.** Padul-15-05 local environment development during the Holocene deduced from a comparison
1086 between different pollen, organic and inorganic geochemistry proxies from the Holocene part of the Padul-
1087 15-05 record and summer and winter insolation for the Sierra Nevada latitude. A) Regional response
1088 determines by Mediterranean forest taxa (%). B) Local response: (a) Summer and winter insolation
1089 calculated for 37° N (Laskar et al., 2004), (b) Ca (norm.) (c) K/Si ratio (clays input), (d) Total organic
1090 carbon percentage (TOC %), (e) *Glomus* type (%) (f), Short-chain (%), (g) Algae percentage from the pollen
1091 analysis (h) Mid-chain (%), (i) Hygrophytes percentage. Beige shadings are showing arid and cold event
1092 during the early and middle Holocene determine by the decline in Mediterranean forest component and
1093 showing the response in the local environment. Proxies were resampled at 80 yr (in bold) by lineal
1094 interpolation using Past software (http://palaeo-electronica.org/2001_1/past/issue1_01.htm). U: Unit.

1095 **Figure 7.** Comparison for the Holocene between different pollen taxa from the Padul-15-05 record with a
1096 previously pollen record in the same area and other pollen and temperature proxies from nearly records in

1097 the western Mediterranean region (see records locations in Supplementary Fig. S8). (a) Deciduous *Quercus*,
1098 Evergreen *Quercus* and Mediterranean forest percentages in the Padul-15-05 record, (b) Deciduous
1099 *Quercus* and Evergreen *Quercus* in a previously record in the Padul peat bog (Pons and Reille, 1988), (c)
1100 Percentage of *Pinus* and *Artemisia* in the nearly Laguna de Rio Seco record, Sierra Nevada (Anderson et
1101 al., 2011), (d) Temperate and Mediterranean forest percentage for the MD95-2043 record, Alboran Sea
1102 (Fletcher and Sánchez-Goñi, 2008), (e) Alkenone sea surface temperature (SST) reconstruction from the
1103 MD01-2444, Alboran Sea (Martrat et al., 2004), (f) Alkenone SST reconstruction from the MD95-2043
1104 record, Alboran Sea (Cacho et al., 1999), (g) Alkenone SST reconstruction from the 434G record, Alboran
1105 Sea (Rodrigo-Gámiz et al., 2014b). Blue shading represents the humidity optimum during the Holocene in
1106 the western Mediterranean region.

1107 **Figure 8.** Holocene climate periodicity from the Padul-15-05 record determine by declines in the
1108 Mediterranean forest component and comparison with other North Atlantic records. (a) Summer and winter
1109 insolation calculated for 37° N (Laskar et al., 2004), (b) Mediterranean forest taxa (c) Ocean stacked
1110 percentage of the Drift Ice Index (reversed) from the North Atlantic (Bond et al., 2001), (d) Total solar
1111 irradiance (TSI) anomaly reconstruction from cosmogenic radionuclide from a Greenland ice core
1112 (Steinhilber et al., 2009), (e) Alkenone sea surface temperature (SST) reconstruction from the MD01-2444,
1113 Alboran Sea (Martrat et al., 2004), (f) Alkenone SST reconstruction from the MD95-2043 record, Alboran
1114 Sea (Cacho et al., 1999), (g) Alkenone SST reconstruction from the 434G record, Alboran Sea (Rodrigo-
1115 Gámiz et al., 2014b). Beige shadings highlight decreases in Mediterranean forest and coldest events related
1116 with decreases in total solar irradiance and decreases in SST. A linear r (Pearson) correlation was calculated
1117 between the Mediterranean forest abundances and the TSI anomaly ($r = 0.43$; $p < 0.001$; between ~ 9.4 and
1118 4.7 cal ka-kyr BP and $r = 0.37$; $p < 0.001$; between 4.7 cal ka-kyr BP and present). In order to obtain equally
1119 spaced time series the Mediterranean forest and the TSI anomaly data were previously resampled at 50
1120 years (linear interpolation), the Mediterranean forest data was detrended (only between 4.7 cal kyr BP to
1121 present) and the TSI anomaly smoothed to a five-point average.

1122 **Table 1.** Modern vegetation belts from Sierra Nevada (El Aallali et al., 1998; Valle, 2003).

1123 **Table 2.** Age data for Padul-15-05 record. All ages were calibrated using R-code package ‘clam 2.2’
1124 employing the calibration curve IntelCal 13 (Reimer et al., 2013) at 95 % of confident range. Note that the
1125 age data for the uppermost ~ 3.27 m were previously shown (Ramos-Román et al., 2018).

1126 **Table 3.** Summary of the *n*-alkane indices from the studied plant, algae and moss samples from the
1127 surroundings of the present-day Padul peatland (For more information see in the Supplementary Figure S2
1128 and S3).

1129 **Table 4.** Linear *r* (Pearson) correlation between geochemical proxies and pollen data from the Padul-15-05
1130 record. Statistical treatment was performed using the Past software ([http://palaeo-](http://palaeo-electronica.org/2001_1/past/issue1_01.htm)
1131 [electronica.org/2001_1/past/issue1_01.htm](http://palaeo-electronica.org/2001_1/past/issue1_01.htm)).

Highlights

- 1.** We carried out a multi-proxy analysis for the last 11.6 cal kyr BP from a new sedimentary record from Padul (Sierra Nevada, Spain).
- 2.** This record shows a long-term climate pattern mostly forced by insolation, showing a significant climate and environmental shift at 4.7 cal kyr BP.
- 3.** Millennial-scale climate oscillations are also characterized in this study by the decrease in Mediterranean forest and local response in the lake level, showing possible atmospheric and climate links between the western Mediterranean and North Atlantic areas.

1 **Millennial-scale cyclical environment and climate variability during the Holocene in the western**
2 **Mediterranean region deduced from a new multi-proxy analysis from the Padul record (Sierra**
3 **Nevada, Spain)**

4

5 María J. Ramos-Román¹, Gonzalo Jiménez-Moreno¹, Jon Camuera¹, Antonio García-Alix^{1,2}, R. Scott
6 Anderson³, Francisco J. Jiménez-Espejo⁴, Dirk Sachse⁵, Jaime L. Toney⁶, José S. Carrión⁷, Cole Webster³,
7 Yurena Yanes⁸

8 ¹ Departamento de Estratigrafía y Paleontología, Universidad de Granada, Spain

9 ² Instituto Andaluz de Ciencias de la Tierra (IACT), CSIC-UGR, Armilla, Spain

10 ³ School of Earth Sciences and Environmental Sustainability, Northern Arizona University, USA.

11 ⁴ Department of Biogeochemistry, Japan Agency for Marine-Earth Science and Technology (JAMSTEC),
12 Japan.

13 ⁵ Helmholtz Centre Potsdam, German Research Centre for Geosciences GFZ, Section 5.1
14 Geomorphology, Organic Surface Geochemistry Lab., Germany

15 ⁶ School of Geographical and Earth Sciences, University of Glasgow, UK □

16 ⁷ Departamento de Biología Vegetal, Facultad de Biología, Universidad de Murcia, Murcia, Spain

17 ⁸ Department of Geology, University of Cincinnati, USA

18

19 *Correspondence to:* María J. Ramos-Román (mjrr@ugr.es)

20 **Abstract**

21 A high-resolution multi-proxy approach, integrating pollen, inorganic and organic geochemical and
22 sedimentological analyses, has been carried out on the Holocene section of the Padul sedimentary record
23 in the southern Iberian Peninsula reconstructing vegetation, environment and climate throughout the last ~
24 11.6 cal kyr BP in the western Mediterranean. The study of the entire Holocene allows us to determine the

25 significant climate shift that occurred during the middle-to-late Holocene transition. The highest occurrence
26 of deciduous forest in the Padul area from ~ 9.5 to 7.6 cal kyr BP represents the Holocene humidity optimum
27 probably due to enhanced winter precipitation during a phase of highest seasonal anomaly and maximum
28 summer insolation. Locally, insolation maxima induced high evaporation, counterbalancing the effect of
29 relatively high precipitation, and triggered very low water table in Padul and the deposition of peat
30 sediments. A transitional environmental change towards more regional aridity occurred from ~ 7.6 to 4.7
31 cal kyr BP and then aridification enhanced in the late Holocene most likely related to decreasing summer
32 insolation. This translated into higher water levels and a sedimentary change at ~ 4.7 cal kyr BP in the Padul
33 wetland, probably related to reduced evaporation during summer in response to decreased seasonality.
34 Millennial-scale variability is superimposed on the Holocene long-term trends. The Mediterranean forest
35 regional climate proxy studied here shows significant cold-arid events around ~ 9.6, 8.5, 7.5, 6.5 and 5.4
36 cal kyr BP with cyclical periodicities (~1100 and 2100 yr) during the early and middle Holocene. A change
37 is observed in the periodicity of these cold-arid events towards ~1430 yr in the late Holocene, with forest
38 declines around ~ 4.7-4, 2.7 and 1.3 cal kyr BP. The comparison between the Padul-15-05 data with
39 published North Atlantic and Mediterranean paleoclimate records suggests common triggers for the
40 observed climate variability, with the early and middle Holocene forest declines at least partially controlled
41 by external forcing (i.e. solar activity) and the late Holocene variability associated with internal mechanisms
42 (oceanic-atmospheric).

43 **Keywords:** Holocene, Padul, wetland, Sierra Nevada, western Mediterranean, atmospheric-oceanic
44 dynamics, wavelet analysis, arid events

45 **1. Introduction**

46 The western Mediterranean region, located in the subtropical latitude (Alpert et al., 2006), is a sensitive
47 area to detect past climate variability and has been the focus of several previous Holocene studies (e.g.,
48 Fletcher et al., 2013; Zielhofer et al., 2017). Present-day climate in this area is characterized by a strong

49 seasonality, principally dominated by dry (hot) summers and wetter (mild) winters (Lionello et al., 2006)
50 and one of the main mechanisms driving climate variations is the North Atlantic Oscillation (NAO)
51 (Hurrell, 1995; Moreno et al., 2005).

52 During the Holocene, orbital-scale (i.e. insolation) variations triggered climate changes that in turn
53 produced significant environmental changes worldwide. Paleoclimate records show a Holocene climatic
54 optimum between 9.5-7.5 cal kyr BP (Dormoy et al., 2009), characterized in the western Mediterranean
55 area by high temperatures and precipitation, which has been related with high summer insolation (Lamb
56 and van der Kaars, 1995; Fletcher and Sánchez-Goñi, 2008; Anderson et al., 2011). Regional climate
57 models described that the most important climatic transition towards cooler and drier conditions during the
58 Holocene occurred around ~ 6 ka (Huntley and Prentice, 1988; Cheddadi et al., 1997). This shift has also
59 been documented in the western Mediterranean, suggesting the establishment of the current NAO-like
60 system at ~ 6 cal kyr BP (Fletcher et al., 2013). However, other studies differ in the timing of this climate
61 shift indicating a transition phase between 7 and 5.5 cal kyr BP (Jalut et al., 2009). These differences could
62 be related with changes in altitudinal vegetation gradient, geomorphological changes in the study area
63 and/or human perturbation of the landscape (Anderson et al., 2011). According to Roberts et al. (2011),
64 combining different proxies indicative of vegetation and geomorphological changes is a useful tool to
65 discern the timing and the main forcing triggering this mid-Holocene environmental changes.

66 During the last few decades, a multitude of continental, marine and ice records worldwide have shown
67 millennial-scales climate variability during the Holocene (e.g. Johnsen et al., 1992; Bar-Matthews et al.,
68 2003; Mayewski et al., 2004). Numerous studies have detected this climate variability in the North Atlantic
69 area (i.e., Bond et al., 2001; Debret et al., 2007, 2009), with a prominent ~ 1500 yr cyclicity throughout the
70 Holocene (Bond et al., 2001). However, others studies have demonstrated that Holocene climate variability
71 was not stationary and exhibited variable periodicity at different times-intervals (Debret et al., 2007; 2009).
72 In this respect, high-resolution Mediterranean records have also shown rapid environmental variability
73 related to millennial-scale climate variability (Cacho et al., 2001; Fletcher and Sánchez-Goñi, 2008; Peyron
74 et al., 2013). Previous palynological analyses from the western Mediterranean showed vegetation responses

75 at millennial-scales that seem to co-vary with climate variability from North Atlantic records,
76 demonstrating hemispheric-scale teleconnections during the Holocene (Combourieu-Nebout et al., 2009;
77 Fletcher et al., 2013; Rodrigo-Gámiz et al., 2014a). Other marine and terrestrial studies found centennial
78 and millennial-scale Holocene frequency climatic patterns (Rodrigo-Gámiz et al., 2014a; Ramos-Román et
79 al., 2016; García-Alix et al., 2017). However, there is a lack of non-stationary time-series analysis at
80 millennial-scales from terrestrial records in the western Mediterranean area, which is necessary to
81 understand terrestrial-ocean-atmospheric dynamics and the connections with high-latitude North Atlantic
82 climate records. This is key for learning about past environmental change and climate variability in the
83 western Mediterranean region.

84 Multi-proxy studies on continental records in southern Iberia and the western Mediterranean that could
85 help understanding this environmental variability during the Holocene are rare. In order to improve our
86 knowledge about this subject, we present a high-resolution multidisciplinary analysis integrating
87 sedimentation, geochemistry, vegetation, and climate change and variability during the Holocene (from
88 ~11.6 cal kyr BP to Present) from the Padul-15-05 wetland record. Previous sedimentary records and
89 paleoecological studies have been carried out on the Padul archive, detecting climate variability from the
90 Pleistocene to the middle Holocene (Florschütz et al., 1971; Pons and Reille, 1988; Ortiz et al., 2004).
91 Nevertheless, a high-resolution multi-proxy analysis on the same sediment samples has never been
92 performed at this site for the entire Holocene epoch. Recently, a multi-proxy analysis [studying pollen,
93 spores, magnetic susceptibility (MS), total organic carbon (TOC) and X-ray fluorescence (XRF)] has been
94 done focusing on the late Holocene part of the Padul-15-05 record. That study shows an aridification trend
95 since ~ 4.7 cal kyr BP and enhanced human influence on the environments in the area since the last 1.5 cal
96 kyr BP (Ramos-Román et al., 2018), renewing the interest to carry out a more complete study for the entire
97 Holocene. The present study uses high-resolution radiocarbon dating, inorganic and organic geochemistry
98 (biomarkers and bulk sediment), pollen, lithology and macrofossil analyses to reconstruct the Padul area
99 paleoenvironmental evolution and millennial-scale vegetation and climate fluctuations in the western
100 Mediterranean region over the last 11,600 years. This research seeks two main goals: 1) understanding

101 regional vegetation changes and local environmental evolution and making climate interpretations during
102 the early, middle and late Holocene, specifically focusing on the transitions, and 2) comparing millennial-
103 scale vegetation and water-level oscillations (regional and local signal) with global climatic events.

104 *1.1. Location and environmental setting*

105 The Padul basin is an endorheic area at around 725 m of elevation at the foothill of the southwestern
106 Sierra Nevada in Andalusia, southern Spain (Fig. 1). Today's climate in the Padul area is characterized by
107 a mean annual temperature of 14.4 °C and a mean annual precipitation of 445 mm, and by hot and dry
108 summers (mean temperature of 22.8 °C and precipitation of 25 mm) and mild and wetter winters (mean
109 temperature of 8 °C and precipitation of 140 mm) (<http://agroclimap.aemet.es/>). The Sierra Nevada
110 mountain range shows strong thermal and precipitation differences due to the altitudinal gradient (from
111 ~700 to more than 3400 m), which controls plant taxa distribution in different bioclimatic vegetation belts
112 due to the variability in temperature and precipitation (Valle Tendero, 2004). According to this
113 climatophilous series classification (Table 1), the Padul basin is situated in the Mesomediterranean
114 vegetation belt (from ~ 600 to 1400 m of elevation), which is largely defined by the dominance of *Quercus*
115 *rotundifolia* (evergreen *Quercus* pollen morphotype) and, to a lesser extent, *Q. faginea* (deciduous *Quercus*
116 pollen morphotype), which is normally accompanied by *Pistacia terebinthus*. *Q. coccifera* (evergreen
117 *Quercus* pollen morphotype) also occur in crests and very sunny rocky outcrops.

118 Sedimentation in the Padul basin results from (1) allochthonous detritic material coming for the
119 surrounding mountains, principally from Sierra Nevada, which is characterized at higher elevations by
120 Paleozoic siliceous metamorphic rocks (mostly mica-schists and quartzites) from the Nevado-Filabride
121 complex and, at lower elevations and acting as bedrock, by Triassic dolomites, limestones and phyllites
122 from the Alpujarride Complex (Sanz de Galdeano et al., 1998), (2) autochthonous organic material coming
123 from plants growing in the wetland area of the basin itself and (3) biogenic carbonates from charophytes,
124 ostracods and gastropod shells, prominent organisms that lived in the lake. The water contribution to the
125 Padul wetland primarily comes from groundwater input and, to a lesser degree, from rainfall. Groundwater

126 comes from different aquifers: the Triassic carbonate aquifers to the north and south edge of the basin, the
127 out-flow of the Granada Basin to the west and the conglomerate aquifer to the east (Castillo Martín et al.,
128 1984; Ortiz et al., 2004). The main water output is through evaporation and evapotranspiration and more
129 recently also by water wells and by canals (locally called “madres”) (Castillo Martín et al., 1984). The
130 canals were built around the end of the XVIII century with the goal of draining the basin water to the Dúrcal
131 river to the southeast for cultivation purposes (Villegas Molina, 1967). In the early 2000s the Padul wetland
132 was placed under environmental protection and the peat mine stopped pumping water out of the basin and
133 the Padul lake increased its size considerably.

134 The Padul-15-05 drilling site is located around 50 m south of the present-day Padul lake-shore area.
135 The edge of the lake area is at present principally dominated by the grass *Phragmites australis*. The lake
136 environment is also characterized by emerged and submerged macrophytes communities dominated by
137 *Chara vulgaris*, *Myriophyllum spicatum*, *Potamogeton pectinatus*, *Potamogeton coloratus*, *Typha*
138 *dominguensis*, *Apium nodiflorum*, *Juncus subnodulosus*, *Carex hispida*, *Juncus bufonius* and *Ranunculus*
139 *muricatus* among others (Pérez Raya and López Nieto, 1991). *Populus alba*, *Populus nigra*, *Ulmus minor*
140 and several species of *Salix* and *Tamarix* grow on the northern lake shore (Ramos-Román et al., 2018).

141 **2. Methodology**

142 *2.1. Padul site core drilling*

143 The Padul-15-05 sediment core (37°00'39.77''N; 3°36'14.06''W) with a length of 42.64 m, was
144 collected in 2015 from the Padul lake shore (Fig. 1). The core was taken with a Rolatec RL-48-L drilling
145 machine equipped with a hydraulic piston corer from the Scientific Instrumentation Center of the University
146 of Granada (CIC-UGR). The sediment core was wrapped in film, put in core boxes, transported and stored
147 in a dark cool room at +4 °C at the University of Granada. In this study, we focus on the uppermost ~ 3.67
148 m from the 42.6-m-long Padul-15-05 core.

149 *2.2. Chronology and sedimentation rates*

150 The age model for the uppermost ~ 3.27 m is based on fourteen AMS radiocarbon dates previously
151 shown in Ramos-Román et al. (2018). Six more radiocarbon samples have been analyzed in the lower part
152 of the study record in order to improve the chronology of older sediments. Three of these samples were
153 rejected, because one plant sample was too young and two gastropod shell samples provided old dates due
154 to the reservoir effect. As a result, the sedimentary record chronology from ~ 4.24 m to 0.21 m depth was
155 constrained using a total of seventeen AMS radiocarbon dates (Table 2). The age model was built using the
156 R-code package ‘Clam 2.2’ employing the calibration curve IntCal 13 (Reimer et al., 2013), a 95%
157 confident range, a smooth spline (type 4) with a 0.20 smoothing value and 1000 iterations (Fig. 2). The
158 chronology of the uppermost 21 cm of the record was built using a linear interpolation between the last
159 radiocarbon date and the top of the record, which was assigned the age when coring (2015 CE).

160 In this paper we followed the three principal subdivisions for the Holocene defined by Walker et al.,
161 2012. They proposed an Early-Middle Holocene boundary at 8.2 cal kyr BP and Middle-Late Holocene at
162 4.2 cal kyr BP.

163 *2.3. Lithology and magnetic susceptibility (MS)*

164 The Padul-15-05 core was split longitudinally and was described in the laboratory with respect to
165 lithology and color (Fig. 3). High-resolution continue scanning images were taken with an Avaatech core
166 scanner at the University of Barcelona (UB). MS was measured with a Bartington MS3 operating with a
167 MS2E sensor. MS measurements (in SI units) were obtained directly from the core surface every 0.5 cm
168 (Fig. 3). Lithological description and MS data of the same record of the uppermost 1.15 m of the record
169 were previously described in Ramos-Román et al. (2018).

170 *2.4. Inorganic geochemistry*

171 High-resolution XRF was applied continuously throughout the core surface, taking measurements of
172 elemental geochemical composition. An Avaatech X-Ray fluorescence (XRF) core scanner® located at the
173 UB was used. Chemical elements were measured in the XRF core scanner at 10 mm of spatial resolution,
174 using 10 s count time, 10 kV X-ray voltage and an X-ray current of 650 μ A for lighter elements and 35 s
175 count time, 30 kV X-ray voltage, X-ray current of 1700 μ A for heavier elements. Thirty-three chemical
176 elements were measured but only the most representative with a significant number of counts were
177 considered (Si, K, Ca, Ti, Fe, Zr, Br, S and Sr). Results for each element are expressed as intensities in
178 counts per second (cps) and normalized for the total sum in cps in every measure (Fig. 4), being the upper
179 part of the record (from 1.15 m to the top) previously shown in Ramos-Román et al. (2018).

180 2.5. Organic geochemistry

181 Several organic geochemical proxies have been studied from bulk sediment samples throughout the
182 record: total organic carbon (TOC), atomic Carbon-Nitrogen ratio (C/N) and atomic Hydrogen-Carbon ratio
183 (H/C). In addition, several indices of leaf wax biomarkers (*n*-alkanes) were calculated: the average chain
184 length (ACL), the carbon preference index (CPI) and the portion of aquatic (Paq). In addition, three new
185 indices have been calculated based on the relative abundance of odd carbon number from nC_{17} to nC_{33}
186 alkanes, except for nC_{27} alkanes (See Section 3.2.2 for justification of new indices).

187 Samples for elemental analyses in bulk sediment were analyzed every 2 or 3 cm throughout the Padul-
188 15-05 record, with a total of 206 samples analyzed. Samples were decalcified with 1:1 HCl to eliminate the
189 carbonate fraction. Carbon, nitrogen and hydrogen content of the decalcified samples were measured in an
190 Elemental Analyzer Thermo Scientific Flash 2000 model at the CIC-UGR. Percentage of TOC (note that
191 TOC of the uppermost 1.15 m of the record was previously described; Ramos-Román et al., 2018), total
192 nitrogen (TN) and total hydrogen (TH) per gram of sediment was calculated from the percentage of organic
193 carbon, nitrogen and hydrogen yielded by the elemental analyzer, and recalculated by the weight of the

194 sample prior to decalcification. The atomic C/N and H/C ratio was calculated from the carbon, nitrogen and
195 hydrogen measurements (Fig. 4).

196 Biomarkers from the Padul-15-05 record were extracted every 5 cm from sedimentary record, with a
197 total of 68 samples analyzed. Furthermore, thirty-one modern plant leaves/algae and bryophyte samples
198 were taken from the surroundings of the Padul basin and analyzed for biomarkers. The total lipid extraction
199 (TLE) from the freeze-dried samples was obtained using an accelerate solvent extractor (ASE) Thermo
200 DIONEX 350, with a dichloromethane:methanol (9:1). Plant biomarkers were extracted manually using
201 dichloromethane:methanol (9:1) by means of sonication and low temperature (38°C). The TLE from plants
202 and sediments was separated into three different fractions using a silica gel column. Before the separation
203 three internal standards were added to the TLE (5 α -androstane, 5 β -androstan-17-one and 5 α -androstan-
204 3 β -ol) in order to assess the biomarker extraction as well as to quantify them. Compounds of the aliphatic
205 fraction (*n*-alkanes) were recovered in the first fraction eluted with Hexane. The *n*-alkanes were identified
206 and quantified using a Gas Chromatography flame detection and mass spectrometry (GC-FID and GC-MS)
207 by means of an Agilent 5975C MSD by comparison to an external *n*-alkane standard mixture from *n*C₁₀ to
208 *n*C₄₀.

209 2.6. Pollen

210 Samples for pollen analysis (1-3 cm³) were taken with a resolution between 1-5 cm throughout the
211 core. A total of 73 samples between 1.15 and 3.67 m have been analysed in this study and were summed to
212 the previous 103 pollen samples analysed between 0-1.15 m (Ramos-Román et al., 2018), with a mean
213 pollen resolution around 65 yr (~ 95 yr between 11.6 and 4.7 cal kyr BP and ~ 50 yr for the last 4,700
214 years). Pollen extraction methods followed a modified Faegri and Iversen, (1989) methodology. Processing
215 included the addition of *Lycopodium* spores for calculation of pollen concentration. Sediment was treated
216 with 10 % NaOH, 10% HCl, 10% HF and the residue was sieved at 250 μ m before an acetolysis solution.
217 Counting was performed using a transmitted light microscope at 400 magnifications to an average pollen

218 count of around 250 terrestrial pollen grains. Fossil pollen was identified using published keys (Beug, 2004)
219 and modern reference collections at the UGR. Pollen counts were transformed to pollen percentages based
220 on the terrestrial pollen sum, excluding aquatics. Non-pollen palynomorphs (NPP) include algal spores.
221 The NPP percentages were also calculated and represented with respect to the terrestrial pollen sum. Several
222 pollen and NPP taxa were grouped according to present-day ecological data in Mediterranean forest,
223 xerophytes and algae (Fig. 5). The Mediterranean forest taxa include *Quercus* total, *Olea*, *Phillyrea*,
224 *Pistacia* and Cistaceae. The Xerophyte group includes *Artemisia*, *Ephedra*, and Amaranthaceae. The Algae
225 group is composed of *Botryococcus*, *Zygnema* type, *Mougeotia* and *Pediastrum*. Zonation was obtained
226 with a cluster analysis using four representative pollen taxa Mediterranean forest, *Pinus* total, Ericaceae and
227 *Artemisia* (Grimm, 1987; Fig. 5).

228 2.7. Statistical analysis

229 Statistical treatment was performed using the *PAST 3.12* software ([Hammer et al., 2001](#)). Principal
230 component analysis (PCA) was conducted on different geochemical elements (XRF data) to clarify the
231 lithological elemental composition of the core (Supplementary; Figure S1). Prior to the PCA analysis, we
232 pretreated the data normalizing the element counts by subtracting the mean and dividing by the standard
233 deviation (Davis and Sampson, 1986). As data spacing was different in all the study proxies, the data were
234 also resampled to the average value of 80-yr (linear interpolation) to obtain equally spaced time series.
235 Posteriorly, a Pearson correlation was made to different organic/inorganic geochemistry and pollen proxies
236 to find affinities between the different proxies.

237 In this study, spectral analysis was accomplished on the Mediterranean forest pollen taxa time series,
238 to identify regional millennial-scale periodicities in the Padul-15-05 record. We used REDFIT software
239 (Schulz and Mudelsee, 2002) on the unevenly spaced pollen time series in order to identify cyclical changes. In
240 addition, we carried out a Wavelet transform analysis by the PAST software (Torrence and Compo, 1998)
241 with the goal of identifying non-stationary cyclical variability in the regional vegetation evolution, the
242 pollen was previously detrended and resampled at 80-yr age increments. In this study, a Morlet wavelet

243 was chosen, the significant level (plotted as contour) corresponded to a p-value = 0.05, and a white-noise
244 model was implemented.

245 *2.8. Correlations for the environment reconstruction*

246 Linear r (Pearson) correlation analyses between the obtained local proxy dataset (MS, Ca, S, Br, Sr,
247 K/Si ratio, C/N ratio, H/C ratio, TOC, short-chain, mid-chain and long-chain abundances, Poaceae, Algae
248 and Hygrophytes) are shown in table 4. These analyses were performed to identify the associations between
249 proxies and to understand environmental change in the Padul area. This analysis assisted us in identifying
250 (a) different proxies characteristic of organic-rich sediments, primarily that peatland environment under
251 very shallow lake conditions (higher TOC, C/N ratio, S, Br, Sr and mid-chain abundance) and (b) a second
252 group of proxies characteristic of deeper shallow water environments depicted by the increase in endogenic
253 carbonates and more influenced by terrestrial-clays input (higher Ca, K/Si, MS, Algae).

254 **3. Results and proxy interpretation**

255 *3.1. Chronology and sedimentary rates*

256 The age-model of the studied Padul-15-05 core (Fig. 2) is constrained by 17 AMS ¹⁴C radiocarbon dates
257 from the top 4.24 m of the record (Table 2). In this work, we studied the uppermost ~ 3.67 m that
258 continuously cover the last ~ 11.6 cal kyr BP. This interval is chronologically constrained by 16 AMS
259 radiocarbon dates. Fifteen distinct sediment accumulation rates (SAR) intervals are differentiated between
260 3.67 m and the top of the record (Fig. 2).

261 *3.2. Lithology, inorganic and organic geochemistry*

262 *3.2.1. Lithology and inorganic geochemistry*

263 Inorganic geochemistry informs us about variations in the lithology and the local depositional
264 environment. Variations in these proxies could also be useful for estimating water level fluctuations in the

265 wetland environment. Sediments bearing aquatic fossil remains (i.e. gastropods and charophytes) as well
266 as being rich in carbonates have previously been related to shallow water lakes (Riera et al., 2004). Lower
267 water levels, more subjected to be occupied by wetland vegetation, and ephemeral lakes are characterized
268 by the increase in organics and clastic input and more influenced by terrestrial-fluvial deposition (Martín-
269 Puertas et al., 2008). Magnetic susceptibility (MS) measures the propensity of the sediments to bring a
270 magnetic charge (Snowball and Sandgren, 2001).

271 Framboidal pyrite (FeS_2) and barite (BaSO_4) with Sr have been found covering exceptionally preserved
272 mammals remains from 40 to 30 ka at the Padul Peat bog (García-Alix et al., 2012) pointing towards a peat-
273 bog environment with enhanced anoxic conditions. The presence of pyrite and organic-sulfur compounds
274 is common in peat bogs (Wieder and Lang, 1988; Feijtel et al., 1989; Chapman, 2001) and other organic
275 rich sediments under anoxic conditions (López-Buendía et al., 2007). Increasing values of organic carbon
276 and bromine have been related with higher organic matter deposition generated in high productivity
277 environments (Kalugin et al., 2007). In marine records, Br XRF scanning counts can be used to estimate
278 sedimentary total organic carbon (Ziegler et al., 2008).

279 A visual lithological inspection was made for the upper ~ 3.67 m of the Padul-15-05 sediment core and
280 was compared with the elemental geochemical composition (XRF) and the MS data (Fig. 3). For the
281 geochemical elements, we conducted a PCA to summarize and better understand the correlation between
282 the visual lithological features and the geochemical signal of the sediments (Supplementary Fig. S1 and
283 Table S1). The PCA in the studied sedimentary sequence identifies three main groups of sediments
284 consisting of clays with variable content in (1) carbonates of endogenic formation with high values of Ca,
285 related with the occurrence of shells and charophyte remains, (2) siliciclastics (Si, K, Ti, Fe, Zr) and (3)
286 vegetal organics (related with S and Br) probably associated with reducing environment under anoxic
287 conditions showing high values of S, Sr and Br. The K/Si ratio was calculated to differentiate the clays
288 input into the basin. The K/Si ratio is based on the fact that clay fraction is enriched in phyllosilicates (illite,
289 muscovite), whereas the coarser particles that are mainly quartz, dolomite and schists. This correlation

290 between K and clay content has been observed in other lacustrine systems (e.g. Lake Enol, Iberian
291 Peninsula) and associated with an increase in detrital input (Moreno et al., 2011). Four different lithological
292 units were identified (Fig. 3). Units 1 and 2 are principally made up of peat sediments and Unit 3 and 4 by
293 clays with variable carbonates (Fig. 3). Unit 1 (SAR ~ 0.04 cm/yr), from the bottom (3.67 m; ~ 11.6 cal kyr
294 BP) to around 2.31 m (~ 7.6 cal kyr BP), is characterized by *facies 1* - dark organic peat – high S, Sr and
295 Br values. Unit 2 (SAR ~ 0.05 cm/yr), from 2.31 to 1.15 m (~ 7.6 to 4.7 cal kyr BP), is also generally
296 characterized by *facies 1* but with the intercalation of three other different *facies*; *facies 2* from 2.31 to 2.21
297 m (~ 7.6 to 7.3 cal kyr BP) depicted by grey clays with gastropod remains (featured by the increase in Ca
298 and K/Si ratio), *facies 3* from 1.95 to 1.85 m (~ 6.6 to 6.4 cal kyr BP) made up of brown clays with the
299 occurrence of gastropods and charophytes (showing a decrease in S, Br and Sr and higher values of Ca) and
300 *facies 4* around 1.46 to 1.40 m (~ 5.7 to 5.4 cal kyr BP) characterized by grey clays (related with the increase
301 in siliciclastic material and clays input). Units 3 (SAR ~ 0.03 cm/yr) and 4 (SAR ~ 0.13 cm/yr) correspond
302 with the uppermost 1.15 m (4.7 cal kyr BP) of the record were previously described in Ramos-Román et al.
303 (2018) as clays with high Ca values and showing an increasing trend in K/Si ratio to the top of the record.

304 3.2.2. Organic geochemistry

305 Variations in TOC, C/N and H/C ratios reflect changes in paleoenvironmental dynamics in bogs and
306 lakes (Meyers and Lallier-Vergés, 1999; Ortiz et al., 2010; García-Alix et al., 2017). TOC concentration is
307 the principal indicator of organic matter content in sediments. Typical organic matter contains 50 % of
308 carbon so the concentration of organic matter in sediments is twice the TOC (Meyers et al., 1999). C/N
309 ratio informs about the proportion of algae and terrestrial vascular plant organic matter in the sediments
310 (Meyers, 1994). Fresh organic matter from algae exhibits molar C/N values that are between 4 and 10,
311 whereas cellulose-rich terrestrial plants show values above 20 and greater (Meyers et al., 1994). H/C values
312 are a good proxy for the source of the organic matter in sediments, as algal/bacterial/amorphous remains
313 are richer in hydrogen than herbaceous and woody plant material, with values over 1.7 indicative of
314 algal/amorphous organisms. In addition, lower values of H/C (<0.8) could also be indicative of organic

315 matter transport or diagenesis after deposition (Talbot, 1988; Talbot and Livingstone, 1989).

316 *N*-alkane biomarker abundance and distribution can provide information about different biological
317 sources of organic matter that accumulated in bog and lake sediments (Meyers and Lallier-Vergés, 1999;
318 Ficken et al., 2000; Sachse et al., 2006). Several of these sources are characterized by distinct predominant
319 *n*-alkane chain-lengths that have been identified according to the biological sources to the sediments : (1)
320 In general, *n*-alkanes with 17 or 19 carbon atoms (nC_{17} or nC_{19}) are found predominantly in algae (Gelpi et
321 al., 1970; Cranwell, 1984) and in photosynthetic bacteria (Cranwell et al., 1987), (2) nC_{21} , nC_{23} and nC_{25}
322 are associated with submerged and floating aquatic plants (Cranwell, 1984; Ficken et al., 2000), while (3)
323 *n*-alkane distribution with predominant $> nC_{27}$, nC_{29} , nC_{31} represents higher terrestrial plant input (Cranwell
324 et al., 1987) as well as emergent macrophytes (e.g. *Juncus* sp., *Typha* sp. or *Phragmites australis*)
325 (Cranwell, 1984; Ogura et al., 1990; Ficken et al., 2000). CPI (illustrating the relative abundance of odd vs.
326 even carbon chain lengths) is a proxy for preservation of organic matter in the sediments, with values lower
327 than 2 indicating diagenetic alteration or algal/bacterial influence and, higher than 2 (see Bush et al., 2013
328 review) indicating terrestrial influence and thermal immaturity of the source rock. Ficken et al. (2000)
329 formulated the Paq (proportion of aquatics) to discern the origin of the organic inputs in the sediments,
330 giving average values for present-day plants of <0.1 for terrestrial plants, 0.1-0.4 for emerged aquatics and
331 0.4-1 for submerged/floating aquatic species.

332 García-Alix et al. (2017), however, showed that the interpretation of these *n*-alkane chain length indices
333 cannot be generalized, and the modern *n*-alkanes distribution of the vegetation in the study site should be
334 well understood prior to paleoenvironmental interpretations from core records. Accordingly, to better
335 constrain the origin of the organic input in the Padul-15-05 record, we analyzed *n*-alkanes from present day
336 terrestrial and aquatic plants as well as algae/bryophyte in the Padul basin area (Supplementary information;
337 Figs. S2 and S3). Our results show that the predominant *n*-alkanes in the samples are nC_{27} , nC_{29} and nC_{31} .
338 There is also a strong odd-over-even carbon number predominance (CPI values higher than 2). This basin
339 is currently dominated by wetland plants, such as *Phragmites australis* with predominant carbon chain
340 between C_{27} and C_{29} *n*-alkane. The Paq for present-day plants average values of 0.16 ± 0.16 for terrestrial

341 plants, 0.29 ± 0.34 for aquatic plants and 0.32 ± 0.21 for algae-bryophyte. ACL average values were around
342 28.23 ± 0.74 for emerged-terrestrial plants, 28.78 ± 1.86 for aquatic plants and 27.97 ± 0.74 for algae-
343 bryophyte (Table 3; Supplementary Fig. S3). These results led us to the need to create three new *n*-alkane
344 indices with the goal of characterizing the source of organic matter in our sediment samples from the Padul-
345 15-05 record, taking in consideration the relative abundances of the odd carbon chains except for nC_{27} (due
346 to higher values in all the plant/algae samples): (1) Short-chain (%), where higher values are typical from
347 algae or bacterial, (2) Mid-chain (%), where higher values are typical of aquatic plants, and (3) Long-chain
348 (%), where higher values are obtained when the source is vascular emerged aquatic or terrestrial plants
349 (Table 3).

- 350 1. Short-chain: $[C_{17}-C_{19}] = [(C_{17}+C_{19})/(C_{17}+C_{19}+C_{21}+C_{23}+C_{25}+C_{29}+C_{31}+C_{33})] \times 100$
351 2. Middle-chain: $[C_{21}-C_{23}-C_{25}] = [(C_{21}+C_{23}+C_{25})/(C_{17}+C_{19}+C_{21}+C_{23}+C_{25}+C_{29}+C_{31}+C_{33})] \times 100$
352 3. Long-chain: $[C_{29}-C_{31}-C_{33}] = [(C_{29}+C_{31}+C_{33})/(C_{17}+C_{19}+C_{21}+C_{23}+C_{25}+C_{29}+C_{31}+C_{33})] \times 100$

353 The results for the organic geochemistry (TOC, C/N ratio, H/C ratio and *n*-alkane indices) from the
354 Padul-15-05 record are illustrated in Figure 4. TOC values range from 0.8 to 61%, with an average value
355 of 27.5 %. Highest TOC values are registered during the deposition of sedimentary Unit 1 averaging values
356 of 41 %, associated with the peatland environment and higher values of anoxic/reducing proxies (showing
357 higher correlation with S, Br; Table 4). Higher TOC variability occurred during Unit 2. The transition
358 between Unit 1 and 2 is marked by a TOC decrease with values around 14 % at ~ 7.6 cal kyr BP. Other
359 decreases occurred between 2-1.89 m (~ 6.9 to 6.4 cal kyr BP) and between 1.48-1.39 m (~ 5.7 to 5.4 cal
360 kyr BP), reaching values around 20 and 30 %, respectively. The transition between Unit 2 and 3 (~ 4.7 cal
361 kyr BP/ ~ 1.13 m) is marked by a significant decline to values below 15 %. The lowest TOC values are
362 recorded during Units 3 and 4 with average values around 4.6 %. Atomic C/N ratios were higher during the
363 lithological Units 1 and 2 and ranged between 53 and 11, with an average value of 26. A decrease in C/N
364 occurred during the transition from Units 2 to 3 down to average values of 17. The lowest values occurred
365 during Unit 1, recording C/N values in a range between 14 and 10. Atomic H/C ratios ranged between 1.13

366 and 6.66 with an average value of 1.65. The lowest values were recorded between the bottom of the record
367 and approximately 0.77 m (~ 3.9 cal kyr BP) with ranging values between 1.13 and 2.26 with an average
368 of 1.39. Highest values are depicted from 0.77 m to the top of the record averaging values of 2.62.

369 The *n*-alkane data obtained from the Padul-15-05 sediments show that shorter carbon chains were
370 abundant during Unit 1. CPI values were higher than 2, averaging values of around 7 and representing an
371 odd over even carbon chain and a good preservation of the organic matter in the sediments, the lowest
372 values, with an average of 2.6, occurred during the Unit 1 around 3.07-2.31 m depth (~ 9.7 to 7.6 cal kyr
373 BP), and the highest values averaging 11.8 occurred between 2.31 and 2.15 m depth (from ~7.5 to 7.2 cal
374 kyr BP). Short-chain abundance shows peaks of higher values at 3.10 m (~9.6 cal kyr BP), 2.55 m (~ 8.5
375 cal kyr BP), 2.30 m (~ 7.5 cal kyr BP), 1.40 m (~ 5.4 cal kyr BP), from 1.10 to 0.8 m (~ 4.6-4 cal kyr BP),
376 0.52 m (~ 2.7 cal kyr BP) and from 0.4-0.33 m (~ 1.3-0.8 cal kyr BP). Mid-chain abundance shows the
377 highest values between the bottom and 2.26 m (between ~11.6 and 7.6 cal kyr BP) with an average of
378 approximately 24 %, depicting a maximum between 2.90 and 2.31 m (~9.5 to 7.6 cal kyr BP) with average
379 values of around 40 %. The lowest values are recorded during the last 1.15 m (~4.7 cal kyr BP). Long-chain
380 abundance shows high values averaging ~ 81 % between 2.26 and 1.40 m (~ 7.5 to 5.4 cal kyr BP) and
381 reached maximum values around 0.60 m (~3.2 cal kyr BP) and between 0.45 m (~ 1.9 cal kyr BP), and the
382 last 0.22 cm (~ 0.1 cal kyr BP).

383 3.3. Pollen and Spores

384 Pollen grains from terrestrial, aquatic species and spores were identified and the taxa higher than around
385 1 % were plotted in the pollen diagrams (Supplementary Figures S4, S5 and S6). The most representative
386 taxa are plotted in a summary pollen diagram (Fig. 5). In this study, we used the variations between
387 Mediterranean forest taxa, xerophytes, hygrophytes and algae for paleoenvironmental and paleoclimatic
388 variability in the study area. The fluctuations in arboreal pollen (AP, including Mediterranean tree species)
389 have previously been used in other nearby Sierra Nevada records as a proxy for regional humidity changes
390 (Jiménez-Moreno and Anderson, 2012; Ramos-Román et al., 2016). The abundance of the Mediterranean
391 woods (i.e., evergreen and deciduous *Quercus*, *Olea*, *Pistacia*) has been used as a proxy for climate change
392 in many other studies in the western Mediterranean region, with higher forest development generally
393 meaning higher humidity (Fletcher and Sánchez-Goñi, 2008; Fletcher et al., 2013). On the other hand,
394 increases in xerophyte pollen taxa (i.e., *Artemisia*, *Ephedra*, *Amaranthaceae*), representative of steppe
395 vegetation, have been used as an indication of aridity in this area (Carrión et al., 2007; Anderson et al.,
396 2011). Variability in wetland angiosperms and algae could be indicative of local change in the surrounding
397 vegetation and lake level fluctuations. Singh et al. (1990) suggested that Cyperaceae and *Typha* could be
398 considered swamp- indicative when co-occurring with freshwater algae (*Cosmarium*, *Zygnemataceae*).
399 Currently, the dominant plant species in the Padul wetland is the common reed, *Phragmites australis*, in
400 fact very common in semi-arid wetlands with shallow water levels (Moro et al., 2004). This species has
401 thrives whenever a wetlands becomes drier (Hudon, 2004). Van Geel et al. (1983) described the occurrences
402 of *Zygnema* and *Mougeotia* as characteristic of shallow lake water environments. The chlorophyceae
403 *Botryococcus* is an indicator of freshwater environments in relatively productive fens, temporary pools,
404 ponds or lakes (Guy-Ohlson, 1992). Clausen (1999) point out that *Botryococcus* abundance is higher in
405 sediment of shallow water lakes and/or littoral environment in deeper lakes. Three pollen zones were
406 visually identified with the help of a cluster analysis using the program CONISS (Grimm, 1987).

407 The pollen results are described subsequently, distinguishing three major phases during the Holocene:

408 3.3.1. From ~ 11.6 to 7.6 cal kyr BP (from ~ 3.67 to 2.31 m)

409 The early and early middle Holocene, from ~ 11.6 to 7.6 cal kyr BP, is characterized by high abundance
410 of Mediterranean forest, averaging relative percentage values of approximately 58%. The most
411 representative arboreal tree taxon between ~ 11.6 to 9.7 cal kyr BP is evergreen *Quercus*, reaching
412 maximum values of around 50%. A decrease in the Mediterranean forest and an increase in hygrophytes
413 and Poaceae occurred between 10.1 and 9.6 cal kyr BP (from 3.28 to 3.01 m). Deciduous *Quercus* show
414 increasing trends between 9.5 and 7.6 cal kyr BP (~ 2.91 to 2.31 m), recording average maxima with values
415 of around 22% at that time. Hygrophytes reach maxima average values of approximately 17%, from ~ 9.8
416 to 8.8 cal kyr BP (from 3.16 to 2.63 m). Algae display a decreasing trend from around 9% (from ~ 11.6 to
417 9.9 cal kyr BP/3.67 to 3.20 m) to 2% (from ~ 9.9 to 7.6 cal kyr BP/3.20 to 2.34 m). These algae decline
418 between ~ 11.6 and 9.9 cal kyr BP is due to the lowering of *Zygnema* spores. An increase in the soil
419 mycorrhizal fungus *Glomus* type occurs from ~9.6 to 9.3 cal kyr BP (from 3.01 to 2.80 m).
420 This transition between the early and middle Holocene is featured by a slight decrease in deciduous *Quercus*
421 and in wetland plants such as Cyperaceae and *Typha* type.

422 3.3.2. From ~ 7.6 to 4.7 cal kyr BP (from ~ 2.34 to 1.15 m)

423 The middle Holocene from ~ 7.6 to 4.7 cal kyr BP is still characterized by high values of Mediterranean
424 forest (averaging values of ~ 58%) interrupted by several events of forest decrease. One of the most
425 significant Mediterranean forest declines (up to 26%) parallel hygrophyte and Poaceae rise between ~ 7.5
426 and 7.3 cal kyr BP (2.28 to 2.21 m). A slight increase in algae also occurred around ~ 7.6 to 7.1 cal kyr BP
427 (2.31 to 2.11 m). A second decrease in the Mediterranean forest occurred at ~ 6 cal kyr BP (from around
428 1.65 m), also characterized by the increase in hygrophytes to maximum values around 40%, and the
429 increase in *Pinus* of around 5 to 12%. A third remarkable decrease in Mediterranean forest occurred
430 between ~ 5.5 to 5.4 cal kyr BP (around 1.43 to 1.39 m), also characterized by the increase of the aquatic

431 component. These three previous events of decrease in forest decline are accompanied by slight *Glomus*
432 type increases.

433 3.3.3. *From ~ 4.7 cal kyr BP to Present (from ~ 1.15 m to top)*

434 The middle to late Holocene transition (~ 4.7 cal kyr BP/~ 1.15 m) is characterized by the decrease in
435 Mediterranean forest, in particular in the deciduous tree taxa, and the increase in *Pinus*, shrubs (i.e.,
436 Ericaceae) and xerophytes and Asteraceae (mainly Cichorioideae) (Ramos-Román et al., 2018).

437 3.4. *Spectral analysis*

438 Spectral analysis was performed on the pollen percentage record in order to find cyclical periodicities
439 in the Mediterranean forest from the Padul-15-05 record using REDFIT analysis (Schulz and Mudelsee,
440 2002) detecting a periodicities of around ~ 2070, 1430 and 1100 yr. Wavelet analyses show significant
441 cycles ($p = 0.05$) in the Mediterranean forest taxa time series with periodicities around ~ 2070 and 1100 yr
442 during the early and middle Holocene period and ~ 1430 yr periodicity since ~ 4.7 cal kyr BP to Present
443 (Supplementary Figure S7).

444 4. Discussion

445 4.1. *Holocene climate change in Padul and the western Mediterranean region*

446 4.1.1. *The earliest Holocene*

447 During the earliest Holocene (~ 11 to 10 cal kyr BP) a transition period from glacial to interglacial
448 conditions occurred in the Padul area and the pollen assemblages were dominated by evergreen *Quercus*
449 and to a lesser extent, mesic forest species such as deciduous *Quercus*. Local environment proxies show a
450 development of a peatland environment in the Padul basin (organic facies featured by higher values of TOC
451 and C/N and lower values of mid-chain, short-chain and S; Fig. 6), which indicate low water levels at that
452 time. The increase in Mediterranean forest taxa may be interpreted as a regional vegetation response to a

453 climate change to warmer and more humid conditions than earlier on during the cold and dry Younger
454 Dryas, agreeing with the increasing trend in SSTs reconstructions from the Alboran Sea (Cacho et al., 1999;
455 Martrat et al., 2004; Rodrigo-Gámiz et al., 2014b; Fig. 7; Supplementary Fig. S8). The observed peak of
456 evergreen *Quercus* is consistent with previously described glacial-interglacial vegetation transition from
457 Southern Europe indicating that a cold-dry steppe was followed by pre-temperate open woodland [including
458 *Juniperus*, *Pinus*, *Betula*, *Quercus*; van der Hammen et al. (1971)]. These results agree with the previous
459 pollen records from Padul, which also show a widespread evergreen *Quercus* forest after the postglacial
460 epoch (Pons and Reille, 1988) and other high-resolution pollen studies in the western Mediterranean region
461 that show a similar forest change with high abundance of Mediterranean taxa (Fletcher and Sanchez-Goñi
462 et al., 2008; Fig. 7). These results are also consistent with vegetation variability in the Middle Atlas
463 Mountains of Morocco depicting high values of evergreen *Quercus rotundifolia* at that time (Lamb and van
464 der Kaars, 1995). A forest expansion is also observed in the nearby, but higher elevation site, Laguna de
465 Rio Seco in Sierra Nevada (Supplementary Fig. S8), but in this case, it is mostly due to *Pinus* expansion
466 after a pollen assemblage dominated by steppe vegetation (Anderson et al., 2011; Fig. 7). This dissimilarity
467 is probably explained by the altitudinal difference between the two sites (Padul=750 m vs. Laguna de Rio
468 Seco=3000 m), being influenced by different vegetation belts (mesomediterranean vs. oromediterranean
469 belt; see Table 1). The continental pollen record of the cave site Carihuela, inland Granada at the
470 supramediterranean altitude, also shows a clear oak dominance during this period (Carrión et al., 1999;
471 Fernández et al., 2007).

472 A punctual increase in algae (principally dominated by *Zygnema* type) also occurred within this peat-
473 dominated and shallow water period at around ~ 10.5 cal kyr BP. We suggest that this increase in algae
474 could probably be linked with an increase in productivity in the wetland resulting from increased
475 temperatures during a warm pulse recorded in the North Atlantic ice record (Bond et al., 2001; Fig. 8).

476 4.1.2. *Early and middle Holocene and Humidity optimum*

477 The early to middle Holocene (from ~ 10 to 4.7 cal kyr BP) in the Padul-15-05 record is featured by

478 the highest values of Mediterranean forest showing the expansion in mesic components (e.g. deciduous
479 *Quercus*), agreeing with the temperate phase of vegetation transition during interglacial periods (described
480 by van der Hammen et al., 1971 and reviewed by Tzedakis et al., 2007; Supplementary Fig. S9). The local
481 Padul wetland environment within this period (~ 10 to 4.7 cal kyr BP) was characterized by generally low
482 water levels, triggering high occurrence of wetland plants, which accumulated in great amounts, generating
483 peat sedimentation related with higher organic content and/or anoxic/reducing conditions and associated
484 geochemical signals (i.e. higher values of TOC, C/N, S and an increase in mid-chain; Figs. 4 and 6). There
485 is an apparent contradiction between the regional vegetation signal, which indicates high humidity, and
486 local sedimentary proxies, which pointing to low water levels in the area. This contradiction could be
487 explained due to very strong evapotranspiration rates during Holocene summer insolation maxima (Laskar
488 et al., 2004) even if annual (mostly winter) precipitation was the highest (Fig. 6). Low lake levels during
489 the regionally humid early Holocene have also been observed in other records from the southern
490 Mediterranean area, pointing to the same high-evaporative summer insolation phenomenon (Lamb and van
491 der Kaars, 1995; Reed et al., 2001; Magny et al., 2007).

492 Despite the overall humid conditions interpreted for the early and middle Holocene, millennial-scale
493 climate variability occurred (see section 4.1.4 below) and wettest conditions are observed between ~ 9.5 to
494 7.6 cal kyr BP in the Padul-15-05 record. This humidity optimum is indicated regionally by the maximum
495 expansion of mesic forest species (deciduous *Quercus*). Our new results from Padul agree with the
496 previously described Holocene climate evolution in the western Mediterranean region, which also show a
497 wetter early and middle Holocene and a transition to drier conditions during the late Holocene (Fletcher et
498 al., 2013; Anderson et al., 2011; Carrión et al., 2010 among others). The maximum in humidity occurred
499 during summer insolation maxima and thus during the warmest Holocene conditions shown by paleoclimate
500 records such as the Greenland ice core record temperature reconstruction (Alley, 2000), the decrease in the
501 Drift Ice Index in the north Atlantic records and in total solar irradiance (TSI) and regionally the SST
502 reconstructions in the Alboran Sea (Bond et al., 2001; Cacho et al., 1999; Rodrigo-Gámiz et al., 2014b;
503 Steinhilber et al., 2009; Figs. 7 and 8). Support for the timing of the Holocene humidity optimum recorded

504 in Padul-15-05 comes from a number of paleoclimatic studies from nearby places. For example, previous
505 pollen results from the Padul sedimentary sequence show a similar increase in deciduous *Quercus* and
506 maximum humidity at the same time (Pons and Reille, 1988; Fig. 7). The nearby alpine site of Laguna de
507 Rio Seco in Sierra Nevada indicates that the early and middle Holocene is characterized by more abundant
508 mesic vegetation and the maximum in algae and aquatic plants, indicating that humid maximum occurred
509 prior to ~ 7.8 cal kyr BP (Anderson et al., 2011). Jimenez-Espejo et al., (2008) in a study in the Algero-
510 Balearic basin described that the end of the Holocene, humid conditions occurred between ~ 7.7 and 7.2 cal
511 kyr BP and a synthesis about circum-Mediterranean vegetation change analysis determined that two
512 principal climatic phases occurred during the early and middle Holocene, with a more humid phase from
513 11 to 7.5 cal kyr BP and a transition phase from 7 to 5.5 cal kyr BP, the later one mostly related to decreasing
514 insolation and the installation of the present climate dynamics (Jalut et al., 2009). Dormoy et al. (2009) also
515 described the maximum in humidity in the Mediterranean region during the early and middle Holocene
516 between 9.5 and 7.5 cal kyr BP, resulting from maximum seasonal anomaly characterized by greatest winter
517 precipitation and minima in precipitation during summer. However, some discrepancies exist about the
518 timing of the mesic maximum within this generally humid period in the Mediterranean region and
519 continental and marine records from southern Iberia and north Africa pointed out that the mesic maximum
520 occurred later on during the middle Holocene (Lamb and van der Kaars, 1995; Carrión, 2002; Fletcher and
521 Sánchez-Goñi, 2008). Supporting our hypothesis, Anderson et al. (2011) suggested that this difference in
522 timing between montane and subalpine forest development and water lake levels could be associated to the
523 different effect that summer insolation maxima and higher seasonality provoked in effective precipitation
524 and water levels during the early Holocene. In lower elevation with higher evaporations rates during
525 summer, compared to higher elevation areas and alpine lakes with lower summer temperatures and higher
526 snowpack during winter and subsequently high lake level.

527 The early Holocene thermal maximum could be explained by maximum orbital-scale summer
528 insolation (Laskar et al., 2004; Figs. 6 and 8). The early Holocene humidity maximum was likely due to
529 enhanced fall/winter precipitation, consistent with global climate models predicting that summer insolation

530 maxima favor the land/sea temperature contrast in the Mediterranean thus enhancing the winter rainfall
531 (Meijer and Tuenter, 2007).

532 This occurred at the same time that the Intertropical Convergence Zone was displaced northward (prior
533 to ~ 6 ka) into the Sahara and Arabian deserts (Gasse and Roberts, 2004). However, Arz et al. (2003) and
534 Tzedakis (2007) concluded that summer monsoon did not reach further than the African subtropical desert
535 during the early and middle Holocene and would not have had a direct influence over the northern
536 Mediterranean coast.

537 Sedimentation at that time in the Padul basin is homogeneous peat but the local proxies show some
538 oscillations (see in section 4.1.4).

539 *4.1.3. End of the humid period and significant environmental change around 4.7 cal kyr BP*

540 The Padul-15-05 record shows the most significant climatic change affecting both regional and local
541 environment at ~ 4.7 cal kyr BP, right at the middle to late Holocene transition. This paleoenvironmental
542 change is regionally depicted by the beginning of a strong decrease in Mediterranean (especially in the
543 deciduous) forest, indicating progressive climate drying conditions, a slight increase in *Pinus*, and an
544 increase in Ericaceae (Ramos-Román et al., 2018). The significant development of heathlands (Ericaceae)
545 during the middle to late Holocene transition could be indicative of reduced insolation under still a relatively
546 humid climate. This agrees with other studies that show that heathlands increased under increasing
547 precession (decreasing summer insolation), suggesting a thriving response to reduced thermal seasonality
548 (Fletcher and Sánchez-Goñi et al., 2008). Similar vegetation changes, with the decline in mesic forest
549 species and the increase in shrubs such as Ericaceae, have previously been recorded in other terrestrial and
550 marine pollen archives from the western Mediterranean region during the transition to the late Holocene
551 (e.g., Carrión 2002; Carrión et al., 2003; 2007; 2010b; Fletcher and Sánchez-Goñi, 2008;) pointing to a
552 regional response to climate aridification and reduction in seasonality (i.e. cooler summers and warmer
553 winters). The timing of this change agrees with Magny et al. (2002) who described the period at 4.5 cal kyr

554 BP, as a crucial transition from wetter to drier climate in the Mediterranean region. In addition, Jalut et al.
555 (2009), described the aridification process in the Mediterranean region since 5.5 cal kyr BP.

556 This climatic change also locally affected the Padul wetland environment, and sedimentation changed
557 drastically from mostly peat (unit 2) to carbonate-rich clays (unit 3) rich in aquatic organisms (charophytes
558 and gastropods; between ~ 4.7 to 1.5 cal kyr BP; Ramos-Román et al., 2018) pointing to an increase in the
559 lake level. This sedimentary change is principally featured in the geochemistry by a decrease in organic
560 content, a decrease in the aquatic plants in the lake [lower values of TOC (Ramos-Román et al., 2018), C/N
561 and generally decrease in mid-chain abundance], an increase in Ca and in the palynomorph record by a
562 continuously increase in algae (principally dominated by *Botryococcus*; Ramos-Román et al., 2018). In
563 addition, a higher terrestrial and detrital input occurred during the aridification trend, observed in the Padul-
564 15-05 sequence by a slight increasing trend in soil erosion (*Glomus*) and clastic input (higher K/Si), most
565 likely due to the decrease in Mediterranean forest in the area.

566 As discussed above, there seems to be a contradiction between regional proxies, showing increased
567 aridity, and local proxies showing increasing lake levels. This could be explained due to varied effect of
568 the orbital-scale decrease in summer insolation in both environments. A decrease in summer insolation
569 would trigger a decrease in the sea surface temperature reducing the wind system and precipitation from
570 sea to shore during winter (Marchal et al., 2002) and would also shorten the length of the growing season
571 thus provoking forest depletion. However, decreasing summer insolation would also reduce the seasonality
572 and would lower evapotranspiration during summer, affecting the evaporation/precipitation balance. This
573 along with the continuous groundwater supply in the Padul basin would explain the increasing lake levels
574 in the Padul wetland during the late Holocene (Fig. 6). Some authors also related this aridification trend to
575 the establishment of the current atmospheric dynamics with a northward shift of the westerlies -and as
576 consequence a long-term NAO-like positive mode- affecting the western Mediterranean region (Magny et
577 al., 2012). In addition, this climatic shift coincided with the end of the African Humid Period (5.5 ka;
578 deMenocal et al., 2000). Shanahan et al. (2015) suggested that the decrease in rainfall at this time shown in

579 the African paleoclimate records (tropical and subtropical Africa) is related to declining summer insolation
580 and the gradual southward migration of the tropical monsoon.

581 A general decreasing trend in SST is recorded in the Alboran Sea since around 4-3 cal kyr BP (Figs. 7
582 and 8; Cacho et al., 1999; Martrat et al., 2004; Rodrigo-Gámiz et al., 2014b), which supports our hypothesis
583 of a lower sea/land temperature contrast. However, the higher resolution study of Rodrigo-Gámiz et al.
584 (2014b) shows increasing SST superimposed between the generally decreasing trend, coinciding with
585 wetter periods such as for example the end of the Iberian-Roman Humid Period.

586 Within the context of regional progressive aridification, the late Holocene (*sensu lato*) from Padul could
587 mainly be divided into two phases, a first phase from ~ 4.7 to 3 cal kyr BP characterized by the slight
588 increasing trend in *Botryococcus* and the declining trend in mid-chain abundance, and a second phase from
589 ~ 3 to 1.5 cal kyr BP featured by maximum values in *Botryococcus* and a minimum in mid-chain abundance
590 (Fig. 6). Relative maxima in Mediterranean forest between ~ 2.6 and 1.6 cal kyr BP, indicating regional
591 humidity, co-occurred with the maximum in *Botryococcus* algae also indicating either high relative lake
592 level and/or more productivity in the lake (Ramos-Román et al., 2018). High relative humidity in this region
593 is supported by the fact that this mild climatic event occurred during the well-known Iberian Roman Humid
594 Period (IRHP) between 2.6 to 1.6 cal kyr BP (Martín-Puertas et al., 2009).

595 The aridification trend enhanced around ~ 1.5 cal kyr BP and culminated with a further environmental
596 change to an ephemeral lake (even emerged during the last centuries). This is deduced by the remarkable
597 increase in detritic sedimentation (K/Si; Fig. 6), probably due to higher soil erosion (increase in *Glomus*
598 type) partially enhanced by human activities in the surroundings of the lake since this time (Ramos-Román
599 et al., 2018), and by a continuous increase in mid-chain, short-chain abundance and wetland plants while
600 *Botryococcus* and other aquatic organisms (especially charophytes) declined. Aquatic plants probably
601 expanded in the Padul wetland area when the water levels dropped. This increasing trend in mid-chain and
602 short-chain abundances started to decline during the last centuries when the wetland became emerged and
603 higher human impact occurred (for more information about human activities see Ramos-Román et al.,
604 2018).

605 The ~ 4.7 to Present natural aridification process was interrupted by millennial-scale climate variability
606 with several especially arid events occurring around ~ 4.7-4, 2.7 and 1.3 cal kyr BP (see next section; 4.1.4)

607 4.1.4. *Millennial-scale Holocene climate variability*

608 In addition to the long-term trends observed in the Padul paleoenvironments, likely driven by
609 insolation-related climate changes during the Holocene, the high-resolution multi-proxy record from Padul-
610 15-05 record shows millennial-scale vegetation, lake level and sedimentary oscillations that can be related
611 with global climate variability and cooling events detected in North Atlantic archives. In this respect, the
612 Padul-15-05 sequence shows arid-cooling climatic events around ~ 9.6, 8.5, 7.5, 6.5, 5.4, 4.7-4, 2.7 and 1.3
613 cal kyr BP, generally identified in both regional (decreases in the Mediterranean forest suggesting regional
614 cooling and aridity) and local proxies (increases in clays input, short-chain, mid-chain and hygrophyte) and
615 with periodicities of about 2100 and 1100 years. These short-scale climatic changes affected sedimentation
616 and local lake level in the Padul environment, generally with increases in carbonate (charophytes and
617 gastropods) and clastic sedimentation, hygrophytes, short-chain and mid-chain abundances pointing to
618 higher lake levels probably triggered by cooling and less evaporation in the wetland, enhanced erosion due
619 to deforestation and increase in plants adapted to more aquatic wetland environments (Fig. 6). Some of
620 these events are manifested in the Padul-15-05 record clearly in both regional and local proxies (~ 9.6, 7.5,
621 5.4, 4.7-4, 2.7, 1.3 cal kyr BP) but some others are more evident in the local signal (for example events at
622 8.5 and 6.5 cal kyr BP). The two latter ones probably indicating that those events were less severe and/or
623 problems recording them sufficiently well in the pollen. During the last ~ 4.7 cal kyr BP, during the
624 establishment of the modern climatic dynamics and the decrease in summer insolation, a shallow lake
625 formed and these cold events are also associated with declines in the lake productivity (for example,
626 reductions in algae before and after the IRHP; Fig. 6).

627 Most of these climatic events have been described in other Mediterranean paleoclimate records, considering
628 the radiocarbon age uncertainties between the different studies. For example, Jalut et al. (2000) also
629 described aridification phases for the western Mediterranean region around ~10.9-9.7, 8.4-7.6 and 5.3- 4.2,

630 4.3-3.4, 2.8-1.7 and 1.3-0.75 cal kyr BP, showing that these events were correlated with glacial advances,
631 ¹⁴C anomalies, North Atlantic records and paleohydrological changes in European mid-latitudes suggesting
632 that they were a regional response to global climate change. Some arid events around ~9.6-9.5, 8.4-8 and
633 6-5.5 cal kyr BP, have been also identified as arid and cool events in a study from the eastern and western
634 Mediterranean region (Dormoy et al., 2009). Fletcher and Zielhofer (2013) detected this rapid climate
635 changes relating these arid periods with high-latitude cooling events around 6-5 and 3.5-2.5 cal kyr BP.
636 Recently, Zielhofer et al. (2017) show a decrease in western Mediterranean winter rain at 11.4, 10.3, 9.2,
637 8.2, 7.2, 6.6, 6.0, 5.4, 5.0, 4.4, 3.5, 2.9, 2.2, 1.9, 1.7, 1.5, 1.0, 0.7, and 0.2 cal kyr BP. They associated these
638 events during the early Holocene with Atlantic coolings probably related with meltwater discharges and
639 weakening of the Atlantic overturning circulation. In contrast, after ~5 cal kyr BP, they related these
640 Atlantic cooling episodes to humid winters and negative NAO conditions evidencing a change in the ocean-
641 atmospheric system in response to the external forcing. In the nearby Sierra Nevada, arid events are detected
642 around 3.8-3.1 and 1.8-0.7 cal kyr BP (Laguna de la Mula; Jiménez-Moreno et al., 2013). Cold and arid
643 events detected in the Padul-15-05 record at ~9.6, 8.5, 7.5, 6.5, 5.4, 4.7-4, 2.7 and 1.3 cal kyr BP have been
644 also identified in North Atlantic records (Bond events 6, 5, 4, 3, 2, 1; Bond et al., 2001; Fig. 8), which
645 indicate that these events were recorded at hemispheric scales. The good correspondence with the timing
646 of these cold events with decreases in solar activity recorded by the TSI anomaly during the Holocene could
647 show a link between them (Steinhilber et al., 2009; Fig. 8). The correlation between the Mediterranean
648 forest from Padul and TSI anomaly ($r = 0.43$; $p < 0.001$ between ~9.4 to 4.7 cal kyr BP and $r = 0.37$; $p <$
649 0.001 between 4.7 cal kyr BP to present) seems to show that a link exists between solar and environmental
650 variability in the Mediterranean area. This would agree with previous studies showing a sun-climate-
651 environment relationship (Zielhofer et al., 2017). However, we are still far to understanding how solar
652 activity affects climate and deeper studies are necessary in order to provide with information about the
653 behavior between solar, climate and environmental relationships and the link between the Mediterranean
654 and North Atlantic regions.

655 4.1.5. *Forcing mechanisms of Holocene millennial-scale climate variability in the western Mediterranean*
656 *region*

657 The time series analysis done on the Mediterranean forest (regional proxy) from the Padul-15-05 record
658 using wavelet analysis shows millennial-scale cyclical periodicities during the early, middle and late
659 Holocene. This analysis helps to understand the relationship between the regional paleoenvironmental
660 periodicity in the proxy data from the Padul record and external (i.e. solar activity) and internal (oceanic-
661 atmospheric dynamics) forcings during the Holocene in the western Mediterranean. Cyclicities of around
662 ~ 2100 yr and ~ 1100 yr are detected in the Mediterranean forest taxa time series with a statistically strong
663 cyclical pattern during the early and middle Holocene (the ~ 1100 yr cycle is absent in the late Holocene),
664 and a predominant ~ 1430 yr cycle between the transition of the middle-late Holocene and during the late
665 Holocene (Supplementary Fig. S7). This later cycle could be carefully linked to human impact, which could
666 have altered the natural climatic signal and is recorded in this area since the last ~ 1500 yr (Ramos-Román
667 et al., 2018).

668 Our results are consistent with similar cyclical patterns detected throughout the North Atlantic records
669 and related with solar activity also describing ~ 2500 and 1000 yr periodicities during the early Holocene
670 (Debret et al., 2007; 2009). A similar periodicity of about 2300 yr is recognized in the $\Delta^{14}\text{C}$ residual series
671 from the Greenland Ice Sheet record (Mayewski et al., 1997). This periodicity has also been evidenced in
672 sea surface temperatures (SST) reconstructions in the Aegean Sea in the NE Mediterranean related with
673 glacier advance and suggesting a solar modulation (Rohling et al., 2002). The ~ 1000 yr periodicity is also
674 established as a signal of solar activity in many other records in the Mediterranean and the North Atlantic
675 region (e.g. Debret; 2007; 2009 and references therein). Previous cyclostratigraphic analysis performed in
676 the nearby Sierra Nevada alpine area also described cyclical climatic fluctuations with periodicities around
677 2200 yr (Jiménez-Espejo et al., 2014). In contrast, other spectral analyses carried out in other records in the
678 North Atlantic and western Mediterranean region detected a periodicity of around ~ 1500 yr (e.g. Bond et
679 al., 2001; Rodrigo-Gámiz et al., 2014a). This ~ 1500 yr cycle is also common in other Sierra Nevada records

680 (Jiménez-Espejo et al., 2014; García-Alix et al., 2017) and was interpreted as a solar and atmospheric-
681 oceanic forcing mechanism. In addition, a cycle of ~ 800 - 760 yr has also been detected in the detailed
682 studied of the late Holocene part of the Padul-15-05 record (Ramos-Román et al., 2018) and in other records
683 in the Sierra Nevada (Ramos-Román et al., 2016). This cycle could be related to the second harmonic of
684 the ~ 1600 - 1500 yr cycle. These results show very mixed interpretations with both solar and/or oceanic
685 forcing mechanisms being described to explain cyclicities in the different proxies. Debret et al. (2009) in a
686 non-stationary time series analysis tried to differentiate the different forcing mechanisms for the different
687 cyclicities and also described an intensification of the ~ 1600 yr period detected in the North Atlantic area
688 (terrestrial and marine records and interpreted of both solar and oceanic origin) in the last 5000 years. Those
689 authors then interpret this cyclical periodicity change as a shift in dynamics from mostly external (solar)
690 forcing to mostly internal (oceanic) forcing.

691 According to this, the results from the Padul-15-05 Holocene record suggest that the regional climate
692 variability during the early and middle Holocene was partially due to external forcing (i.e. solar irradiance)
693 and variability during the late Holocene (since ~ 4.7 cal kyr BP) was dominated by the effect of internal
694 forcing (atmospheric-oceanic dynamic) -established since the NAO system influencing the western
695 Mediterranean region- enhanced since ~ 5 cal kyr BP (Debret et al., 2007; 2009). Fletcher et al. (2013)
696 described a shift in the millennial-scale periodicity since around ~ 6 cal kyr BP related with the
697 establishment of the actual climate system in the western Mediterranean region. The similarities between
698 the millennial-scale oscillations observed in the Padul-15-05 record with the total solar irradiance anomaly
699 (TSI) and cooling events in the North Atlantic region (e.g. Bond et al., 2001; Steinhilber et al., 2009; Fig.
700 8) support the solar-atmospheric-oceanic link in the Atlantic-western Mediterranean region previously
701 suggested (Debret et al., 2009).

702 **5. Conclusions**

703 Variations in regional and local paleoenvironmental and paleoclimate proxies from the Padul-15-05
704 Holocene record helped to interpret climate and paleoenvironmental change during the last 11,600 years in

705 southern Iberia and the western Mediterranean region. The comparison of our record with other regional
706 and global oceanic-atmospheric-terrestrial studies aided to comprehend the origin of these
707 paleoenvironmental changes.

708 The early and middle Holocene was characterized by overall humid and warm conditions and a
709 humidity optimum between ~ 9.5 and 7.6 cal kyr BP, humid winters and very hot and dry summers and a
710 higher seasonality, occurred in this area due to summer insolation maxima. These interpretations come from
711 the highest occurrence of deciduous tree species and humid conditions in the local environment (higher
712 mid-chain abundance) in the Padul-15-05 core. Summer insolation maxima translated into very high
713 evaporation rates and lowest lake level conditions triggering the abundance of wetland plants and the
714 deposition of peat related with the higher TOC. A transition phase towards drier conditions is recorded in
715 the middle Holocene between ~ 7.6 and 4.7 cal kyr BP through a decrease in deciduous forest and a higher
716 water level variability mainly associated with variations in Ca, S, K/Si ratio and TOC content. This
717 environmental change was probably due to a reduction in seasonality and decreasing summer insolation,
718 which also locally triggered less evaporation and the alternation of water level increase within a peatland
719 environment. This climate transition culminated in the Padul area with a significant environmental change
720 at ~ 4.7 cal kyr BP, featured by a regional aridification trend that produced a decreasing trend in the
721 Mediterranean forest. Precipitation decreased in the late Holocene but the decrease in summer insolation
722 locally triggered less evaporation and the development of a shallow water lake environment and a
723 significant sedimentary change characterized by higher values of Ca an increasing trend in clay minerals
724 (K/Si ratio), and the decrease in TOC. The Padul shallow lake environment became ephemeral since ~ 1.5
725 cal kyr BP and even emerged during the last centuries probably induced by human impact.

726 The Padul-15-05 record also shows millennial-scale climate variability with declines in Mediterranean
727 forest showing cool-arid events and variability in the lake level around 9.6 , 8.5 , 7.5 , 6.5 , 5.4 , $4.7-4$, 3 , 2.7
728 and 1.3 cal kyr BP, associated with cold events in the North Atlantic records. According to the regional
729 (Mediterranean forest taxa) paleoclimate results from the non-stationary time-series analyses, climate
730 during the early and middle Holocene could have been influenced by external solar forcing with typical

731 periodicities around 1100 and 2100 yrs, and the last ~ 4700 years could have been associated with an
732 internal oceanic/atmospheric control (also in part related with solar forcing) as periodicities changed
733 towards ~ 1430 yr in the regional paleoclimate proxy. However, this later periodicity has to be taken
734 carefully as human impact is evident in the area during the last 1500 yr, probably altering somehow the
735 climatic record.

736 We would like to emphasise on the importance of carrying out multi-proxy analyses containing both
737 regional and local signals and a non-stationary time-series analysis in order to clarify the links between
738 terrestrial-oceanic-atmospheric connections in Holocene paleoclimatic studies.

739 **Acknowledgments**

740 This work was supported by the project P11-RNM-7332 funded by Consejería de Economía,
741 Innovación, Ciencia y Empleo de la Junta de Andalucía, the project CGL2013-47038-R funded by
742 Ministerio de Economía y Competitividad of Spain and fondo Europeo de desarrollo regional FEDER and
743 the research group RNM0190 (Junta de Andalucía). M. J. R.-R. acknowledges the predoctoral and
744 postdoctoral funding provided by Consejería de Economía, Innovación, Ciencia y Empleo de la Junta de
745 Andalucía (P11-RNM-7332). J.C. acknowledges the PhD funding provided by Ministerio de Economía y
746 Competitividad (CGL2013-47038-R). J.S.C. acknowledges the support of projects CGL-BOS-2012-34717,
747 CGL-BOS 2015-68604, and Fundación Séneca 19434/PI/14. A.G.-A. was also supported by a Ramón y
748 Cajal Fellowship RYC-2015-18966 of the Spanish Government (Ministerio de Economía y Competitividad).
749 Javier Jaimez (CIC-UGR) is thanked for graciously helping with the coring, the drilling equipment and
750 logistics. We would also like to thank to two anonymous reviewers and the editor (Fabienne Marret-Davies)
751 for their valuable suggestions.

752 **References**

- 753 Alpert, P., Baldi, M., Ilani, R., Krichak, S., Price, C., Rodó, X., Saaroni, H., Ziv, B., Kishcha, P., Barkan, J., Mariotti,
754 A., Xoplaki, E., 2006. Chapter 2 Relations between climate variability in the Mediterranean region and the
755 tropics: ENSO, South Asian and African monsoons, hurricanes and Saharan dust. *Developments in Earth and*
756 *Environmental Sciences* 4, 149–177. doi:10.1016/S1571-9197(06)80005-4
- 757 Anderson, R.S., Jiménez-Moreno, G., Carrión, J.S., Pérez-Martínez, C., 2011. Postglacial history of alpine vegetation,
758 fire, and climate from Laguna de Río Seco, Sierra Nevada, southern Spain. *Quaternary Science Reviews* 30,
759 1615–1629. doi:https://doi.org/10.1016/j.quascirev.2011.03.005
- 760 Arz, H.W., Lamy, F., Pätzold, J., Müller, P.J., Prins, M., 2003. Mediterranean Moisture Source for an Early-Holocene
761 Humid Period in the Northern Red Sea. *Science* 300, 118. doi:10.1126/science.1080325
- 762 Bar-Matthews, M., Ayalon, A., Gilmour, M., Matthews, A., Hawkesworth, C.J., 2003. Sea–land oxygen isotopic
763 relationships from planktonic foraminifera and speleothems in the Eastern Mediterranean region and their
764 implication for paleorainfall during interglacial intervals. *Geochimica et Cosmochimica Acta* 67, 3181–3199.
765 doi:https://doi.org/10.1016/S0016-7037(02)01031-1
- 766 Beug, H.-J.: Leitfaden der Pollenbestimmung für Mitteleuropa und angrenzende Gebiete, Fisch. Stuttg., Leitfaden der
767 Pollenbestimmung für Mitteleuropa und angrenzende Gebiete, Friedrich Pfeil, München, 61, 2004.
- 768 Bond, G., Kromer, B., Beer, J., Muscheler, R., Evans, M.N., Showers, W., Hoffmann, S., Lotti-Bond, R., Hajdas, I.,
769 Bonani, G., 2001. Persistent Solar Influence on North Atlantic Climate During the Holocene. *Science* 294,
770 2130. doi:10.1126/science.1065680
- 771 Cacho, I., Grimalt, J.O., Pelejero, C., Canals, M., Sierro, F.J., Flores, J.A., Shackleton, N., 1999. Dansgaard-Oeschger
772 and Heinrich event imprints in Alboran Sea paleotemperatures. *Paleoceanography* 14, 698–705.
773 doi:10.1029/1999PA900044
- 774 Cacho, I., Grimalt, J.O., Canals, M., Sbaiffi, L., Shackleton, N.J., Schönfeld, J., Zahn, R., 2001. Variability of the
775 western Mediterranean Sea surface temperature during the last 25,000 years and its connection with the
776 Northern Hemisphere climatic changes. *Paleoceanography* 16, 40–52. doi:10.1029/2000PA000502
- 777 Carrión, J.S., 2002. Patterns and processes of Late Quaternary environmental change in a montane region of
778 southwestern Europe. *Quaternary Science Reviews* 21, 2047–2066. doi:https://doi.org/10.1016/S0277-
779 3791(02)00010-0
- 780 Carrión, J.S., Fernández, S., González-Sampériz, P., Gil-Romera, G., Badal, E., Carrión-Marco, Y., López-Merino,
781 L., López-Sáez, J.A., Fierro, E., Burjachs, F., 2010b. Expected trends and surprises in the Lateglacial and
782 Holocene vegetation history of the Iberian Peninsula and Balearic Islands. *Review of Palaeobotany and*
783 *Palynology* 162, 458–475. doi:http://dx.doi.org/10.1016/j.revpalbo.2009.12.007
- 784 Carrión, J.S., Munuera, M., Navarro, C., Burjachs, F., Dupré, M., Walker, M.J., 1999. The palaeoecological potential
785 of pollen records in caves: the case of Mediterranean Spain. *Quaternary Science Reviews* 18, 1061–1073.
786 doi:10.1016/S0277-3791(98)00002-X
- 787 Carrión, J.S., Sánchez-Gómez, P., Mota, J.F., Yll, R., Chaín, C., 2003. Holocene vegetation dynamics, fire and grazing
788 in the Sierra de Gádor, southern Spain. *The Holocene* 13, 839–849. doi:10.1191/0959683603hl662rp
- 789 Carrión, J.S., Fuentes, N., González-Sampériz, P., Quirante, L.S., Finlayson, J.C., Fernández, S., Andrade, A., 2007.
790 Holocene environmental change in a montane region of southern Europe with a long history of human
791 settlement. *Quaternary Science Reviews* 26, 1455–1475. doi:https://doi.org/10.1016/j.quascirev.2007.03.013
- 792 Castillo Martín, A., Benavente Herrera, J., Fernández Rubio, R., Pulido Bosch, A., 1984. Evolución y ámbito
793 hidrogeológico de la laguna de Padul (Granada). *Las Zonas Húmedas en Andalucía; Monografías de DGMA-*
794 *MOPU*.
- 795 Chapman, S.J., 2001. Sulphur Forms in Open and Afforested Areas of Two Scottish Peatlands. *Water, Air, and Soil*
796 *Pollution* 128, 23–39. doi:10.1023/A:1010365924019
- 797 Cheddadi, R., Yu, G., Guiot, J., Harrison, S.P., Prentice, I.C., 1997. The climate of Europe 6000 years ago. *Climate*
798 *Dynamics* 13, 1–9. doi:10.1007/s003820050148
- 799 Clausen, A., 1999. Palaeoenvironmental significance of the green alga *Botryococcus* in the lacustrine rotliedend
800 (upper carboniferous - lower permian). *Historical Biology* 13, 221–234. doi:10.1080/08912969909386582
- 801 Combourieu-Nebout, N., Peyron, O., Dormoy, I., Desprat, S., Beaudouin, C., Kotthoff, U., Marret, F., 2009. Rapid
802 climatic variability in the west Mediterranean during the last 25 000 years from high resolution pollen data.
803 *Clim. Past* 5, 503–521. doi:10.5194/cp-5-503-2009
- 804 Cranwell, P., Eglinton, G., Robinson, N., 1987. Lipids of aquatic organisms as potential contributors to lacustrine
805 sediments—II. *Organic Geochemistry* 11, 513–527.

806 Cranwell, P.A., 1984. Lipid geochemistry of sediments from Upton Broad, a small productive lake. *Organic*
807 *Geochemistry* 7, 25–37. doi:10.1016/0146-6380(84)90134-7

808 Davis, J.C., Sampson, R.J., 1986. *Statistics and data analysis in geology*. Wiley New York.

809 Debret, M., Bout-Roumazeilles, V., Grousset, F., Desmet, M., McManus, J.F., Massei, N., Sebag, D., Petit, J.-R.,
810 Copard, Y., Trentesaux, A., 2007. The origin of the 1500-year climate cycles in Holocene North-Atlantic
811 records. *Clim. Past* 3, 569–575. doi:10.5194/cp-3-569-2007

812 Debret, M., Sebag, D., Crosta, X., Massei, N., Petit, J.-R., Chapron, E., Bout-Roumazeilles, V., 2009. Evidence from
813 wavelet analysis for a mid-Holocene transition in global climate forcing. *Quaternary Science Reviews* 28,
814 2675–2688. doi:https://doi.org/10.1016/j.quascirev.2009.06.005

815 deMenocal, P., Ortiz, J., Guilderson, T., Sarnthein, M., 2000. Coherent High- and Low-Latitude Climate Variability
816 During the Holocene Warm Period. *Science* 288, 2198–2202. doi:10.1126/science.288.5474.2198

817 Dormoy, I., Peyron, O., Combourieu Nebout, N., Goring, S., Kotthoff, U., Magny, M., Pross, J., 2009. Terrestrial
818 climate variability and seasonality changes in the Mediterranean region between 15 000 and 4000 years BP
819 deduced from marine pollen records. *Clim. Past* 5, 615–632. doi:10.5194/cp-5-615-2009

820 El Aallali, A., Nieto, J. M. L., Raya, F. A. P., and Mesa, J. M.: Estudio de la vegetación forestal en la vertiente sur de
821 Sierra Nevada (Alpujarra Alta granadina), *Itinera Geobot.*, 11, 387–402, 1998.

822 Faegri, K., Iversen, J., 1989. *Textbook of Pollen Analysis*. Wiley, New York.

823 Feijtel, T.C., Salingar, Y., Hordijk, C.A., Sweerts, J.P.R.A., Van Breemen, N., Cappenberg, T.E., 1989. Sulfur cycling
824 in a dutch moorland pool under elevated atmospheric S-deposition. *Water, Air, and Soil Pollution* 44, 215–
825 234. doi:10.1007/BF00279256

826 Fernández, S., Fuentes, N., Carrión, J.S., González-Sampériz, P., Montoya, E., Gil, G., Vega-Toscano, G., Riquelme,
827 J.A., 2007. The Holocene and Upper Pleistocene pollen sequence of Carihuela Cave, southern Spain. *Geobios*
828 40, 75–90. doi:10.1016/j.geobios.2006.01.004

829 Ficken, K.J., Li, B., Swain, D., Eglinton, G., 2000. An n-alkane proxy for the sedimentary input of submerged/floating
830 freshwater aquatic macrophytes. *Organic geochemistry* 31, 745–749.

831 Fletcher, W.J., Sánchez-Goñi, M.F., 2008. Orbital- and sub-orbital-scale climate impacts on vegetation of the western
832 Mediterranean basin over the last 48,000 yr. *Quaternary Research* 70, 451–464.
833 doi:10.1016/j.yqres.2008.07.002

834 Fletcher, W.J., Zielhofer, C., 2013. Fragility of Western Mediterranean landscapes during Holocene Rapid Climate
835 Changes. *Long-term degradation of fragile landscape systems* 103, 16–29. doi:10.1016/j.catena.2011.05.001

836 Fletcher, W.J., Debret, M., Goñi, M.F.S., 2013. Mid-Holocene emergence of a low-frequency millennial oscillation
837 in western Mediterranean climate: Implications for past dynamics of the North Atlantic atmospheric
838 westerlies. *The Holocene* 23, 153–166. doi:10.1177/0959683612460783

839 Florschütz, F., Amor, J.M., Wijmstra, T.A., 1971. Palynology of a thick quaternary succession in southern Spain.
840 *Palaeogeography, Palaeoclimatology, Palaeoecology* 10, 233–264. doi:http://dx.doi.org/10.1016/0031-
841 0182(71)90049-6

842 García-Alix, A., Delgado Huertas, A., Martín Suárez, E., 2012. Unravelling the Late Pleistocene habitat of the
843 southernmost woolly mammoths in Europe. *Quaternary Science Reviews* 32, 75–85.
844 doi:10.1016/j.quascirev.2011.11.007

845 García-Alix, A., Jiménez-Espejo, F.J., Toney, J.L., Jiménez-Moreno, G., Ramos-Román, M.J., Anderson, R.S.,
846 Ruano, P., Queralt, I., Delgado Huertas, A., Kuroda, J., 2017. Alpine bogs of southern Spain show human-
847 induced environmental change superimposed on long-term natural variations. *Scientific Reports* 7, 7439.
848 doi:10.1038/s41598-017-07854-w

849 Gasse, F., Roberts, C.N., 2004. Late Quaternary Hydrologic Changes in the Arid and Semiarid Belt of Northern Africa.
850 In: Diaz, H.F., Bradley, R.S. (Eds.), *The Hadley Circulation: Present, Past and Future*. Springer Netherlands,
851 Dordrecht, pp. 313–345. doi:10.1007/978-1-4020-2944-8_12

852 Geel, B. van, Hallewas, D.P., Pals, J.P., 1983. A late holocene deposit under the Westfriese Zeedijk near Enkhuizen
853 (Prov. of Noord-Holland, The Netherlands): Palaeoecological and archaeological aspects. *Review of*
854 *Palaeobotany and Palynology* 38, 269–335. doi:http://dx.doi.org/10.1016/0034-6667(83)90026-X

855 Gelpi, E., Schneider, H., Mann, J., Oró, J., 1970. Hydrocarbons of geochemical significance in microscopic algae.
856 *Phytochemistry* 9, 603–612. doi:10.1016/S0031-9422(00)85700-3

857 Grimm, E.C., 1987. CONISS: a Fortran 77 program for stratigraphically constrained cluster analysis by the method
858 of incremental sum of squares. *Comput. Geosci.* 13, 13-35

859 Guy-Ohlson, D., 1992. Botryococcus as an aid in the interpretation of palaeoenvironment and depositional processes.
860 *Review of Palaeobotany and Palynology* 71, 1–15. doi:http://dx.doi.org/10.1016/0034-6667(92)90155-A

- 861 Hammer, O., Harper, D.A.T., Ryan, P.D., 2001. PAST: paleontological statistics software package for education and
862 data analysis. *Palaeontologia Electronica* 4 (1), 9.
- 863 Hudon, C., 2004. Shift in wetland plant composition and biomass following low-level episodes in the St. Lawrence
864 River: looking into the future. *Canadian Journal of Fisheries and Aquatic Sciences* 61, 603–617.
865 doi:10.1139/f04-031
- 866 Huntley, B., Prentice, I.C., 1988. July Temperatures in Europe from Pollen Data, 6000 Years Before Present. *Science*
867 241, 687–690. doi:10.1126/science.241.4866.687
- 868 Hurrell, J.W., 1995. Decadal Trends in the North Atlantic Oscillation: Regional Temperatures and Precipitation.
869 *Science* 269, 676. doi:10.1126/science.269.5224.676
- 870 Jalut, G., Esteban Amat, A., Bonnet, L., Gauquelin, T., Fontugne, M., 2000. Holocene climatic changes in the Western
871 Mediterranean, from south-east France to south-east Spain. *Palaeogeography, Palaeoclimatology,*
872 *Palaeoecology* 160, 255–290. doi:10.1016/S0031-0182(00)00075-4
- 873 Jalut, G., Dedoubat, J.J., Fontugne, M., Otto, T., 2009. Holocene circum-Mediterranean vegetation changes: Climate
874 forcing and human impact. *Quaternary International* 200, 4–18.
875 doi:https://doi.org/10.1016/j.quaint.2008.03.012
- 876 Jimenez-Espejo, F.J., Martínez-Ruiz, F., Rogerson, M., González-Donoso, J.M., Romero, O.E., Linares, D.,
877 Sakamoto, T., Gallego-Torres, D., Rueda Ruiz, J.L., Ortega-Huertas, M., Perez Claros, J.A., 2008. Detrital
878 input, productivity fluctuations, and water mass circulation in the westernmost Mediterranean Sea since the
879 Last Glacial Maximum. *Geochemistry, Geophysics, Geosystems* 9, n/a-n/a. doi:10.1029/2008GC002096
- 880 Jiménez-Espejo, F.J., García-Alix, A., Jiménez-Moreno, G., Rodrigo-Gámiz, M., Anderson, R.S., Rodríguez-Tovar,
881 F.J., Martínez-Ruiz, F., Giral, S., Delgado Huertas, A., Pardo-Igúzquiza, E., 2014. Saharan aeolian input and
882 effective humidity variations over western Europe during the Holocene from a high altitude record. *Chemical*
883 *Geology* 374–375, 1–12. doi:10.1016/j.chemgeo.2014.03.001
- 884 Jiménez-Moreno, G., Anderson, R.S., 2012. Holocene vegetation and climate change recorded in alpine bog sediments
885 from the Borreguiles de la Virgen, Sierra Nevada, southern Spain. *Quaternary Research* 77, 44–53.
886 doi:https://doi.org/10.1016/j.yqres.2011.09.006
- 887 Jiménez-Moreno, G., García-Alix, A., Hernández-Corbalán, M.D., Anderson, R.S., Delgado-Huertas, A., 2013.
888 Vegetation, fire, climate and human disturbance history in the southwestern Mediterranean area during the
889 late Holocene. *Quat. Res.* 79, 110–122. https://doi.org/10.1016/j.yqres.2012.11.008
- 890 Johnsen, S.J., Clausen, H.B., Dansgaard, W., Fuhrer, K., Gundestrup, N., Hammer, C.U., Iversen, P., Jouzel, J.,
891 Stauffer, B., Steffensen, J.P., 1992. Irregular glacial interstadials recorded in a new Greenland ice core. *Nature*
892 359, 311–313. doi:10.1038/359311a0
- 893 Kalugin, I., Daryin, A., Smolyaninova, L., Andreev, A., Diekmann, B., Khlystov, O., 2007. 800-yr-long records of
894 annual air temperature and precipitation over southern Siberia inferred from Teletskoye Lake sediments.
895 *Quaternary Research* 67, 400–410. doi:https://doi.org/10.1016/j.yqres.2007.01.007
- 896 Kaushal, S., Binford, M.W., 1999. Relationship between C:N ratios of lake sediments, organic matter sources, and
897 historical deforestation in Lake Pleasant, Massachusetts, USA. *Journal of Paleolimnology* 22, 439–442.
898 doi:10.1023/A:1008027028029
- 899 Lamb, H.F., Kaars, S. van der, 1995. Vegetational response to Holocene climatic change: pollen and
900 palaeolimnological data from the Middle Atlas, Morocco. *The Holocene* 5, 400–408.
901 doi:10.1177/095968369500500402
- 902 Laskar, J., Robutel, P., Joutel, F., Gastineau, M., Correia, A.C.M., Levrard, B., 2004. A long-term numerical solution
903 for the insolation quantities of the Earth, *Astron. Astrophys.*, 428, 261–285. doi:10.1051/0004-
904 6361:20041335
- 905 Lionello, P., Malanotte-Rizzoli, P., Boscolo, R., 2006. *Mediterranean climate variability*. Elsevier.
- 906 Magny, M., Beaulieu, J.-L. de, Drescher-Schneider, R., Vannière, B., Walter-Simonnet, A.-V., Miras, Y., Millet, L.,
907 Bossuet, G., Peyron, O., Brugiapaglia, E., Leroux, A., 2007. Holocene climate changes in the central
908 Mediterranean as recorded by lake-level fluctuations at Lake Accesa (Tuscany, Italy). *Quaternary Science*
909 *Reviews* 26, 1736–1758. doi:http://dx.doi.org/10.1016/j.quascirev.2007.04.014
- 910 Magny, M., Peyron, O., Sadori, L., Ortu, E., Zanchetta, G., Vannière, B., Tinner, W., 2012. Contrasting patterns of
911 precipitation seasonality during the Holocene in the south- and north-central Mediterranean. *Journal of*
912 *Quaternary Science* 27, 290–296. doi:10.1002/jqs.1543
- 913 Marchal, O., Cacho, I., Stocker, T.F., Grimalt, J.O., Calvo, E., Martrat, B., Shackleton, N., Vautravers, M., Cortijo,
914 E., Van Kreveld, S., Andersson, C., Koç, N., Chapman, M., Saffi, L., Duplessy, J.-C., Sarnthein, M., Turon,
915 J.-L., Duprat, J., Jansen, E., 2002. Apparent long-term cooling of the sea surface in the northeast Atlantic and

- 916 Mediterranean during the Holocene. *Quaternary Science Reviews* 21, 455–483. doi:10.1016/S0277-
917 3791(01)00105-6
- 918 Martín-Puertas, C., Valero-Garcés, B.L., Mata, M.P., González-Sampériz, P., Bao, R., Moreno, A., Stefanova, V.,
919 2008. Arid and humid phases in southern Spain during the last 4000 years: the Zoñar Lake record, Córdoba.
920 *The Holocene* 18, 907–921. doi:10.1177/0959683608093533
- 921 Martín-Puertas, C., Valero-Garcés, B.L., Brauer, A., Mata, M.P., Delgado-Huertas, A., Dulski, P., 2009. The Iberian-
922 Roman Humid Period (2600-1600 cal yr BP) in the Zoñar Lake varve record (Andalucía, southern Spain).
923 *Quaternary Research* 71, 108–120. doi:10.1016/j.yqres.2008.10.004
- 924 Martrat, B., Grimalt, J.O., López-Martínez, C., Cacho, I., Sierro, F.J., Flores, J.A., Zahn, R., Canals, M., Curtis, J. H.,
925 Hodell, D. A., 2004. Abrupt Temperature Changes in the Western Mediterranean over the Past 250000 years.
926 *Science* 306, 1762. <https://doi.org/10.1126/science.1101706>
- 927 Mayewski, P.A., Meeker, L.D., Twickler, M.S., Whitlow, S., Yang, Q., Lyons, W.B., Prentice, M., 1997. Major
928 features and forcing of high-latitude northern hemisphere atmospheric circulation using a 110,000-year-long
929 glaciochemical series. *Journal of Geophysical Research: Oceans* 102, 26345–26366. doi:10.1029/96JC03365
- 930 Mayewski, P.A., Rohling, E.E., Stager, J.C., Karlén, W., Maasch, K.A., Meeker, L.D., Meyerson, E.A., Gasse, F.,
931 Kreveld, S. van, Holmgren, K., Lee-Thorp, J., Rosqvist, G., Rack, F., Staubwasser, M., Schneider, R.R.,
932 Steig, E.J., 2004. Holocene climate variability. *Quaternary Research* 62, 243–255.
933 doi:<https://doi.org/10.1016/j.yqres.2004.07.001>
- 934 Meijer, P.T., Tuenter, E., 2007. The effect of precession-induced changes in the Mediterranean freshwater budget on
935 circulation at shallow and intermediate depth. *Journal of Marine Systems* 68, 349–365.
936 doi:10.1016/j.jmarsys.2007.01.006
- 937 Meyers, P.A., 1994. Preservation of elemental and isotopic source identification of sedimentary organic matter.
938 *Chemical Geology* 114, 289–302. doi:10.1016/0009-2541(94)90059-0
- 939 Meyers, P.A., Lallier-Vergés, E., 1999. Lacustrine Sedimentary Organic Matter Records of Late Quaternary
940 Paleoclimates. *Journal of Paleolimnology* 21, 345–372. doi:10.1023/A:1008073732192
- 941 Moreno, A., Cacho, I., Canals, M., Grimalt, J.O., Sánchez-Goñi, M.F., Shackleton, N., Sierro, F.J., 2005. Links
942 between marine and atmospheric processes oscillating on a millennial time-scale. A multi-proxy study of the
943 last 50,000 yr from the Alboran Sea (Western Mediterranean Sea). *Quaternary Science Reviews* 24, 1623–
944 1636. doi:<https://doi.org/10.1016/j.quascirev.2004.06.018>
- 945 Moreno, A., López-Merino, L., Leira, M., Marco-Barba, J., González-Sampériz, P., Valero-Garcés, B.L., López-Sáez,
946 J.A., Santos, L., Mata, P., Ito, E., 2011. Revealing the last 13,500 years of environmental history from the
947 multiproxy record of a mountain lake (Lago Enol, northern Iberian Peninsula). *Journal of Paleolimnology*
948 46, 327–349. doi:10.1007/s10933-009-9387-7
- 949 Moro, M.J., Domingo, F., López, G., 2004. Seasonal transpiration pattern of *Phragmites australis* in a wetland of semi-
950 arid Spain. *Hydrological Processes* 18, 213–227. doi:10.1002/hyp.1371
- 951 Ogura, K., Machihara, T., Takada, H., 1990. Diagenesis of biomarkers in Biwa Lake sediments over 1 million years.
952 *Organic Geochemistry* 16, 805–813.
- 953 Ortiz, J.E., Torres, T., Delgado, A., Julià, R., Lucini, M., Llamas, F.J., Reyes, E., Soler, V., Valle, M., 2004. The
954 palaeoenvironmental and palaeohydrological evolution of Padul Peat Bog (Granada, Spain) over one million
955 years, from elemental, isotopic and molecular organic geochemical proxies. *Organic Geochemistry* 35, 1243–
956 1260. doi:<https://doi.org/10.1016/j.orggeochem.2004.05.013>
- 957 Ortiz, J.E., Torres, T., Delgado, A., Llamas, J.F., Soler, V., Valle, M., Julià, R., Moreno, L., Díaz-Bautista, A., 2010.
958 Palaeoenvironmental changes in the Padul Basin (Granada, Spain) over the last 1Ma based on the biomarker
959 content. *Palaeogeography, Palaeoclimatology, Palaeoecology* 298, 286–299.
960 doi:10.1016/j.palaeo.2010.10.003
- 961 Pérez Raya, F., López Nieto, J., 1991. Vegetación acuática y helofítica de la depresión de Padul (Granada). *Acta Bot.*
962 *Malacitana* 16, 373–389.
- 963 Peyron, O., Magny, M., Goring, S., Joannin, S., Beaulieu, J.-L. de, Brugiapaglia, E., Sadori, L., Garfí, G., Kouli, K.,
964 Ioakim, C., Combourieu-Nebout, N., 2013. Contrasting patterns of climatic changes during the Holocene
965 across the Italian Peninsula reconstructed from pollen data. *Clim. Past* 9, 1233–1252. doi:10.5194/cp-9-1233-
966 2013
- 967 Pons, A., Reille, M., 1988. The holocene- and upper pleistocene pollen record from Padul (Granada, Spain): A new
968 study. *Palaeogeography, Palaeoclimatology, Palaeoecology* 66, 243–263.
969 doi:[http://dx.doi.org/10.1016/0031-0182\(88\)90202-7](http://dx.doi.org/10.1016/0031-0182(88)90202-7)
- 970 Ramos-Román, M.J., Jiménez-Moreno, G., Anderson, R.S., García-Alix, A., Toney, J.L., Jiménez-Espejo, F.J.,
971 Carrión, J.S., 2016. Centennial-scale vegetation and North Atlantic Oscillation changes during the Late

- 972 Holocene in the southern Iberia. *Quaternary Science Reviews* 143, 84–95.
973 doi:<https://doi.org/10.1016/j.quascirev.2016.05.007>
- 974 Ramos-Román, M.J., Jiménez-Moreno, G., Camuera, J., García-Alix, A., Anderson, R.S., Jiménez-Espejo, F.J.,
975 Carrión, J.S., 2018. Holocene climate aridification trend and human impact interrupted by millennial- and
976 centennial-scale climate fluctuations from a new sedimentary record from Padul (Sierra Nevada, southern
977 Iberian Peninsula). *Clim. Past.*, 14 (1), 117-137. <https://doi.org/10.5194/cp-14-117-2018>
- 978 Reed, J.M., Stevenson, A.C., Juggins, S., 2001. A multi-proxy record of Holocene climatic change in southwestern
979 Spain: the Laguna de Medina, Cádiz. *The Holocene* 11, 707–719. doi:10.1191/09596830195735
- 980 Reimer, P.J., Bard, E., Bayliss, A., Beck, J.W., Blackwell, P.G., Ramsey, C.B., Buck, C.E., Cheng, H., Edwards, R.L.,
981 Friedrich, M., Grootes, P.M., Guilderson, T.P., Hafliðason, H., Hajdas, I., Hatté, C., Heaton, T.J., Hoffmann,
982 D.L., Hogg, A.G., Hughen, K.A., Kaiser, K.F., Kromer, B., Manning, S.W., Niu, M., Reimer, R.W., Richards,
983 D.A., Scott, E.M., Southon, J.R., Staff, R.A., Turney, C.S.M., Plicht, J. van der, 2013. IntCal13 and Marine13
984 Radiocarbon Age Calibration Curves 0–50,000 Years cal BP. *Radiocarbon* 55, 1869–1887.
985 doi:10.2458/azu_js_rc.55.16947
- 986 Riera, S., Wansard, G., Julià, R., 2004. 2000-year environmental history of a karstic lake in the Mediterranean Pre-
987 Pyrenees: the Estanya lakes (Spain). *Catena*, 55, 293–324. doi:[https://doi.org/10.1016/S0341-](https://doi.org/10.1016/S0341-8162(03)00107-3)
988 [8162\(03\)00107-3](https://doi.org/10.1016/S0341-8162(03)00107-3)
- 989 Rodrigo-Gámiz, M., Martínez-Ruiz, F., Rodríguez-Tovar, F.J., Jiménez-Espejo, F.J., Pardo-Igúzquiza, E., 2014a.
990 Millennial- to centennial-scale climate periodicities and forcing mechanisms in the westernmost
991 Mediterranean for the past 20,000 yr. *Quaternary Research* 81, 78–93.
992 doi:<https://doi.org/10.1016/j.yqres.2013.10.009>
- 993 Rodrigo-Gámiz, M., Martínez-Ruiz, F., Rampen, S.W., Schouten, S., Sinninghe Damsté, J.S., February 1, 2014b. Sea
994 surface temperature variations in the western Mediterranean Sea over the last 20 kyr: A dual-organic proxy
995 (UK'37 and LDI) approach. *Paleoceanography* 29, 87–98. doi:10.1002/2013PA002466
- 996 Rohling, E., Mayewski, P., Abu-Zied, R., Casford, J., Hayes, A., 2002. Holocene atmosphere-ocean interactions:
997 records from Greenland and the Aegean Sea. *Climate Dynamics* 18, 587–593. doi:10.1007/s00382-001-
998 0194-8
- 999 Sachse, D., Radke, J., Gleixner, G., 2006. δD values of individual n-alkanes from terrestrial plants along a climatic
1000 gradient – Implications for the sedimentary biomarker record. *Organic Geochemistry* 37, 469–483.
1001 doi:10.1016/j.orggeochem.2005.12.003
- 1002 Sanz de Galdeano, C., El Hamdouni, R., Chacón, J., 1998. Neotectónica de la fosa del Padul y del Valle de Lecrín.
1003 Itinerarios Geomorfológicos por Andalucía Oriental, Publicacions de la Universitat de Barcelona, Barcelona
1004 65–81.
- 1005 Schulz, M., Mudelsee, M., 2002. REDFIT: estimating red-noise spectra directly from unevenly spaced paleoclimatic
1006 time series. *Computers & Geosciences* 28, 421–426. doi:[https://doi.org/10.1016/S0098-3004\(01\)00044-9](https://doi.org/10.1016/S0098-3004(01)00044-9)
- 1007 Shanahan, T.M., McKay, N.P., Hughen, K.A., Overpeck, J.T., Otto-Bliesner, B., Heil, C.W., King, J., Scholz, C.A.,
1008 Peck, J., 2015. The time-transgressive termination of the African Humid Period. *Nature Geoscience* 8, 140.
- 1009 Singh, G., Wasson, R.J., Agrawal, D.P., 1990. Vegetational and seasonal climatic changes since the last full glacial in
1010 the Thar Desert, northwestern India. *The Proceedings of the 7th International Palynological Congress (Part*
1011 *I)* 64, 351–358. doi:10.1016/0034-6667(90)90151-8
- 1012 Snowball, I., Sandgren, P., 2001. Application of mineral magnetic techniques to paleolimnology. *Developments in*
1013 *Paleoenvironmental Research. Tracking Environmental Change Using Lake Sediments: Physical and*
1014 *Geochemical Methods* 2, 217–237.
- 1015 Steinhilber, F., Beer, J., Fröhlich, C., 2009. Total solar irradiance during the Holocene. *Geophysical Research Letters*
1016 36, 19. doi:10.1029/2009GL040142
- 1017 Talbot, M., 1988. The origins of lacustrine oil source rocks: evidence from the lakes of tropical Africa. *Geological*
1018 *Society, London, Special Publications* 40, 29–43.
- 1019 Talbot, M.R., Livingstone, D.A., 1989. Hydrogen index and carbon isotopes of lacustrine organic matter as lake level
1020 indicators. *The Phanerozoic Record of Lacustrine Basins and Their Environmental* 70, 121–137.
1021 doi:10.1016/0031-0182(89)90084-9
- 1022 Torrence, C., Compo, G.P., 1998. A Practical Guide to Wavelet Analysis. *Bulletin of the American Meteorological*
1023 *Society* 79, 61–78. doi:10.1175/1520-0477(1998)079<0061:APGTWA>2.0.CO;2
- 1024 Tzedakis, P., 2007. Seven ambiguities in the Mediterranean palaeoenvironmental narrative. *Quaternary Science*
1025 *Reviews* 26, 2042–2066.
- 1026 Valle, F.: Mapa de series de vegetación de Andalucía 1: 400 000, Editorial Rueda, Madrid, 2003.

- 1027 Valle Tendero, F., 2004. Modelos de Restauración Forestal: Datos botánicos aplicados a la gestión del Medio Natural
1028 Andaluz II: Series de vegetación. Consejería de Medio Ambiente de la Junta de Andalucía, Sevilla.
- 1029 Villegas Molina, F., 1967. Laguna de Padul: Evolución geológico-histórica. Estudios Geográficos 28, 561.
- 1030 Wieder, R.K., Lang, G.E., 1988. Cycling of inorganic and organic sulfur in peat from Big Run Bog, West Virginia.
1031 Biogeochemistry 5, 221–242. doi:10.1007/BF02180229
- 1032 Walker, M. J., Berkelhammer, M., Björck, S., Cwynar, L. C., Fisher, D. A., Long, A. J., Lowe, J. J., Newnham, R.
1033 M., Rasmussen, S. O. and Weiss, H., 2012. Formal subdivision of the Holocene Series/Epoch: a Discussion
1034 Paper by a Working Group of INTIMATE (Integration of ice-core, marine and terrestrial records) and the
1035 Subcommission on Quaternary Stratigraphy (International Commission on Stratigraphy). J. Quaternary Sci.,
1036 27: 649-659. doi:10.1002/jqs.2565
- 1037 Ziegler, M., Jilbert, T., Lange, G.J. de, Lourens, L.J., Reichert, G., 2008. Bromine counts from XRF scanning as an
1038 estimate of the marine organic carbon content of sediment cores. Geochemistry, Geophysics, Geosystems 9.
- 1039 Zielhofer, C., Fletcher, W.J., Mischke, S., De Batist, M., Campbell, J.F.E., Joannin, S., Tjallingii, R., El Hamouti, N.,
1040 Junginger, A., Stele, A., Bussmann, J., Schneider, B., Lauer, T., Spitzer, K., Strupler, M., Brachert, T.,
1041 Mikdad, A., 2017. Atlantic forcing of Western Mediterranean winter rain minima during the last 12,000
1042 years. Quaternary Science Reviews 157, 29–51. doi:10.1016/j.quascirev.2016.11.037

1043 **Figure captions**

1044 **Figure 1.** Location and pictures of Padul wetland. (a) Location of Padul wetland in Sierra Nevada, southern
1045 Iberian Peninsula, with an inset showing south western Europe. (b) Padul basin area showing the coring
1046 location. (c) Picture of Padul wetland, peat bog and crops area in the Padul basin, and the alluvial fans and
1047 Sierra Nevada mountains in the background. Picture from M.J. Ramos-Román. Software use: Above, Sierra
1048 Nevada map was performed using the GIS software Global Mapper (<http://www.globalmapper.com>) and
1049 modified with Adobe Illustrator. The inset map (the western Mediterranean region) was created with Adobe
1050 Illustrator (<https://www.adobe.com/>). Below, left, is the Google earth image
1051 (<http://www.google.com/earth/index.html>) of the Padul basin showing the coring locations. ☒

1052 **Figure 2.** Picture of the Padul-15-05 sediment core (images were taken with an Avaatech core scanner at
1053 the University of Barcelona) with the age-depth model showing the part of the record that was studied here
1054 (red rectangle) corresponding with the last ~11.600 years, based on a previous age-depth model (Ramos-
1055 Román et al., 2018). The sediment accumulation rates (SAR; unit= cm/yr) between radiocarbon dates are
1056 marked. See the body of the text for the explanation of the age reconstructions.

1057 **Figure 3.** Inorganic geochemistry results for the ~3.67 m of the upperpart from Padul 15-05 record. Picture
1058 of the Padul-15-05 record, facies interpretations with paleontology, magnetic susceptibility (MS) and X-
1059 ray fluorescence (XRF). XRF elements (Ca, Sr, Br, S, Si, K, Ti, Fe, Zr) are represents as counts per second
1060 normalized to the total counts (norm.). (a) MS in SI, (b) Calcium normalized (Ca norm.) (c) Strontium
1061 normalized (Sr norm.) (d) Bromine normalized (Br norm.) (e) Sulfur normalized (S norm.) (f) Silica
1062 normalized (Si norm.), (g) Potassium normalized (K norm.), (h) Titanium normalized (Ti norm.), (i) Iron
1063 normalized (Fe norm.), (j) Zirconium normalized (Zr norm.), (k) K/Si ratio. Note that uppermost ~ 1.15 m
1064 inorganic geochemistry results of the record were previously shown in Ramos-Román et al. (2018).

1065 **Figure 4.** Organic geochemistry results for the ~3.67 m of the upperpart (Holocene part) from Padul-15-05
1066 record and comparison with inorganic index calculated from the PCA analysis performed to XRF elements

1067 in the same record. (a) K/Si ratio, (b) Ca (norm.), (c) Total organic carbon percentage (TOC %), (d) Carbon-
1068 Nitrogen ratio (C/N), (e) Hydrogen-Carbon ratio (H/C), (f) Average chain length (ACL), (g) Carbon
1069 preference index (CPI), (h) Short-chain (%), (i) Mid-chain (%), (j) Long-chain (%). Note that the uppermost
1070 ~ 1.15 m TOC values were previously shown (Ramos-Román et al., 2018).

1071 **Figure 5.** Percentages of selected pollen taxa and non-pollen palynomorphs (NPPs) from the Holocene part
1072 of Padul-15-05 record, represented with respect to terrestrial pollen sum. Silhouettes show 7-time
1073 exaggerations of pollen percentages. Tree and shrubs are showing in green, herbs and grasses in yellow,
1074 aquatics in dark blue, algae in blue and fungi in brown. The Mediterranean forest taxa is composed of
1075 *Quercus* total, *Olea*, *Phillyrea* and *Pistacia*. The xerophyte group includes *Artemisia*, *Ephedra*, and
1076 *Amaranthaceae*. The hygrophytes group is composed by *Cyperaceae* and *Typha* type. Algae group is formed
1077 by *Zygea* type, *Botryococcus*, *Mougeotia* and *Pediastrum*. U: Unit. Note that uppermost ~ 1.15 m pollen
1078 and NPPs results of the record were previously depicted (Ramos-Román et al., 2018).

1079 **Figure 6.** Padul-15-05 local environment development during the Holocene deduced from a comparison
1080 between different pollen, organic and inorganic geochemistry proxies from the Holocene part of the Padul-
1081 15-05 record and summer and winter insolation for the Sierra Nevada latitude. A) Regional response
1082 determines by Mediterranean forest taxa (%). B) Local response: (a) Summer and winter insolation
1083 calculated for 37° N (Laskar et al., 2004), (b) Ca (norm.) (c) K/Si ratio (clays input), (d) Total organic
1084 carbon percentage (TOC %), (e) *Glomus* type (%) (f), Short-chain (%), (g) Algae percentage from the pollen
1085 analysis (h) Mid-chain (%), (i) Hygrophytes percentage. Beige shadings are showing arid and cold event
1086 during the early and middle Holocene determine by the decline in Mediterranean forest component and
1087 showing the response in the local environment. Proxies were resampled at 80 yr (in bold) by lineal
1088 interpolation using Past software (http://palaeo-electronica.org/2001_1/past/issue1_01.htm). U: Unit.

1089 **Figure 7.** Comparison for the Holocene between different pollen taxa from the Padul-15-05 record with a
1090 previously pollen record in the same area and other pollen and temperature proxies from nearly records in

1091 the western Mediterranean region (see records locations in Supplementary Fig. S8). (a) Deciduous *Quercus*,
1092 Evergreen *Quercus* and Mediterranean forest percentages in the Padul-15-05 record, (b) Deciduous
1093 *Quercus* and Evergreen *Quercus* in a previously record in the Padul peat bog (Pons and Reille, 1988), (c)
1094 Percentage of *Pinus* and *Artemisia* in the nearly Laguna de Rio Seco record, Sierra Nevada (Anderson et
1095 al., 2011), (d) Temperate and Mediterranean forest percentage for the MD95-2043 record, Alboran Sea
1096 (Fletcher and Sánchez-Goñi, 2008), (e) Alkenone sea surface temperature (SST) reconstruction from the
1097 MD01-2444, Alboran Sea (Martrat et al., 2004), (f) Alkenone SST reconstruction from the MD95-2043
1098 record, Alboran Sea (Cacho et al., 1999), (g) Alkenone SST reconstruction from the 434G record, Alboran
1099 Sea (Rodrigo-Gámiz et al., 2014b). Blue shading represents the humidity optimum during the Holocene in
1100 the western Mediterranean region.

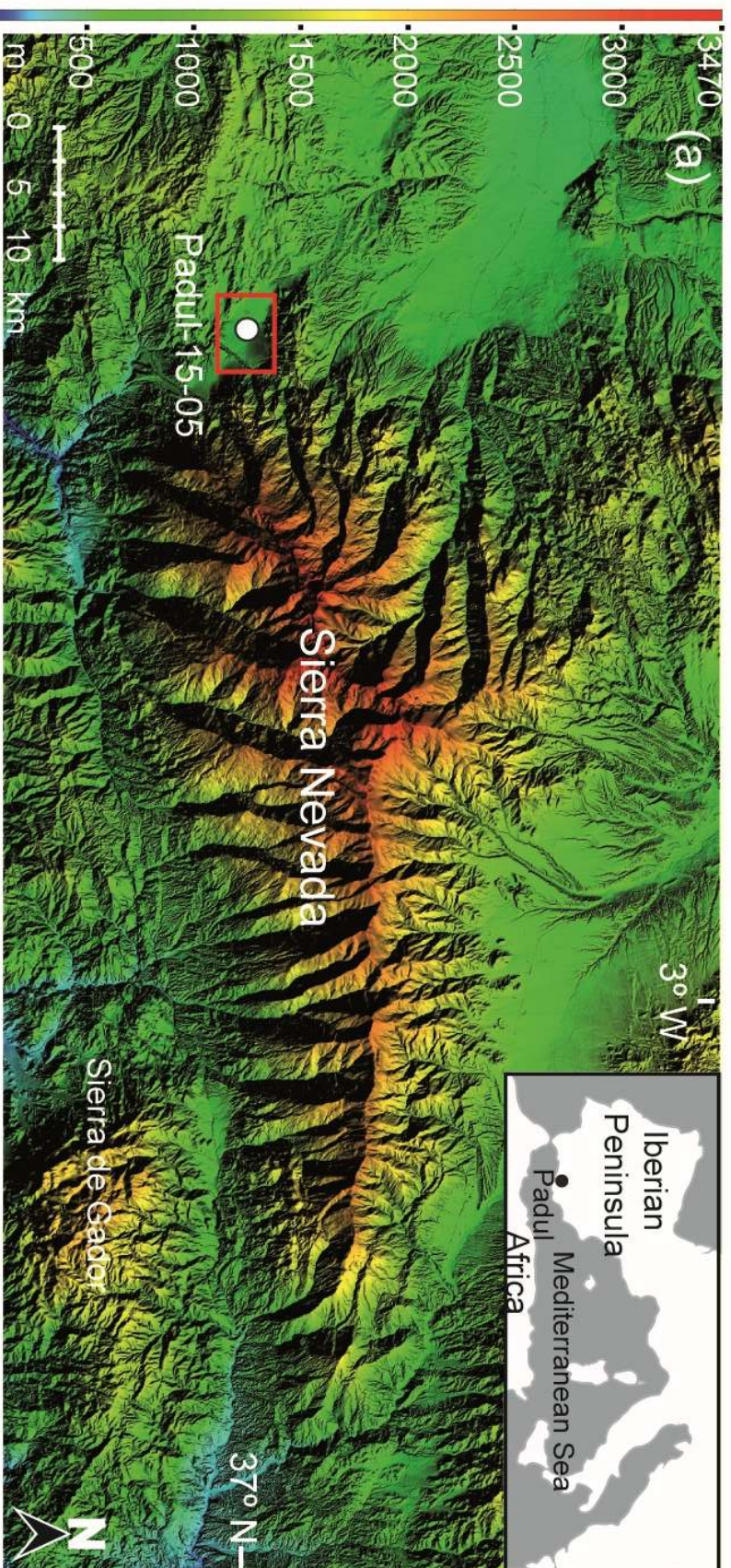
1101 **Figure 8.** Holocene climate periodicity from the Padul-15-05 record determine by declines in the
1102 Mediterranean forest component and comparison with other North Atlantic records. (a) Summer and winter
1103 insolation calculated for 37° N (Laskar et al., 2004), (b) Mediterranean forest taxa (c) Ocean stacked
1104 percentage of the Drift Ice Index (reversed) from the North Atlantic (Bond et al., 2001), (d) Total solar
1105 irradiance (TSI) anomaly reconstruction from cosmogenic radionuclide from a Greenland ice core
1106 (Steinhilber et al., 2009), (e) Alkenone sea surface temperature (SST) reconstruction from the MD01-2444,
1107 Alboran Sea (Martrat et al., 2004), (f) Alkenone SST reconstruction from the MD95-2043 record, Alboran
1108 Sea (Cacho et al., 1999), (g) Alkenone SST reconstruction from the 434G record, Alboran Sea (Rodrigo-
1109 Gámiz et al., 2014b). Beige shadings highlight decreases in Mediterranean forest and coldest events related
1110 with decreases in total solar irradiance and decreases in SST. A linear r (Pearson) correlation was calculated
1111 between the Mediterranean forest abundances and the TSI anomaly ($r = 0.43$; $p < 0.001$; between ~ 9.4 and
1112 4.7 cal kyr BP and $r = 0.37$; $p < 0.001$; between 4.7 cal kyr BP and present). In order to obtain equally
1113 spaced time series the Mediterranean forest and the TSI anomaly data were previously resampled at 50
1114 years (linear interpolation), the Mediterranean forest data was detrended (only between 4.7 cal kyr BP to
1115 Present) and the TSI anomaly smoothed to a five-point average.

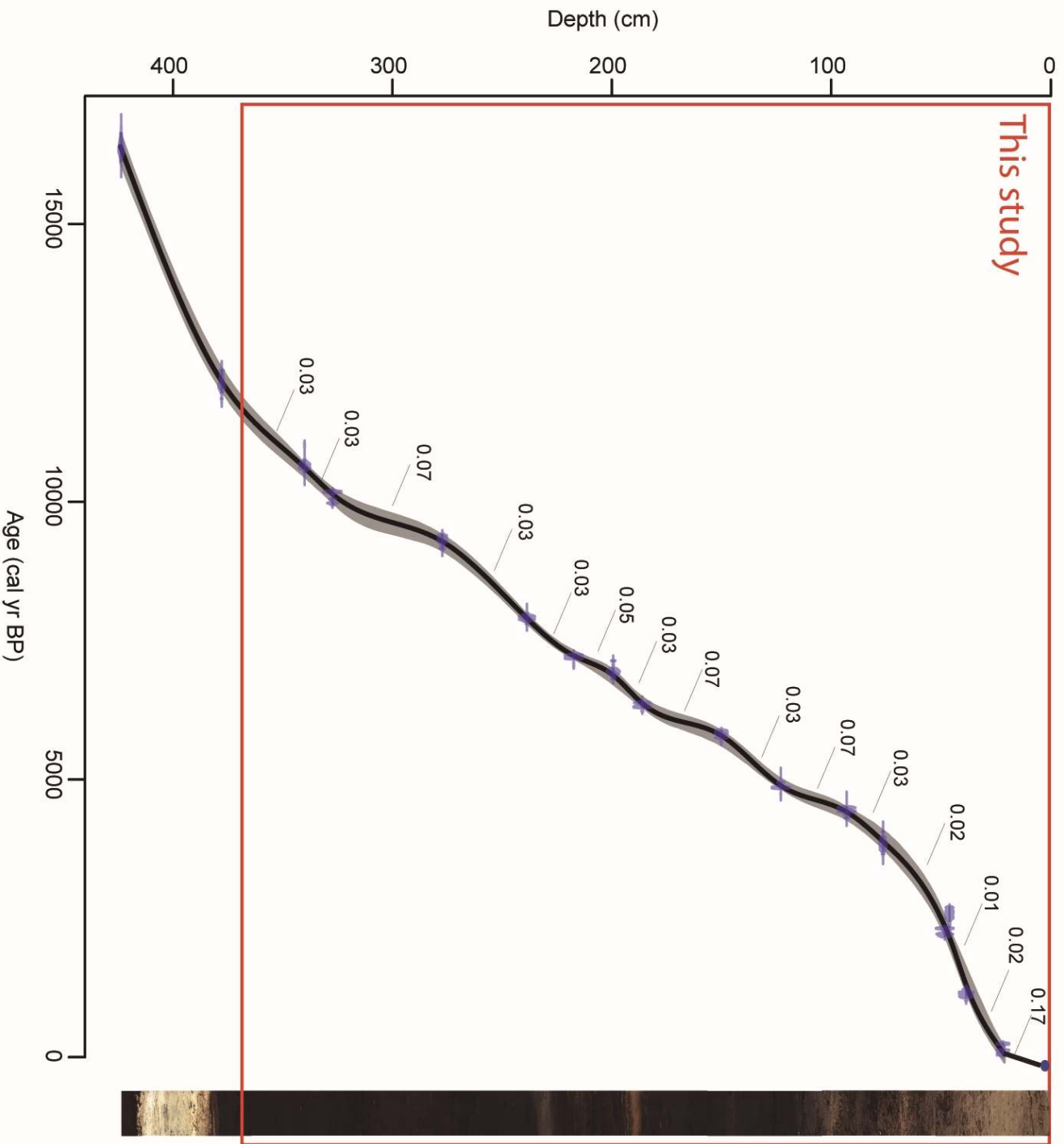
1116 **Table 1.** Modern vegetation belts from Sierra Nevada (El Aallali et al., 1998; Valle, 2003).

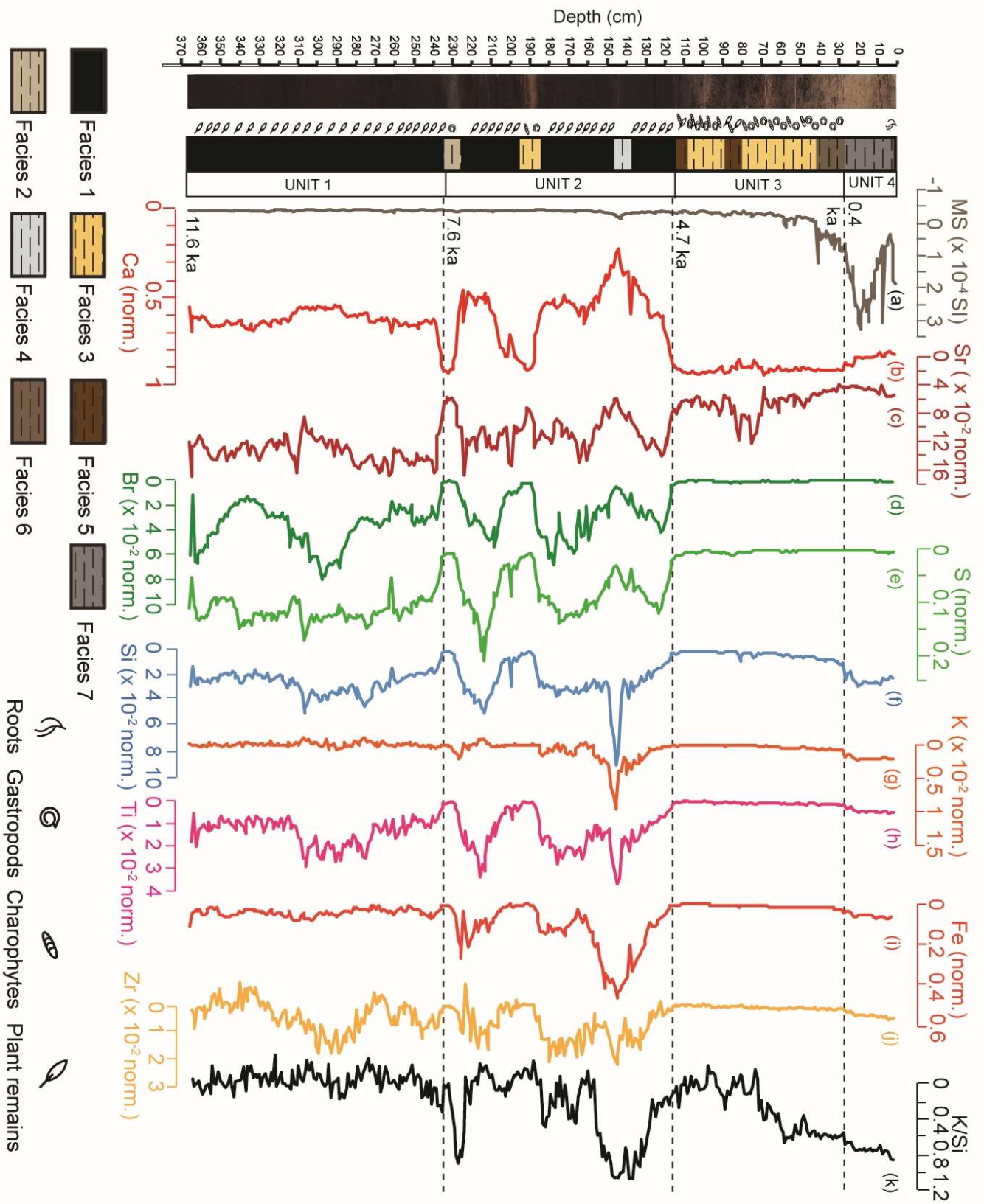
1117 **Table 2.** Age data for Padul-15-05 record. All ages were calibrated using R-code package ‘clam 2.2’
1118 employing the calibration curve IntelCal 13 (Reimer et al., 2013) at 95 % of confident range. Note that the
1119 age data for the uppermost ~ 3.27 m were previously shown (Ramos-Román et al., 2018).

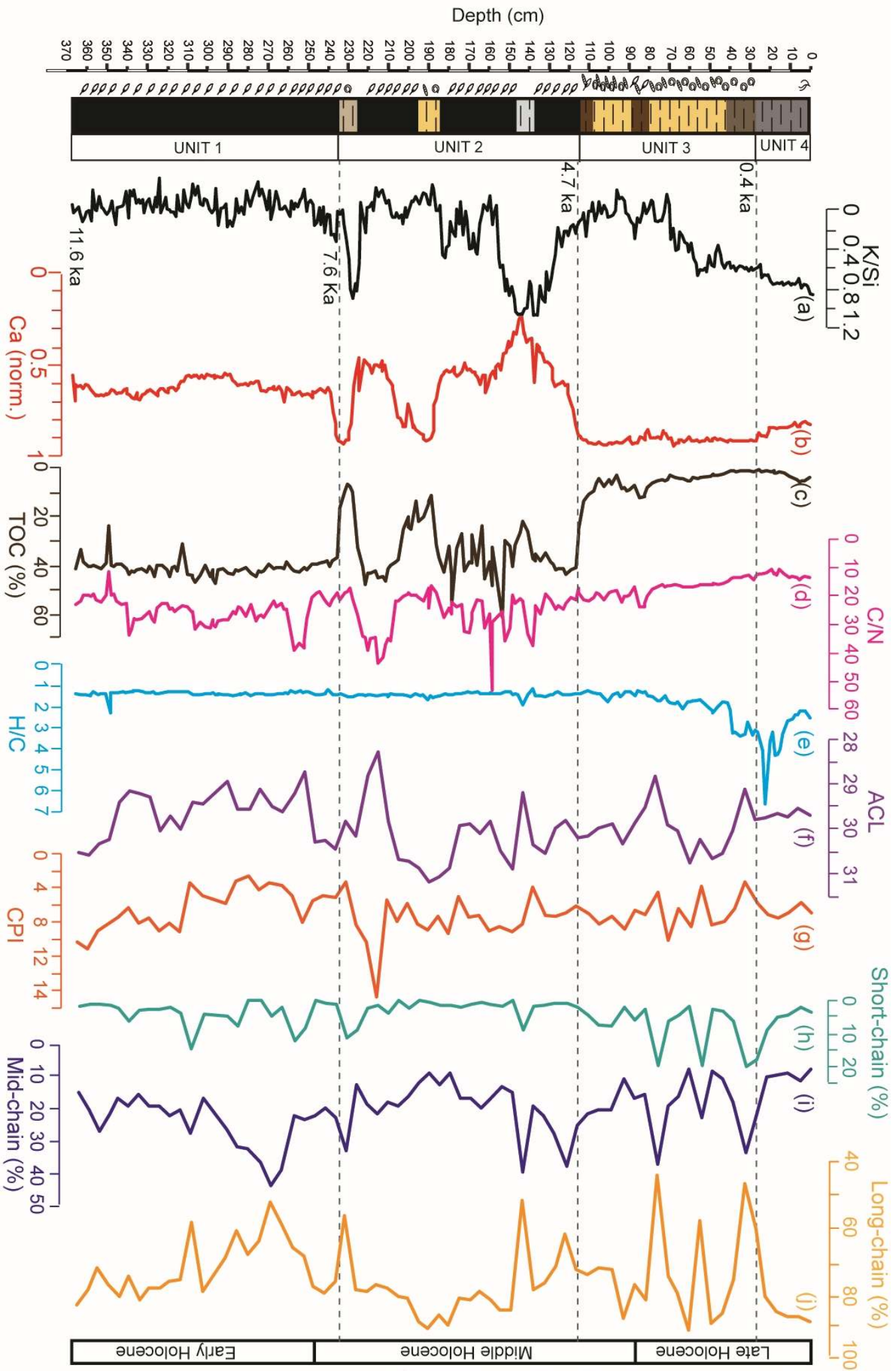
1120 **Table 3.** Summary of the *n*-alkane indices from the studied plant, algae and moss samples from the
1121 surroundings of the present-day Padul peatland (For more information see in the Supplementary Figure S2
1122 and S3).

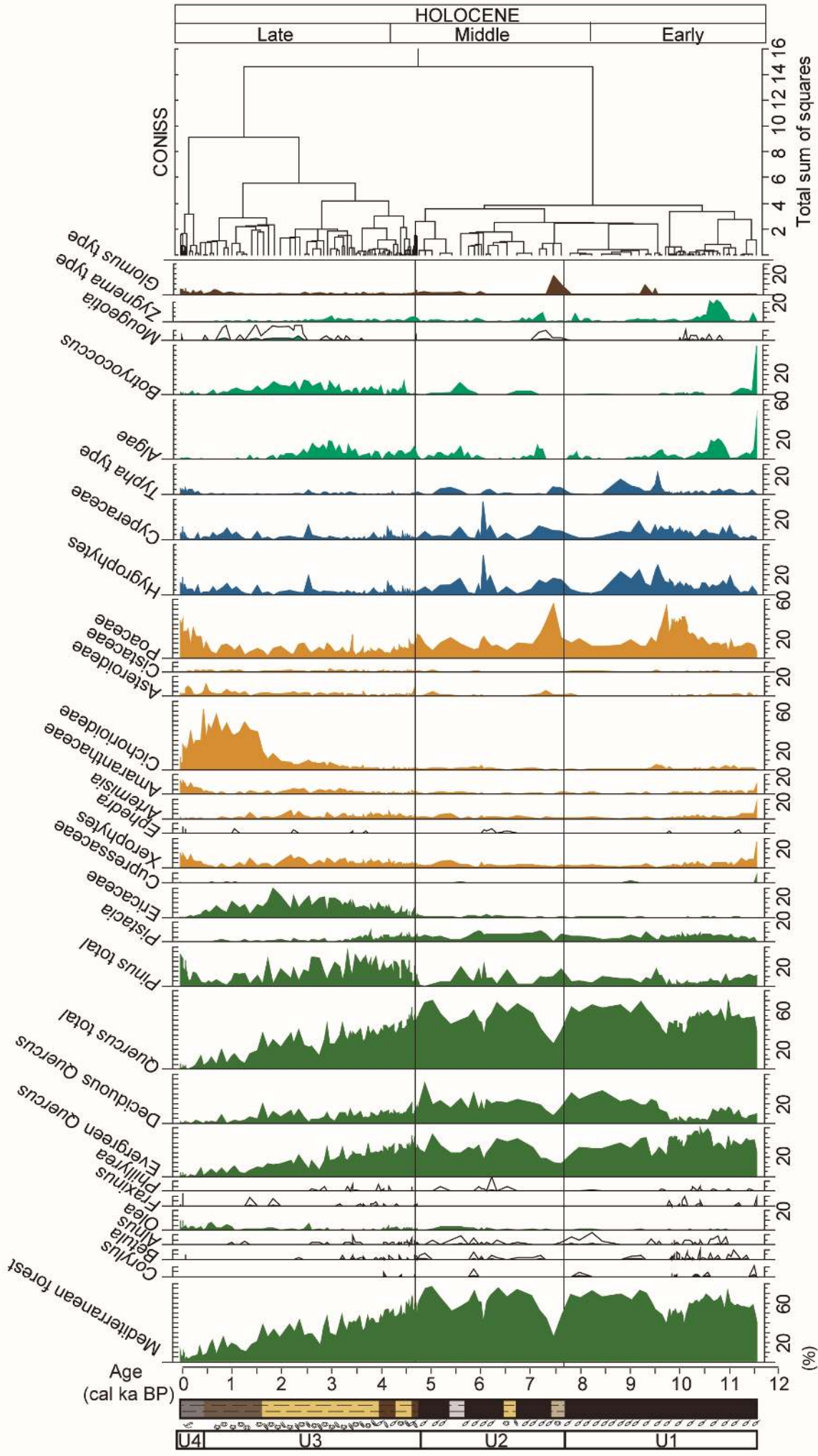
1123 **Table 4.** Linear *r* (Pearson) correlation between geochemical proxies and pollen data from the Padul-15-05
1124 record. Statistical treatment was performed using the Past software ([http://palaeo-](http://palaeo-electronica.org/2001_1/past/issue1_01.htm)
1125 [electronica.org/2001_1/past/issue1_01.htm](http://palaeo-electronica.org/2001_1/past/issue1_01.htm)).





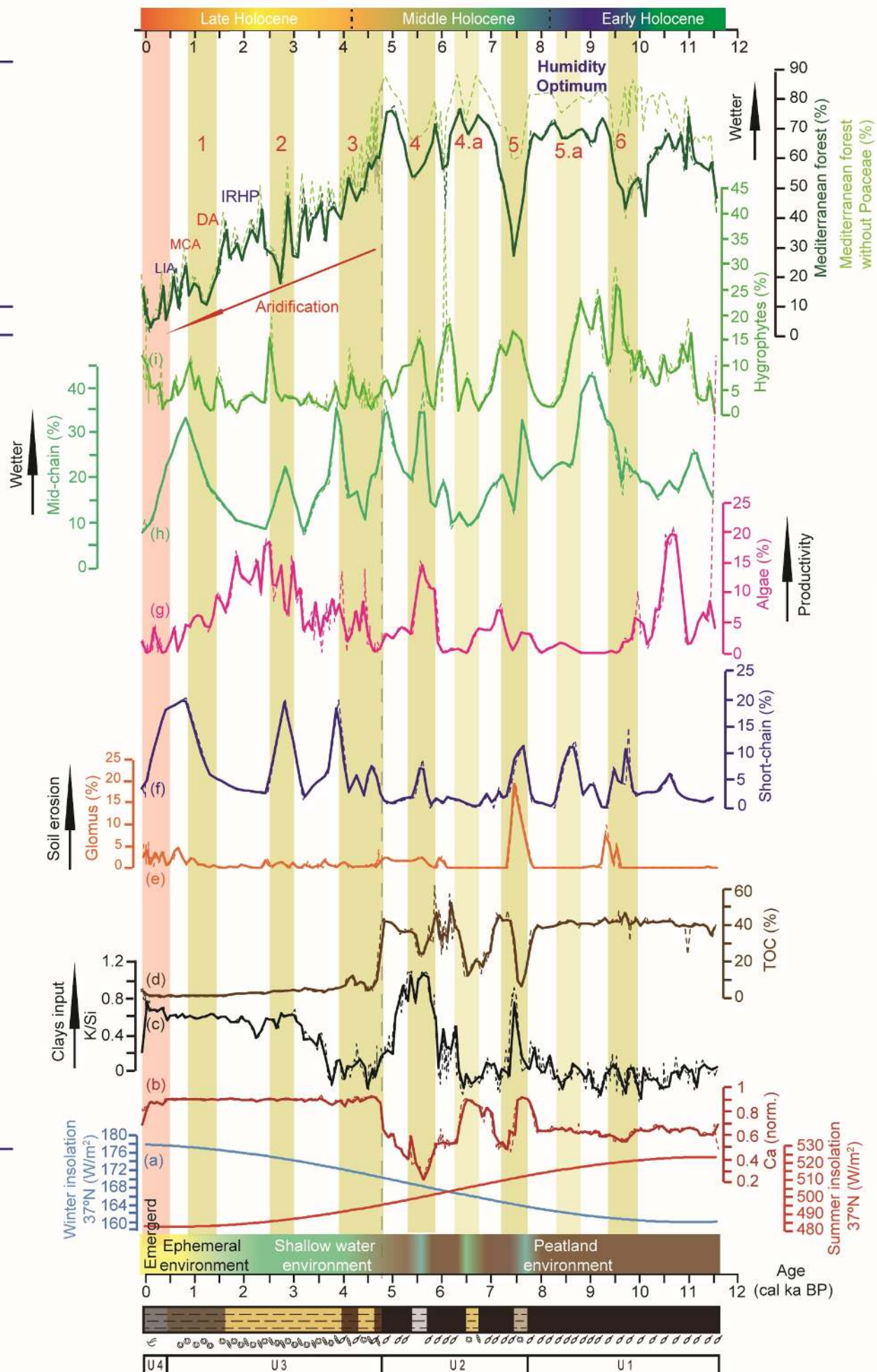


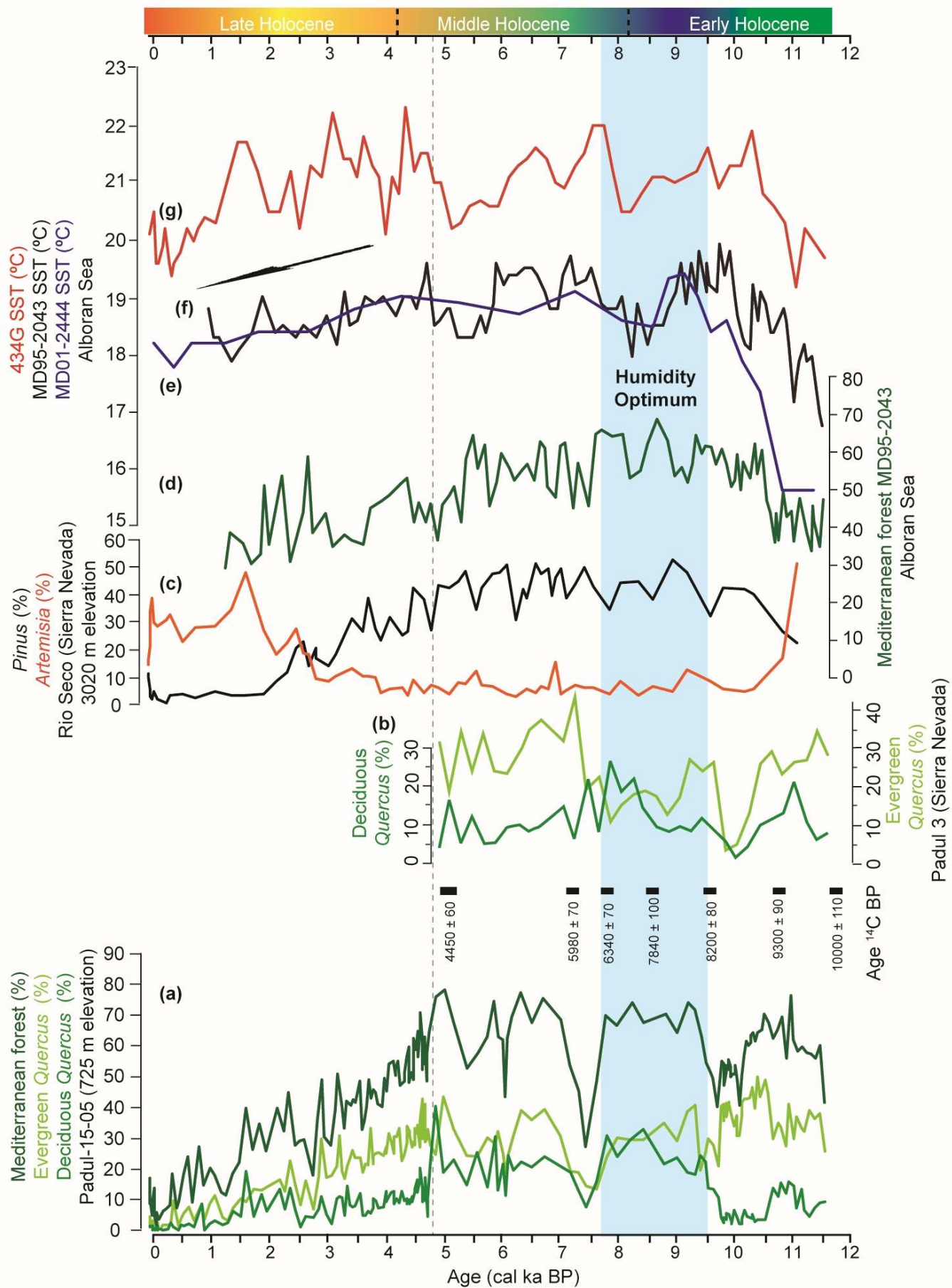


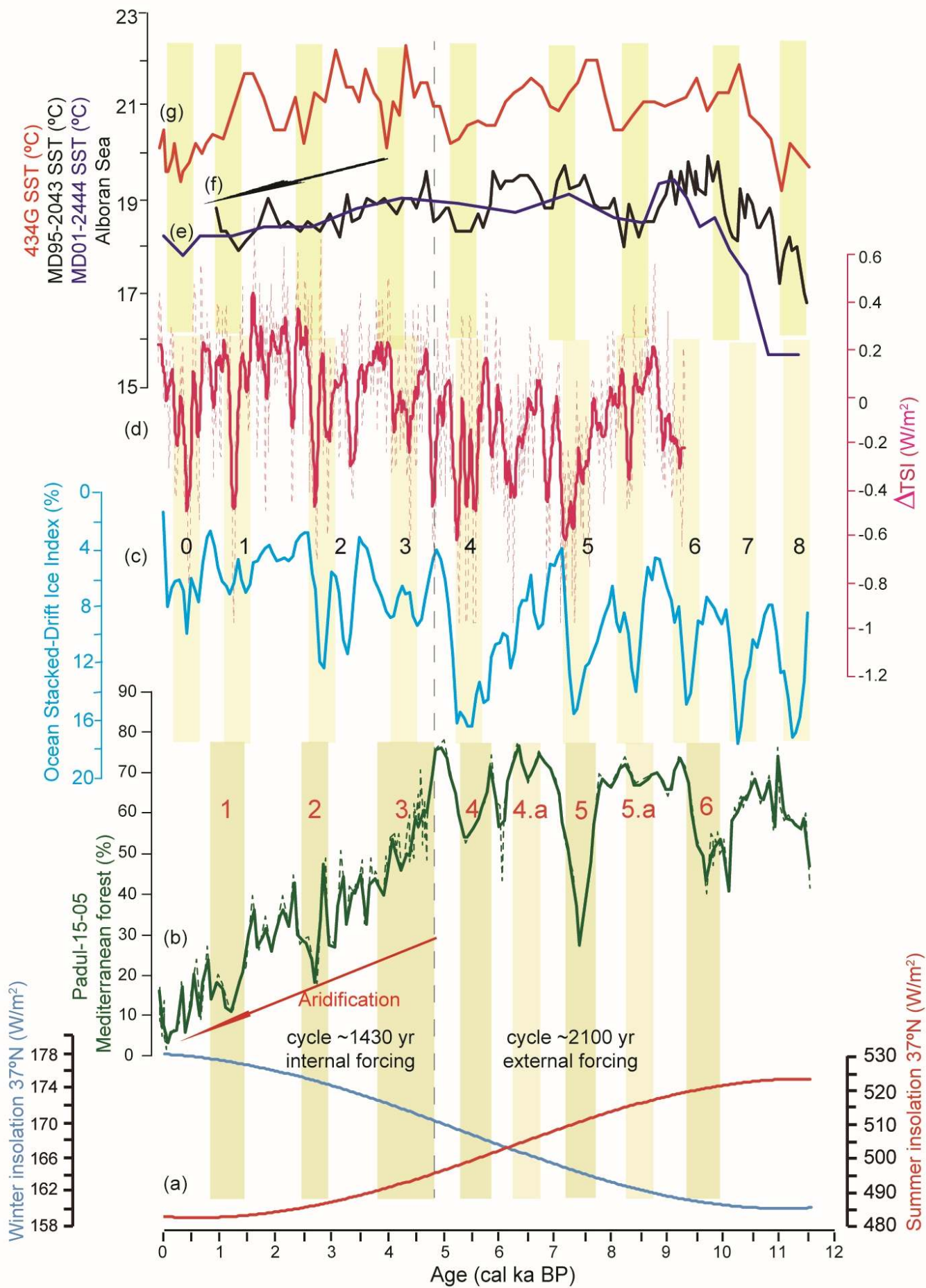


(A) Regional

(B) Local







Vegetation belt	Elevation (m)	Main taxa
Crioromediterranean	> 2800	Tundra vegetation including members of Poaceae, Asteraceae, Brassicaceae, Gentianaceae, Scrophulariaceae and Plantaginaceae.
Oromediterranean	1900-2800	<i>Pinus sylvestris</i> , <i>P. nigra</i> and <i>Juniperus</i> spp. and other shrubs such as species of Fabaceae, Cistaceae and Brassicaceae. ☒
Supramediterranean	1400-1900	<i>Quercus pyrenaica</i> , <i>Q. faginea</i> and <i>Q. rotundifolia</i> and <i>Acer opalus</i> ssp. ☒ <i>granatense</i> and other trees and shrubs, with some species of Fabaceae, Thymelaeaceae, Cistaceae and <i>Artemisia</i> sp.
Mesomediterranean	600-1400	<i>Quercus rotundifolia</i> , some shrubs, herbs and plants as <i>Juniperus</i> sp., and some species of Fabaceae, Cistaceae and Liliaceae

Laboratory number ^a	Core	Material	Depth (cm)	Age (¹⁴ C yr BP \pm 1 σ)	Calibrated age (cal yr BP) 95% confidence interval	Median age (cal yr BP)
Reference ages			0	2015CE	-65	-65
D-AMS 008531	Padul-13-01	Plant remains	21.67	103 \pm 24	23-264	125
Poz-77568	Padul-15-05	Org. bulk sed.	38.46	1205 \pm 30	1014-1239	1130
BETA-437233	Padul-15-05	Plant remains	46.04	2480 \pm 30	2385-2722	2575
Poz-77569	Padul-15-05	Org. bulk sed.	48.21	2255 \pm 30	2158-2344	2250
BETA-415830	Padul-15-05	* Shell	71.36	3910 \pm 30	4248-4421	4345
BETA- 437234	Padul-15-05	Plant remains	76.34	3550 \pm 30	3722-3956	3840
BETA-415831	Padul-15-05	Org. bulk sed.	92.94	3960 \pm 30	4297-4519	4430
Poz-74344	Padul-15-05	Plant remains	122.96	4295 \pm 35	4827-4959	4870
BETA-415832	Padul-15-05	Plant remains	150.04	5050 \pm 30	5728-5900	5815
Poz-77571	Padul-15-05	Plant remains	186.08	5530 \pm 40	6281-6402	6340
Poz-74345	Padul-15-05	Plant remains	199.33	6080 \pm 40	6797-7154	6935
BETA-415833	Padul-15-05	Org. bulk sed.	217.36	6270 \pm 30	7162-7262	7210
Poz-77572	Padul-15-05	Org. bulk sed.	238.68	7080 \pm 50	7797-7999	7910
Poz-74347	Padul-15-05	Plant remains	277.24	8290 \pm 40	9138-9426	9295
BETA-415834	Padul-15-05	Plant remains	327.29	8960 \pm 30	9932-10221	10105
Poz-77573	Padul-15-05	Plant remains	340.04	9420 \pm 50	10514-10766	10640
Poz-74348	Padul-15-05	* Plant ramains	375.62	9120 \pm 50	10199-10412	10305
Poz-79815	Padul-15-05	Org. Bulk sed.	377.83	10310 \pm 50	11847-12388	12145
Poz-79817	Padul-15-05	* Shell	411.02	13910 \pm 60	16588-17088	16840
Poz-79818	Padul-15-05	* Shell	414.89	14130 \pm 50	17001-17419	17210
Poz-77574	Padul-15-05	Org. Bulk sed.	423.65	13580 \pm 80	16113-16654	16385

* Rejected data

^a Sample number assigned at radiocarbon laboratory

Samples	n-alkane indices					
	Paq	ACL	CPI	Short-chain (%)	Mid-chain (%)	Long-chain (%)
Algae- Bryophyte	0.32 ± 0.21	27.97 ± 0.74	9.52 ± 7.69	13.02 ± 21.07	35.26 ± 19.82	51.71 ± 33.84
Aquatics plants	0.29 ± 0.34	28.78 ± 1.86	11.60 ± 7.35	1.33 ± 4.40	28.36 ± 32.44	70.31 ± 34.64
Terrestrial	0.16 ± 0.16	28.23 ± 0.74	20.64 ± 10.84	-	17.44 ± 19.34	82.56 ± 19.34

	C/N ratio	H/C ratio	TOC	MS	Peacece	Algae	Hydrophyte	Short-chain	Mid-chain	Long-chain	S	Br	K/Si	Ca	Sr
C/N ratio		5.33E-16	6.30E-33	9.48E-13	9.41E-07	7.14E-02	2.11E-10	3.67E-05	0.0093249	9.69E-01	2.15E-30	1.24E-13	4.56E-08	1.05E-24	5.60E-20
H/C ratio	-0.60595		4.97E-16	1.25E-54	0.24997	0.83873	0.014101	1.36E-11	0.16571	0.040739	4.80E-11	3.45E-08	1.03E-10	9.55E-09	9.85E-17
TOC	0.79396	-0.60645		1.03E-12	8.08E-08	0.00097023	5.41E-10	1.26E-11	0.00011256	0.80183	2.41E-65	1.04E-36	1.02E-10	2.05E-39	6.36E-49
MS	-0.54666	0.90279	-0.54594		0.58699	0.64816	0.018814	2.33E-09	1.03E-01	0.12274	4.44E-09	2.02E-07	2.83E-11	1.60E-06	4.34E-15
Peacece	0.39277	-0.095815	0.42633	-0.045323		0.00096771	5.25E-07	0.37586	5.61E-01	0.99854	8.46E-08	0.00018098	0.019496	6.83E-06	0.00031762
Algae	-0.14967	-0.016988	-0.27025	-0.038078	-0.27031		0.0028618	0.6669	9.08E-05	0.0073904	0.0043751	8.23E-05	0.00030366	0.13141	0.00039267
Hydrophyte	0.49514	-0.20278	0.4852	-0.19424	0.40108	-0.24514		0.29595	1.53E-08	0.00034311	1.54E-12	5.19E-10	0.016645	1.67E-10	1.44E-06
Short-chain	-0.33565	0.52387	-0.52465	0.4706	-0.074081	0.036044	-0.087385		0.0010611	5.42E-22	6.36E-08	1.93E-08	4.50E-05	8.70E-08	2.48E-11
Mid-chain	0.21524	-0.11572	0.31522	-0.13612	0.048675	-0.31926	0.44853	0.26917		1.93E-48	5.05E-05	3.19E-03	6.52E-02	0.00011163	3.23E-05
Long-chain	0.0032797	-0.17016	0.021023	-0.12875	-0.00015362	0.2216	-0.29331	-0.6921	-0.88146		0.66657	0.66508	5.68E-01	0.7461	0.99199
S	0.77416	-0.51013	0.93201	-0.46179	0.42573	-0.23457	0.54234	-0.43076	0.32998	-0.036081		9.63E-42	3.78E-12	4.77E-34	5.58E-40
Br	0.56396	-0.43716	0.81996	-0.41423	0.30507	-0.32002	0.48565	-0.44574	0.24327	0.036253	0.84907		2.40E-07	8.36E-27	7.26E-26
K/Si	-0.43366	0.50252	-0.50258	0.51532	-0.19316	0.29481	-0.1979	0.33204	-0.15353	-0.047753	-0.53426	-0.41189		0.22728	2.33E-21
Ca	-0.72099	0.45282	-0.83631	0.38503	-0.36269	0.12543	-0.49757	0.42671	-0.31537	0.027119	-0.80209	-0.74218	0.110054		5.65E-19
Sr	0.6649	-0.61781	0.88208	-0.59051	0.2939	-0.28956	0.38657	-0.51813	0.33788	0.00084107	0.83951	0.73296	-0.68263	-0.65119	

Supplementary Information

Millennial-scale cyclical environment and climate variability during the Holocene in the western Mediterranean region deduced from a new multi-proxy analysis from the Padul record (Sierra Nevada, Spain)

María J. Ramos-Román¹, Gonzalo Jiménez-Moreno¹, Jon Camuera¹, Antonio García-Alix^{1,2}, R. Scott Anderson³, Francisco J. Jiménez-Espejo⁴, Dirk Sachse⁵, Jaime L. Toney⁶, José S. Carrión⁷, Cole Webster³, Yurena Yanes⁸

¹ Departamento de Estratigrafía y Paleontología, Universidad de Granada, Spain

² Instituto Andaluz de Ciencias de la Tierra (IACT), CSIC-UGR, Armilla, Spain

³ School of Earth Sciences and Environmental Sustainability, Northern Arizona University, USA.

⁴ Department of Biogeochemistry, Japan Agency for Marine-Earth Science and Technology (JAMSTEC), Japan.

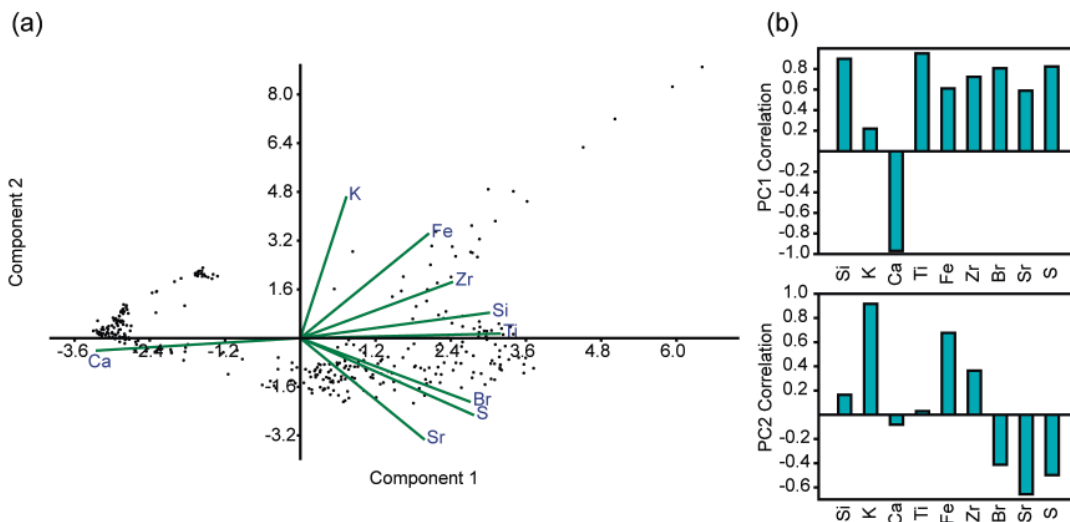
⁵ Helmholtz Centre Potsdam, German Research Centre for Geosciences GFZ, Section 5.1 Geomorphology, Organic Surface Geochemistry Lab., Germany

⁶ School of Geographical and Earth Sciences, University of Glasgow, UK

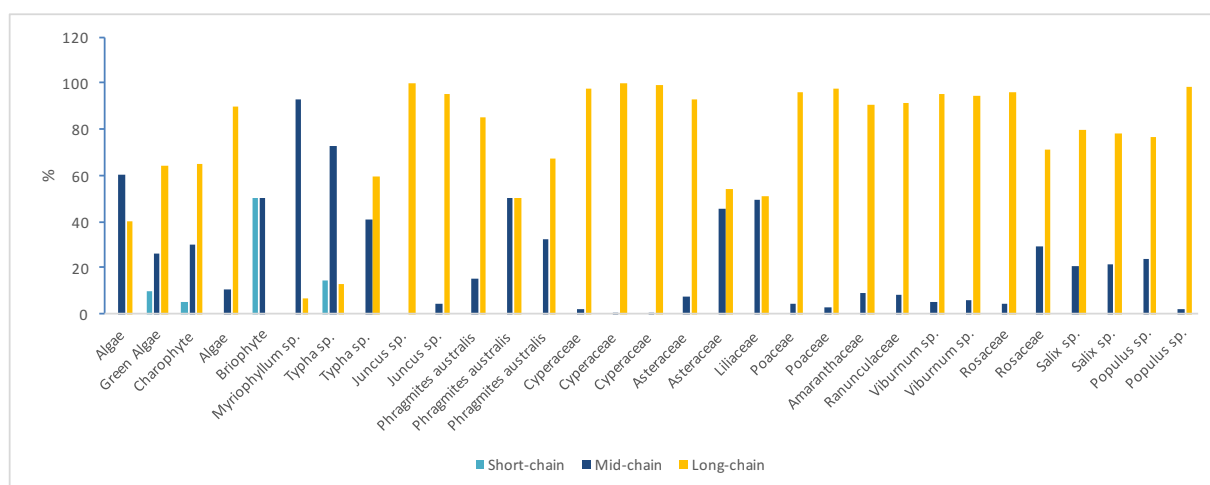
⁷ Departamento de Biología Vegetal, Facultad de Biología, Universidad de Murcia, Murcia, Spain

⁸ Department of Geology, University of Cincinnati, USA

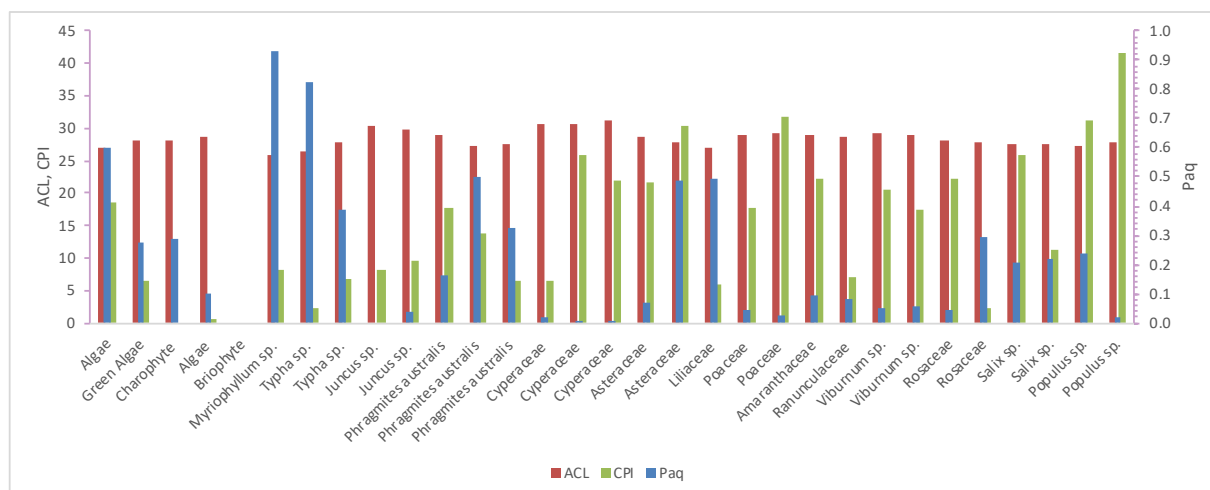
Supplementary Figures



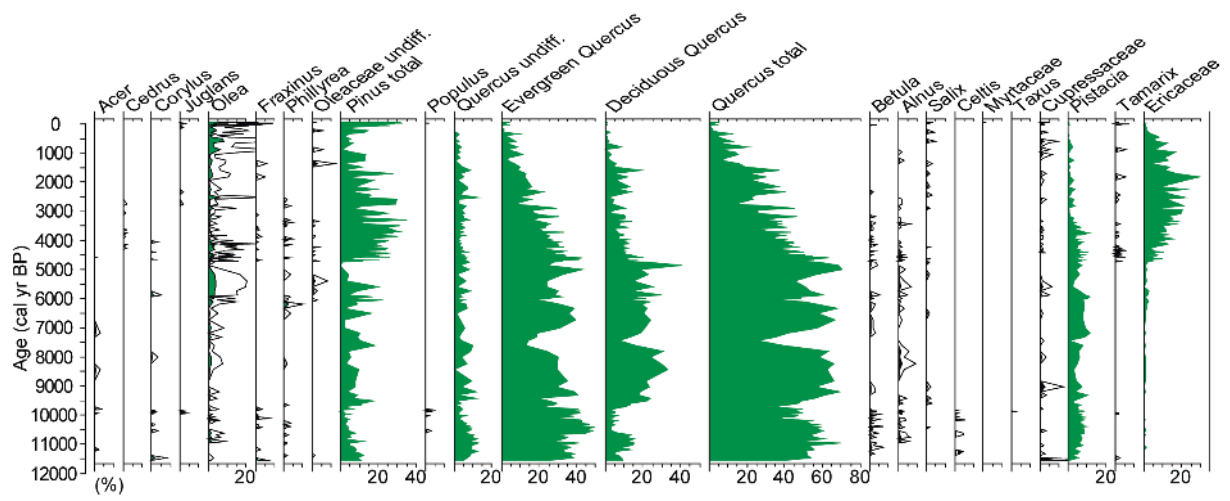
Supplementary Figure S1. X-ray fluorescence (XRF) PCA results from the Padul-15-05 record. (a) Biplot figure and (b) loadings (correlation) of the most significant components; PC1 (above) and PC2 (below). Statistical analysis was performed using Past software (http://palaeo-electronica.org/2001_1/past/issue1_01.htm).



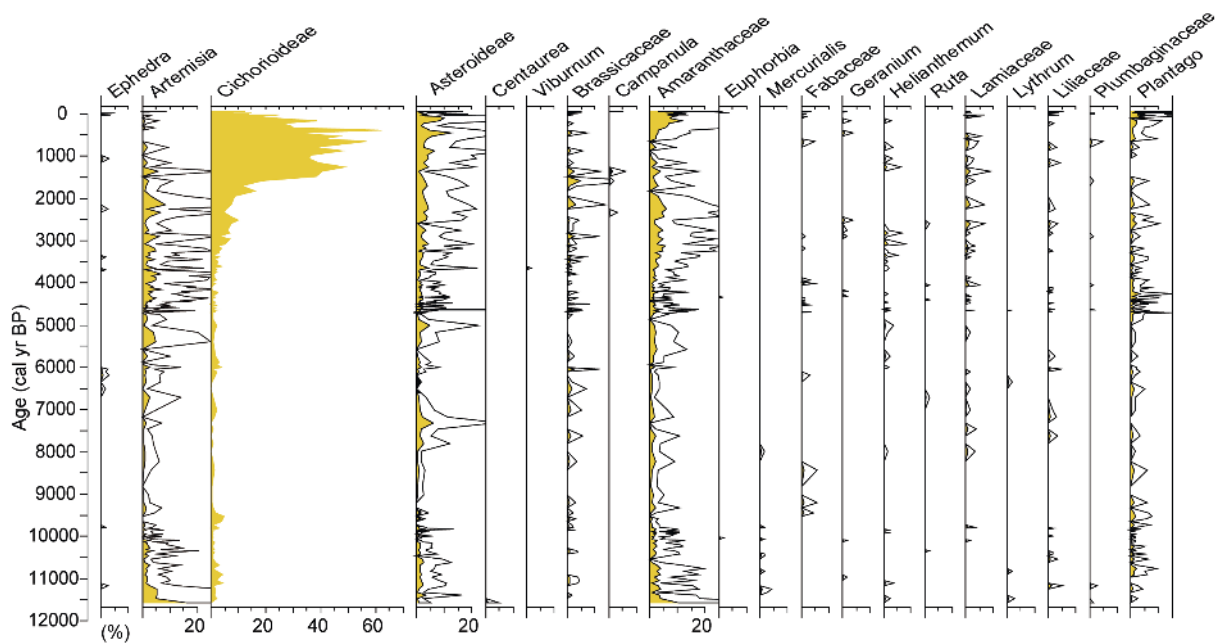
Supplementary Figure S2. *n*-alkane indices [Short-chain, Mid-chain and Long-chain (%)] from the algae, bryophyte and plant samples studies in the surroundings of the present-day Padul lake.



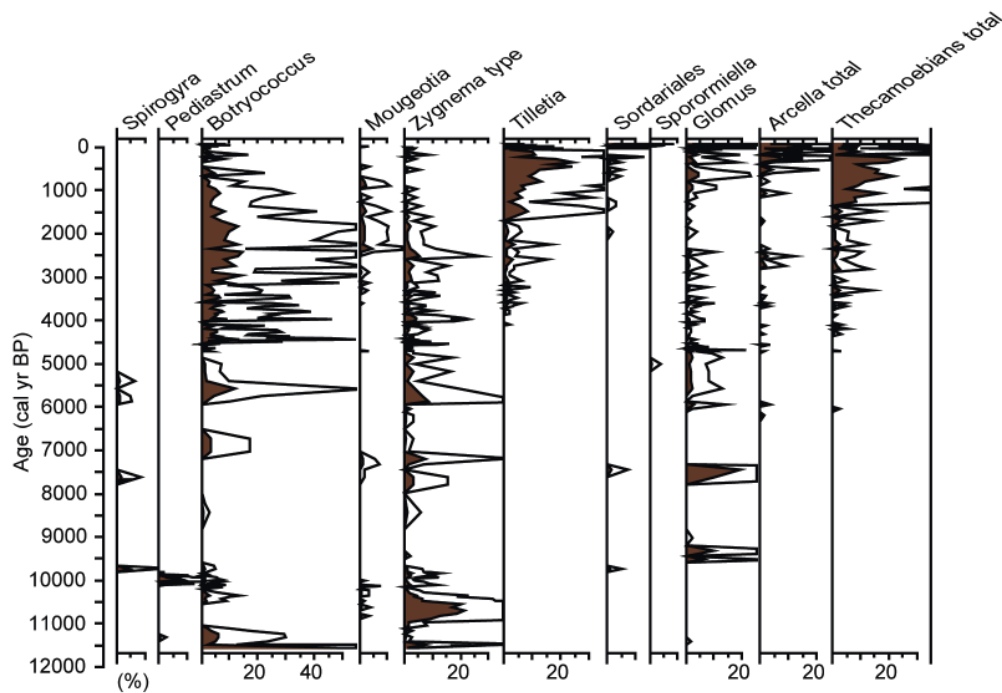
Supplementary Figure S3. *n*-alkane indices (Paq, ACL and CPI) from the algae, bryophyte and plant samples studies in the surroundings of the present-day Padul lake.



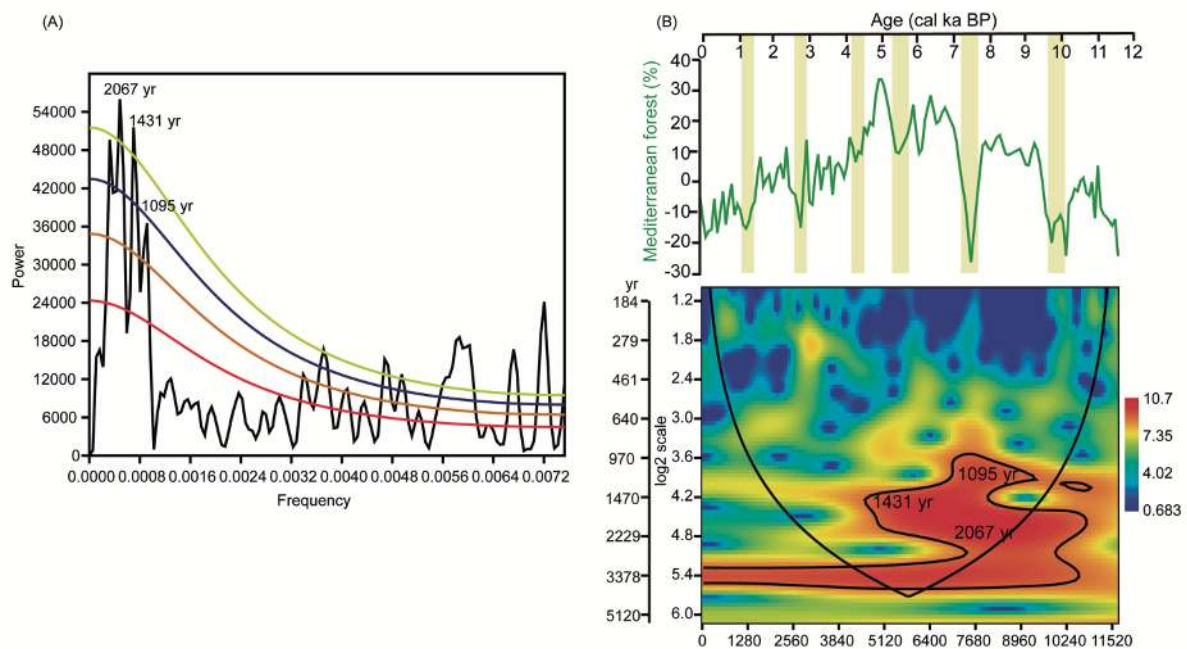
Supplementary Figure S4. Pollen percentages of major tree and shrubs pollen taxa from the Padul-15-05 record. Pollen curve are exaggerated 5x in some taxa (black silhouette).



Supplementary Figure S5. Pollen percentages of major herbs pollen taxa from the Padul-15-05. Pollen curve are exaggerated 5x in some taxa (black silhouette).

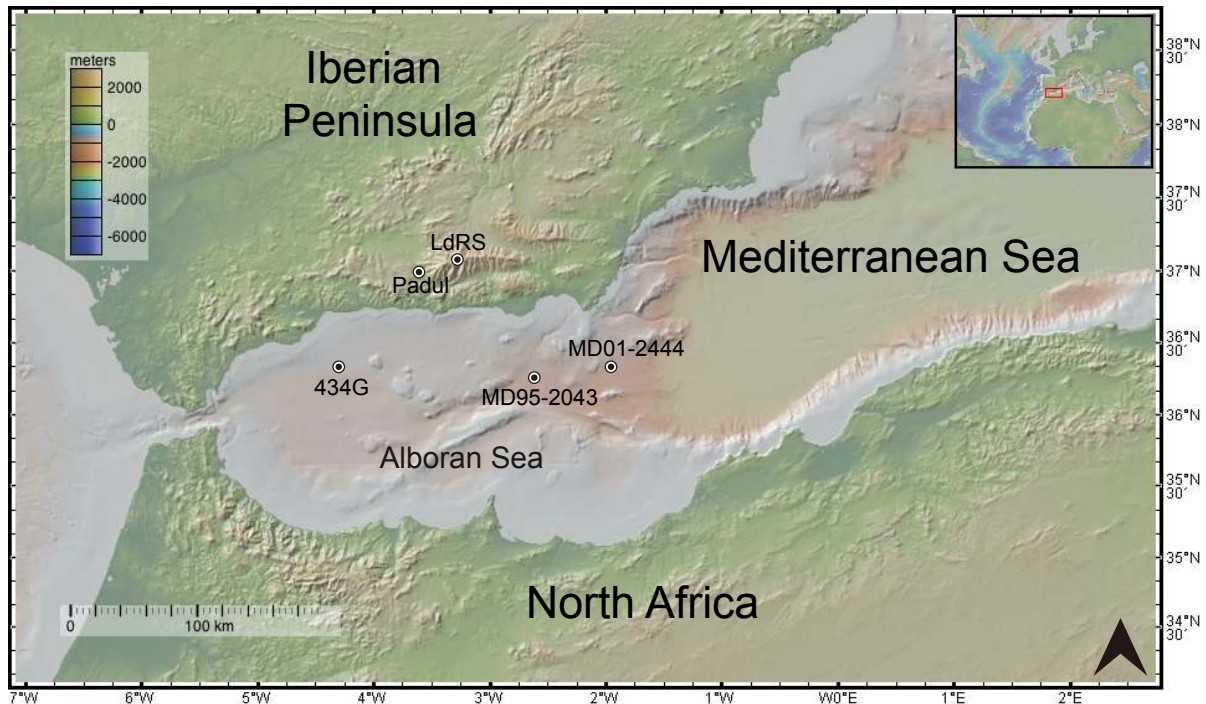


Supplementary Figure S6. Pollen percentages of major non-pollen palynomorphs from the Padul-15-05. Pollen curve are exaggerated 5x in some taxa (black silhouette).

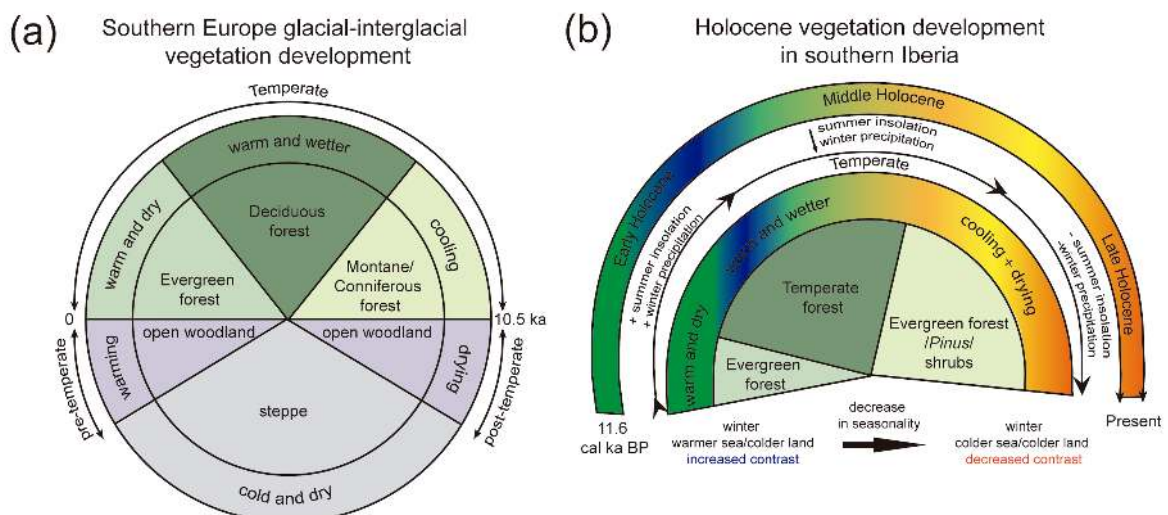


Supplementary Figure S7. Wavelet analysis results from the local and regional proxies from Padul-15-05 record. (A) Spectral analysis of Mediterranean forest (%). AR (1) red noise (red line). Confident levels are marked: 80 % (orange line), 90% (blue line) and 95 % (green line) and the significant periodicities above the 80 % confident level are shown. (B) *Above*. Mediterranean forest taxa (%) detrended and lineally interpolated to 80 yr; shading indicate Mediterranean forest

declines with a ~2067 yr of periodicity until ca. 5.5 cal ka BP and a ~1431 yr of periodicity since ca. 5 cal ka BP. Statistical analysis was performed using Past software (http://palaeo-electronica.org/2001_1/past/issue1_01.htm).



Supplementary Figure S8. Location of different terrestrial and marine records in the north western Mediterranean region. The map was performed using the software GeoMapApp (<http://www.geomapapp.org>) and modified with Adobe Illustrator.



Supplementary Figure S9. (A) Vegetation succession during an idealized glacial-interglacial cycle in southern Europe with sufficient moisture availability during a precessional period (modified from Tzedakis,

2007). (B) Vegetation/climate succession in southern Iberia since ~11.6 cal ka BP.

Supplementary tables

PC	Eigenvalue	% variance
1	5.2735	58.594
2	2.31664	25.74
3	0.575871	6.3986
4	0.327842	3.6427
5	0.213153	2.3684
6	0.168962	1.8774
7	0.077899	0.86554
8	0.0461336	0.5126
9	1.82E-17	2.02E-16

Supplementary Table S1. X-ray fluorescence (XRF) PCA results from Padul-15-05 record. Eigenvalue, and percentage of variance explained with the different Principal Components. Statistical analysis was performed using Past software (http://palaeo-electronica.org/2001_1/past/issue1_01.htm).